ANNUAL REPORT 1997

Department of Optoelectronics

University of Ulm

Contents

Improving Performances 1

Articles **2**

62% Wall-plug Efficiency InGaAs/AlGaAs Laser Diode Arrays 2

Semiconductor Lasers using Lateral Confinement by Native-Oxide Layers 6

Fabrication of Vertical Facets in AlGaAs Using CAIBE 12

Fabrication and Characterization of Broad-Area Lasers with Dry Etched Mirrors 16

High-Quality Single-Layer Antireflection Coating 20

Gas Source Molecular Beam Epitaxy of InAlGaP/InGaP MQW-Lasers 24

Efficient Single-Mode Oxide Confined GaAs VCSELs 27

Highly Efficient Single-Mode Oxide Confined GaAs VCSELs 33

Bias-Free 2.5 Gb/s Data Transmission 38

Oxide Confined 2D VCSEL Arrays for High-Density Inter/Intra-Chip Interconnects 43

CW-Operation of a Diode Cascade InGaAs Quantum Well VCSEL 48

Bottom Emitting VCSELs for High cw Optical Output Power 52

Oxide Confined Vertical-Cavity Semiconductor Optical Amplifier for 980 nm Wavelength 57

Progress Towards Long Wavelength VCSELs 61

Design and Modeling of Long Wavelenth Fused VCSEL Cavities 62

Low Threshold 1.3 μm-InAsP/InGaAsP Quantum Well Lasers 66

Wafer-Fused Long-Wavelength VCSELs 71

Device Performance of Ultra-Violet Emitting Diodes Grown by MBE 76

MOVPE Growth of InGaN MQW LEDs 81

Blue Light-Emitting Diodes on GaN Substrates, Growth and Characterization . 86

GaN Based LEDs with Different Recombination Zones 92

Lists of Publications **98**

Ph.D. Theses 98

Diploma Theses and Semester Projects 99

Talks and Seminars 102

Publications and Conference Contributions 106

Department of Optoelectronics
University of Ulm

Albert-Einstein-Allee 45
D-89069 Ulm, Germany
Fax: +49–731/50–26049
Phone: +49–731/50–

Head of Department:

Prof. Dr.	Karl Joachim Ebeling	–26051	karl.ebeling@e-technik.uni-ulm.de

Assistant Head of Department:

Prof. Dr.	Peter Unger	–26054	unger@sunrise.e-technik.uni-ulm.de

Cleanroom Management:

Dr.-Ing.	Jürgen Mähnß	–26053	juergen.maehnss@e-technik.uni-ulm.de

Senior Research Assistant:

Dr.-Ing.	Rainer Michalzik	–26048	rainer.michalzik@e-technik.uni-ulm.de

Secretaries:

	Christine Bunk	–26050	karl.ebeling@e-technik.uni-ulm.de
	Sükran Kilic	–26059	

Research Staff:

Dipl.-Phys.	Hin Yiu Anthony Chung	–26043	hin-yin.chung@e-technik.uni-ulm.de
Dipl.-Ing.	Eckard Deichsel	–26057	eckard.deichsel@e-technik.uni-ulm.de
Dipl.-Ing.	Franz Eberhard	–26039	franz.eberhard@e-technik.uni-ulm.de
Dipl.-Ing.	Matthias Golling	–26043	matthias.golling@e-technik.uni-ulm.de
Dipl.-Ing.	Martin Grabherr	–26036	martin.grabherr@e-technik.uni-ulm.de
Dipl.-Ing.	Jörg Heerlein	–26046	joerg.heerlein@e-technik.uni-ulm.de
Dipl.-Phys.	Roland Jäger	–26040	roland.jaeger@e-technik.uni-ulm.de
Dipl.-Ing.	Jürgen Joos	–26035	juergen.joos@e-technik.uni-ulm.de
Dipl.-Phys.	Günter Jost	–26046	guenter.jost@e-technik.uni-ulm.de
Dipl.-Phys.	Christian Jung	–26036	christian.jung@e-technik.uni-ulm.de
Dr.rer.nat.	Markus Kamp	–26454	kamp@sunrise.e-technik.uni-ulm.de
Dipl.-Ing.	Roger King	–26035	roger.king@e-technik.uni-ulm.de
Dipl.-Ing.	Christoph Kirchner	–26040	christoph.kirchner@e-technik.uni-ulm.de
M.S.	Safwat William Mahmoud	–26044	safwat.mahmoud@e-technik.uni-ulm.de
Dipl.-Ing.	Ulrich Martin	–26038	ulrich.martin@e-technik.uni-ulm.de
Dipl.-Phys.	Markus Mayer	–26452	markus.mayer@e-technik.uni-ulm.de
Dipl.-Phys.	Michael Miller	–26452	michael.miller@e-technik.uni-ulm.de
Dipl.-Phys.	Arthur Pelzmann	–26452	arthur.pelzmann@e-technik.uni-ulm.de
Dipl.-Phys.	Markus Schauler	–26039	markus.schauler@e-technik.uni-ulm.de
Dipl.-Ing.	Wolfgang Schmid	–26044	wolfgang.schmid@e-technik.uni-ulm.de
Dipl.-Phys.	Peter Schnitzer	–26037	peter.schnitzer@e-technik.uni-ulm.de
Dr.-Ing.	Georgi Stareev	–26043	georgi.stareev@e-technik.uni-ulm.de
Dipl.-Ing.	Veit Schwegler	–26043	veit.schwegler@e-technik.uni-ulm.de
Dipl.-Ing.	Dieter Wiedenmann	–26037	dieter.wiedenmann@e-technik.uni-ulm.de

Technical Staff:

Margit Kohler	–260 41	
Sophie Pfetsch	–260 41	sophie.pfetsch@e-technik.uni-ulm.de
Susanne Menzel	–260 41	
Rudolf Rösch	–260 38	rudolf.roesch@e-technik.uni-ulm.de
Josef Theisz	–260 30	

Improving Performances

As in recent years, research of the Department has concentrated on vertical cavity laser diodes (VCSELs), optical interconnects, high power edge emitting laser diodes, as well as GaN based light emitting diodes (LEDs). Highlights in VCSEL research achievements include record high cw output powers of single-mode VCSELs (4.8 mW), large-area multi-mode VCSELs (350 mW), and 3 x 3 VCSEL arrays (650 mW) as well as demonstration of the first diode cascade VCSEL. Sub half-milliamp 1 x 16 VCSEL arrays with 40 % wallplug efficiency, 4 x 8 VCSEL arrays with 8 Gbit/s data transmission capability per channel, and 2.5 Gibt/s bias-free data transmission with high efficiency low threshold VCSELs set new benchmarks for optical interconnect performance. Considerable progress in high power edge emitting lasers has led to broad-area devices with 63 % wallplug efficiency (just 3 % below the world record), laser diodes with 5.7 W cw output power, and hybrid optical amplifiers with above 500 mW high quality beam power. In GaN research, novel homoepitaxial LEDs on GaN substrates and UV LEDs attracted broad interest. In cooperation with the Department of Electronic Devices and Circuits GaN field effect transistors with excellent high temperature characteristics have been produced.

The Department's success in research is due to tremendous efforts of Ph.D. students and excellent support by the technical personnel. The various scientific achievements have led to numerous invitations to international conferences. Two former students, Ulrich Fiedler and Zheng Dai, received their Ph.D. degrees and now have attractive positions in industry or research organizations. In total 17 diploma theses and 12 semester projects were completed. All staff was happy to have Prof. Anders Larsson from Chalmers University Göteborg, Sweden, as a distinguished Guest Professor in the Department. We also enjoyed having Prof. Bart van Zhegbroeck from Colorado State University again in our Department for a couple of weeks.

The many research projects of the Department have been generously supported by the German Science Foundation, the Federal Ministry of Research and Technology, the Volkswagen Foundation, the ACTs and MEL-ARI Programs of the European Community, and a special program of the local Government of the State of Baden-Württemberg, all of which are gratefully acknowledged. Cooperation with industry, in particular Daimler-Benz Research and Siemens AG has been further strengthened. For his achievements in VCSEL research and technology transfer to industry the Head of the Department received the Karl Heinz Beckurts-Prize, the former technology transfer prize of the Federal Government.

Both Professors of the Department have time-consuming extra duties. Peter Unger was elected as the Chairman of the committee responsible for examination affairs in the Faculty and the Head of the Department still serves as an elected Vice-President of the University.

K. J. Ebeling, January 1998

62% Wall-plug Efficiency InGaAs/AlGaAs Laser Diode Arrays

Jörg Heerlein and Roland Jäger

High efficiency InGaAs/AlGaAs laser diode arrays with a maximum optical output power of 2.7 W in continuous wave (CW) operation at an emission wavelength of $\lambda = 980\,nm$ have been developed. A maximum wall-plug efficiency of $\eta = 62\,\%$ at room temperature has been achieved for 500-μm-long laser array devices consisting of 20 stripes with an aperture width of 5 μm and a spacing of 7 μm mounted junction-side-down on a diamond heatspreader.

1. Introduction

High-power, large-area multimode laser diodes are important for a wide range of applications including laser beam printers, pumping of fiber amplifiers and solid state lasers, and material processing. The maximum optical CW power in broad-area lasers is typically limited by the onset of a reversible thermal roll over or by an irreversible catastrophic optical mirror damage (COMD). The COMD effect is accelerated by a thermal runaway effect and filamentations. To increase the maximum optical power, low differential resistances, small optical losses and large electro-optical conversion efficiencies are necessary. The properties of the laser device can be improved further by a junction-side-down mounting for an efficient cooling and by special geometries to suppress local filamentations. In this work, we present our improved epitaxial quality in terms of efficiencies, losses and resistances. Therefore, gain-guided laser diode arrays mounted junction-side down on diamond heat spreaders have been fabricated and investigated. A schematic drawing of a laser diode array with 20 stripes is depicted in Fig. 1.

2. Device Structure

The epitaxial structure used in this work consists of an 8-nm-thick $In_{0.2}Ga_{0.8}As$ quantum well surrounded by 40-nm-thick GaAs barrier layers and 100-nm-thick $Al_xGa_{1-x}As$ graded index layers where the Al mole fraction is linearly graded from 5 % to 30 %. The p- and n-dopands are C and Si, respectively. The top contact consists of a highly doped ($2{\cdot}10^{20}\,cm^{-3}$) cap layer and an evaporated TiPtAu contact metallization. The lateral active area which consists of 20 5-μm-wide stripes has been defined by wet chemical etching. The structures have been passivated by a 100-nm-thick Si_3N_4 layer deposited by

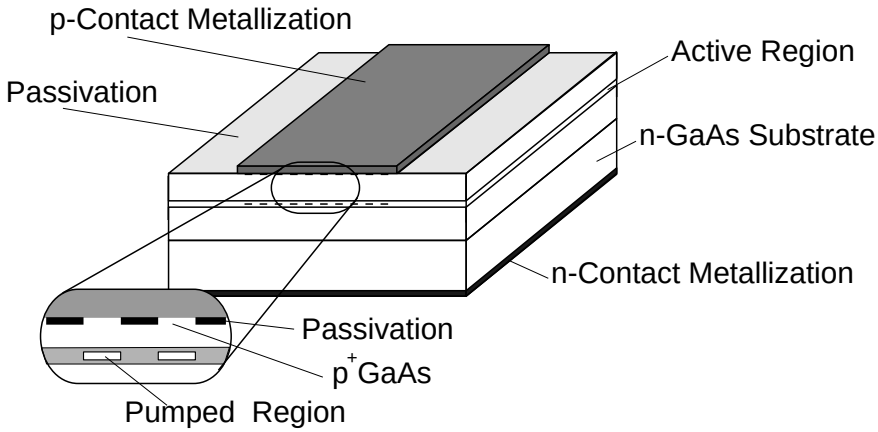

Fig. 1. Schematic drawing of a gain guided laser array.

a sputter deposition system. After cleaving, the lasers have been soldered junction-side down on a diamond heatspreader which is mounted by thermal compression bonding on a copper heat sink.

3. Experimental Results

For the characterization of the epitaxial quality, broad-area lasers with an aperture width of 100 μm have been fabricated and measured under pulsed conditions. For long cavities the threshold current density is $j_{\mathrm{th}} = 120\,\mathrm{A/cm^2}$. Measurements of threshold current densities for different temperatures in the range of 0-20 °C show a T_0 value of 210 K. Internal efficiencies η_{i} and intrinsic losses α_{i} are 87 % and $2.2\,\mathrm{cm^{-1}}$, respectively. The series resistance, as determined by the slope of the IV curve, was typically 0.22-0.3 Ω for a 500 μm laser. The turn-on voltage V_0 of the IV characteristic is 1.3 V. From measurements of the vertical far field pattern we determined the full width at half maximum (FWHM) of the fast axis divergence angle to be $\Theta_{\mathrm{FWHM}} = 41\,°$.

All laser diode arrays consist of 20 5-μm-wide stripes with different spacings of 7 μm up to 13 μm. The optical output characteristic of a 500-μm-long laser array with a spacing of 7 μm taken at a heatsink temperature of 20 °C is shown in Fig. 2. A total maximum output power of 2.7 W CW is obtained at a current of 3.5 A at the point where thermal roll over occurs. The laser array exhibits a threshold current of 120 mA, corresponding to a current density of $240\,\mathrm{A/cm^2}$. The differential efficiency is 81% and remains constant up to ~1.7 W From the IV characteristic in Fig. 3 we get a differential resistance of 170 mΩ and a turn-on voltage V_0 of 1.3 V. Also shown in Fig. 3 is the total wall-plug efficiency versus operating current which shows a peak value of 62 % at an optical power of ~700 mW.

An optical emission spetrum of a 500-μm-long laser array at an operating current of $1.2 \cdot I_{\mathrm{th}}$ and $7.3 \cdot I_{\mathrm{th}}$, respectively, is depicted in Fig. 4 and indicates operation at $\lambda = 978$ nm near threshold. To compare the spectral width of broad area and array structures

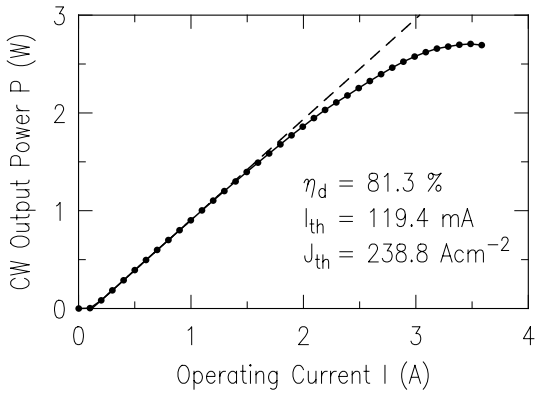

Fig. 2. Optical output characteristic in CW operation for a 500-μm-long uncoated laser diode array with an aperture width of 5 μm and a spacing of 7 μm. The laser is mounted junction-side down on a diamond heat spreader.

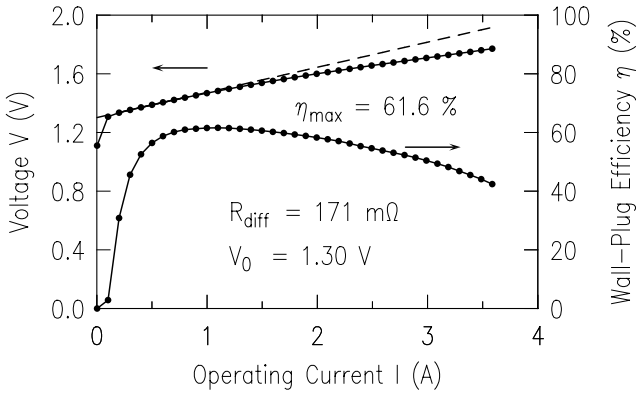

Fig. 3. *IV* characteristic and wall-plug efficiency η of the same device as in Fig. 2. All measurements have been taken at room temperature (20 °C).

we measured the spectral width $\Delta\lambda_{10\,\mathrm{dB}}$ where the intensity is decreased to a value of 10 % of the maximum. At high optical output powers, $\Delta\lambda_{10\,\mathrm{dB}}$ is two times smaller for arrays than for broad area lasers. For example, at an optical output power of 800 mW the spectral width of a broad area laser is $\Delta\lambda_{10\,\mathrm{dB}} = 7.6\,\mathrm{nm}$ and for a laser array (stripe width 5 μm, spacing 10 μm) $\Delta\lambda_{10\,\mathrm{dB}}$ is 3.9 nm.

The thermal resistance of a mounted laser has been measured by using the correlation of emission wavelength shift and temperature rise. In theory, the wavelength shift of the band gap for an $In_{0.2}Ga_{0.8}As$ quantum well is $\Delta\lambda/\Delta T = 0.32\,\mathrm{nm/K}$. In experiment, we

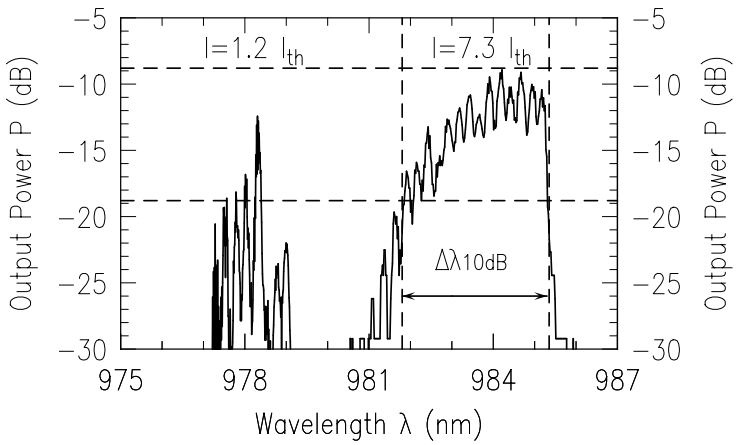

Fig. 4. Optical emission spectrum of a 500-μm-long laser array with an aperture width of 5 μm and a spacing of 7 μm at an operating current of $1.2{\cdot}I_{\mathrm{th}}$ and $7.3{\cdot}I_{\mathrm{th}}$, respectively.

found a value of $0.333 \pm 0.004\,\mathrm{nm/K}$. Using

$$R_{\mathrm{th}} = \frac{\Delta\lambda}{0.33\mathrm{nm/K}} \cdot \frac{1}{P_{\mathrm{d}}} = \frac{\Delta T}{\Delta P_{\mathrm{d}}}$$

with the power dissipation $P_{\mathrm{d}} = V\,I$ - P_{opt} we have determined the thermal resistances $\mathrm{R_{th}}$. For a broad area laser of a size of $500\,\mu\mathrm{m} \times 100\,\mu\mathrm{m}$ we determined $\mathrm{R_{th}}$ to be 28.4 K/W. For laser arrays with the same cavity length and a spacing of the stripes of $7\,\mu\mathrm{m}$ and $13\,\mu\mathrm{m}$ the thermal resistance is 18.4 K/W and 17 K/W, respectively. The reduced thermal resistance of the laser array leads to higher optical output powers in CW operation.

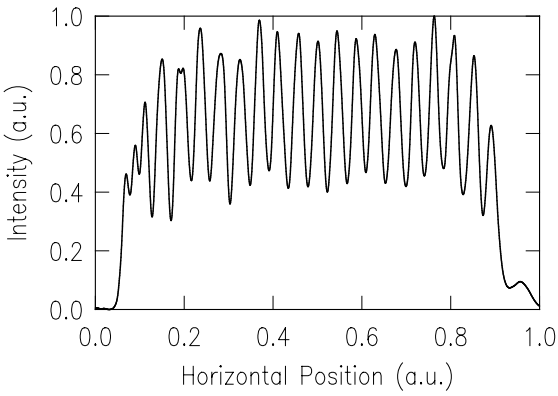

Fig. 5. Optical near-field pattern at the facet of a laser diode array with an aperture width of $5\,\mu\mathrm{m}$ and a spacing of $10\,\mu\mathrm{m}$. $I = 12 \cdot I_{\mathrm{th}}$.

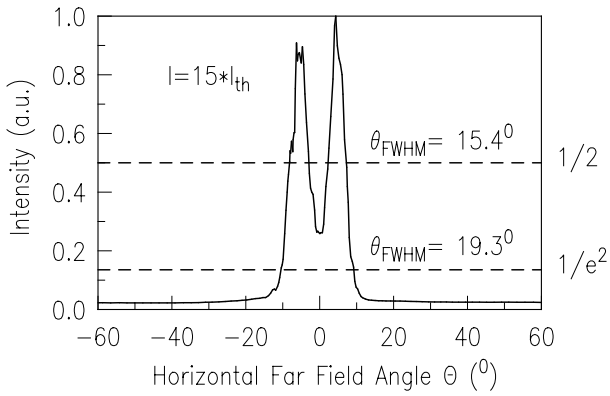

Fig. 6. Far-field distribution of the device shown in Fig. 5 taken at 15 times threshold current.

The optical near-field pattern has been measured by imaging the laser facet on a beam analysis system. Broad area lasers show an irregular intensity distribution including spontaneous filamentations. This behavior leads also to a strong and irregular far field distribution in the slow axis. The FWHM of the far-field angle Θ_{FWHM} increases from 4.1° ($I = 2 \cdot I_{\mathrm{th}}$) to 14° ($I = 20 \cdot I_{\mathrm{th}}$) due to thermal lensing. In contrast to broad-area lasers, laser arrays show an even modulation of the intensity. For arrays with a small spacing, there is only a weak intensity modulation leading to a broad and little modulated far-field pattern. Fig. 5 shows a strong modulated intensity distribution of an array with a stripe width of $5\,\mu\mathrm{m}$ and a spacing of $10\,\mu\mathrm{m}$ at 12 times threshold current. The contributing far-field pattern depicted in Fig. 6 shows two symmetric side lobes. The charactersitic side lobes in the horizontal far field are independent of the operating current. Arrays with a larger spacing of $13\,\mu\mathrm{m}$ show small side maxima between the pumped region due to higher super modes. This leads to a far-field pattern with typical two side lobes and a small peak in the center. As for broad-area lasers also for arrays the FWHM of the horizontal far field angle Θ_{FWHM} increases for higher operating currents but the shape of the far-field pattern stays stabler for arrays.

Semiconductor Lasers using Lateral Confinement by Native-Oxide Layers

Jörg Heerlein

We report on results of wet-oxidized narrow-stripe laser diodes operating in single lateral and longitudinal mode around an emission wavelength of 850 nm. Devices with an active width of 4–10 µm achieved output powers of up to 240 mW in continuous wave operation at room temperature. Furthermore, we have analyzed the lateral waveguiding using the effective index method. We found, that the effective refractive index step can be adjusted exactly by the thickness of the AlAs layer and its distance to the graded index separate confinement heterostructure (GRINSCH) region.

1. Introduction

Large optical-power index-guided single-stripe lasers operating in a single lateral mode are promising devices as light sources for various optical systems such as laser-beam printers, optical data storage devices, for pumping of fiber amplifiers and of solid state lasers, and for frequency doubling. Therefore, ridge-waveguide lasers and buried heterostructure lasers have been widely investigated. Recent improvements in the performance of vertical-cavity surface-emitting lasers (VCSELs) have been achieved using a selective wet oxidation process for injected current confinement and lateral index guiding. Wall-plug efficiencies and multi-mode output powers have been increased up to 57 % and 180 mW, respectively [1], [2]. For stripe lasers, an oxidized layer also provides advantages for electrical and optical confinement.

Fig. 1 shows a schematic drawing of a native-oxide confined narrow-stripe laser. A thin AlAs layer above the active region has been wet oxidized in a hot steam atmosphere from the side walls. The active lateral geometry is defined by the width of the oxidized AlAs layer. Using this technique, the refractive index of the AlAs layer is reduced to a value of $n \sim 1.6$ for the Al_xO_y. This leads to a lower effective refractive index n_2 beside the active laser stripe, building a lateral index guiding. The effective refractive-index step Δn_{eff} can be adjusted exactly and reproducibly by the thickness of the AlAs layer and its distance to the active region during the epitaxial growth. In case of a conventional ridge-waveguide structure, the index guiding has to be defined by the etch depth beside the active region. Since there is a strong dependence between etch depth and effective refractive index, a homogeneous technological reproduction of the index step is rather difficult.

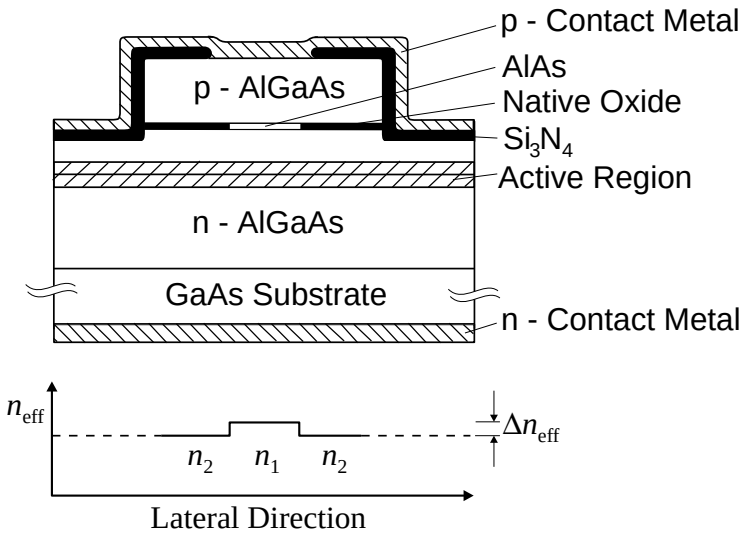

Fig. 1. Schematic drawing of a narrow-stripe laser with an AlAs layer above the active region which is oxidized from the side walls.

Furthermore, the isolating Al_xO_y layer provides an aperture for a homogeneous, non-dissipative current injection without surface recombinations. Compared to a ridge-waveguide structure, the p-side contact resistance and the series resistance are reduced due to a larger contact area. First Caracci, Kish et al. [3] presented encouraging results on native-oxide index-guided AlGaAs/GaAs lasers where a 400-nm-thick AlGaAs confinement layer was oxidized. InGaAs/AlGaAs lasers with native-oxide top- and bottom-confined narrow stripes were fabricated with 300-nm-thick oxidized AlGaAs layers showing optical output powers of 35 mW per facet for a 2.5 μm aperture [4]. InGaAs/AlGaAs lasers with 100-nm-thick AlAs layers were presented showing threshold currents of 1.7 mA [5]. In this paper we present the results on GaAs quantum well GRINSCH lasers exhibiting maximum optical output powers of 240 mW with wall-plug efficiencies of nearly 40 % in continuous wave operation without mounting on subcarriers.

2. Device Structure

The epitaxial structure which is grown by molecular beam epitaxy (MBE) consists of a single GaAs quantum well surrounded by graded-index AlGaAs layers and $Al_{0.5}Ga_{0.5}As$ cladding layers. A thin AlAs layer is positioned in a distance of 200 nm above the GRIN-SCH region.

After wet-chemical mesa etching, a selective oxidation of the 100-nm-thick AlAs layer in a 390 °C hot steam atmosphere is carried out. At an oxidation rate of about 1 μm/min, the width of the oxidized region can be controlled with an accuracy better than 1 μm. Devices with an active lateral width of $W = 4 \ldots 10\,\mu$m have been fabricated in this way.

3. Mode Analysis

For calculating the effective refractive index of the GRINSCH structure surrounded by the cladding layer including an AlAs or Al_xO_y layer we used the Maxwell equations for planar waveguides. Since the gain of transversal electric (TE-) modes in quantum well structures of this material system is much larger than for the perpendicular polarization (transveral magnetic, TM-modes), we take into account only the component equation for the electric field E_y in the plane of the well.

$$\frac{d^2E_y}{dx^2} + \left[n^2(x)k^2 - \beta^2\right] E_y = 0$$

with the refractive index n, vacuum wave number k and the beam propagation constant β. A superposition of trigonometric and exponential functions are employed for the solutions of the differential equation. The solutions are subject to the boundary conditions of decay at $y = \pm\infty$, field and derivative continuity at all interfaces. The GRIN layers are approximated by 50 layers each of equal thickness and constant refractive index. For the determination of the refractive indices of the layers we use a model published by Adachi [6]. The effective refractive index step $\Delta n_{\text{eff}} = n_1 - n_2$ between lateral active region and oxidized region has been calculated and plotted in Fig. 2 as a function of the distance d which is defined as the distance from the AlAs layer to the edge of the GRINSCH region. The thickness t of the AlAs layer is 100 nm. In Fig. 3 the dependence of the index step as a function of AlAs layer thickness t is depicted. The AlAs layer is positioned in a distance d of 200 nm to the GRINSCH region.

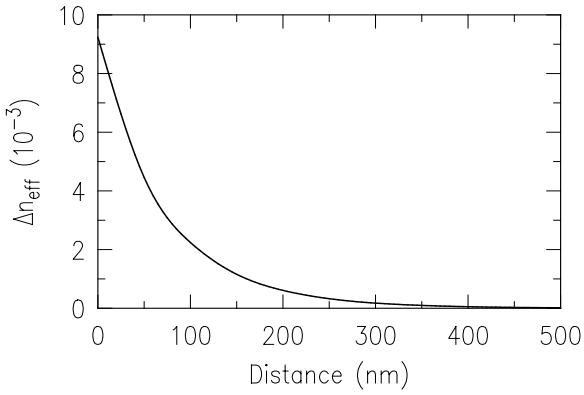

Fig. 2. Lateral effective refractive index step $\Delta n_{\text{eff}} = n_1 - n_2$ between lateral active and oxidized region as a function of the distance from the AlAs layer to the GRINSCH region.

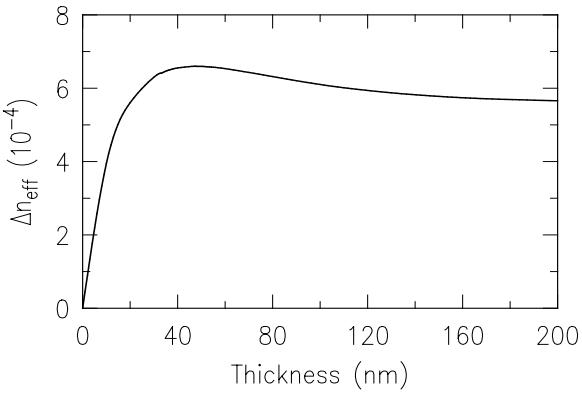

Fig. 3. Effective refractive index step Δn_{eff} as a function of the thickness of the AlAs layer.

For index-guided modes, there is a discrete spectrum of allowed modes within the range $kn_1 > \text{Re}\{\beta_m\} > kn_2$, with the effective refractive index n_1 of the active region and the effective refractive index n_2 of the cladding region. There is also a cut-off condition

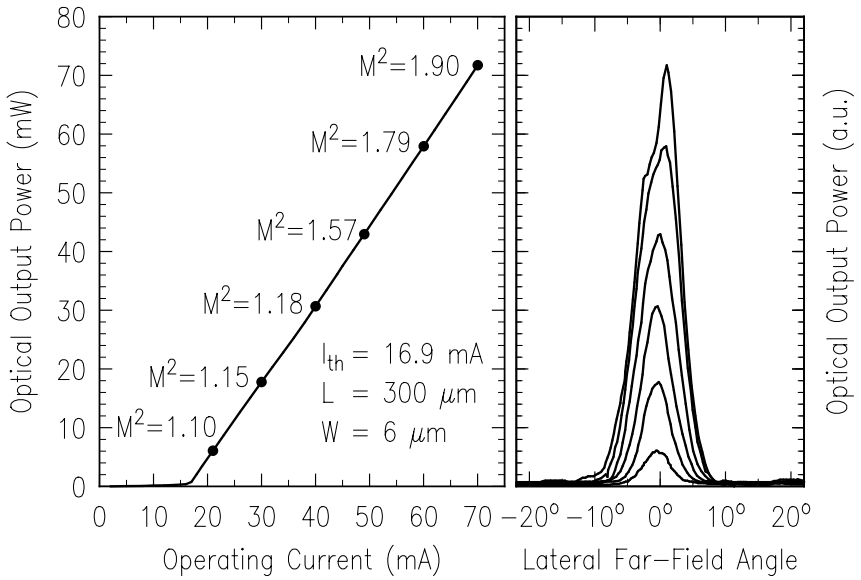

Fig. 4. Output characteristic of an oxidized laser with an active area of $300 \cdot 6\,\mu\mathrm{m}^2$. Beam quality factors M^2 between 1.1 and 1.2 have been measured below 30 mW. The corresponding nearly gaussian far-field patterns are depicted on the right hand side.

for each mode, when the optical field is not longer confined by the waveguide. This occurs when $\mathrm{Re}\{\beta_m\} = kn_2$. Such modes are referred to as radiation modes. The cut-off condition for higher order modes can be estimated by

$$\Delta n \leq \frac{\lambda^2}{8w^2\overline{n}}$$

with $\overline{n}$ the mean value of the refractive indexes n_1, n_2, the vacuum wavelength λ and the aperture width w. As an example, for building a single-mode waveguide with a stripe width of $w = 4\,\mu$m and $\lambda = 850\,$nm, the index step Δn has to be lower than $1.7{\cdot}10^{-3}$. In our device the effective refractive-index step is $\Delta n_{\mathrm{eff}} = 6{\cdot}10^{-4}$ which leads to a weak index guiding.

4. Device Characteristics

For the characterization of the epitaxial laser structure, broad-area lasers have been fabricated. The internal quantum efficiency η_{i} and the intrinsic losses α_{i} were determined from the reciprocal differential quantum efficiency versus cavity length L. Taking into account a mirror reflectivity R of 30 %, the internal quantum efficiency and the intrinsic losses can be calculated to be 90 % and $4.1\,\mathrm{cm}^{-1}$, respectively. For $2\,\mathrm{mm} \cdot 100\,\mu$m large devices, threshold current densities of $130\,\mathrm{Acm}^{-2}$ have been measured under pulsed conditions. These results predict that the epitaxially-grown laser structure offers a good quality for single-mode laser diodes.

Single mode lasers with a native-oxide lateral-confinement layer have been fabricated from these epitaxial qualities. All devices have been tested as cleaved at room temperature under continuous wave (CW) operation without mounting on a heat sink. In the light-current characteristics, the sum of the output powers of both facets are plotted.

Fig. 4 depicts the CW output characteristic of an oxide-confined laser with a cavity length of $L = 300\,\mu$m and an aperture width of $W = 6\,\mu$m. The threshold current I_{th} is 17 mA. The beam quality factor M^2 has been measured in the horizontal direction to be below 1.2 up to an optical power of 45 mW (aperture width = $6\,\mu$m). The M^2 for various operating curents are listed in the output characteristic. On the right hand side, the far-field patterns at different operating current levels are shown. The output beam is nearly diffraction limited, characterized by a gaussian intensity distribution.

The optical emission spectrum is depicted on the right hand side of Fig. 5 at an operating current 20 mA and 60 mA, respectively. The peak emission wavelength is $\lambda = 842$ nm near threshold. In case of a $300\,\mu$m long laser diode, the free spectral range is 0.31 nm. Up to an optical output power of 60 mW, we found a nearly constant side-mode suppression of 30 dB. For higher optical output powers the longitudinal emission spectrum becomes multi mode. This behavior can be seen in Fig. 5 where the values of the side-mode supression are listed in the output characteristic.

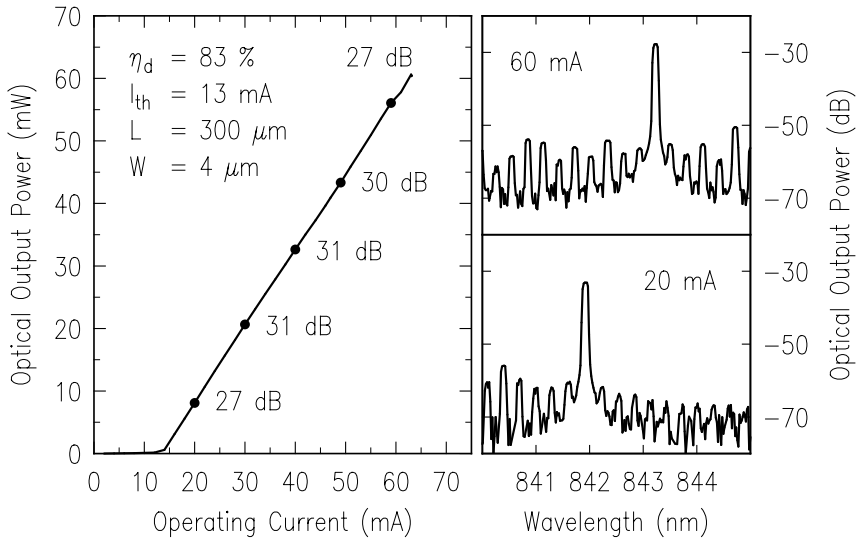

Fig. 5. Optical output characteristic and inserted side mode suppression of the longitudinal modes for a $300\,\mu$m long laser with a current aperture w of $4\,\mu$m. The diagrams on the right hand side show spectra at currents of 20 mA (at bottom) and 60 mA (at top).

Considerable high maximum total output powers of up to 240 mW have been achieved for laser diodes with an active area of $750 \cdot 10\,\mu\mathrm{m}^2$ as depicted in Fig. 6. The series resistance is $2.6\,\Omega$. Threshold current I_{th} and differential quantum efficiency η_{d} are 31 mA and 60 %, respectively. The wall-plug efficiency η stays nearly constant for a wide operation range with a maximum value of 38 %.

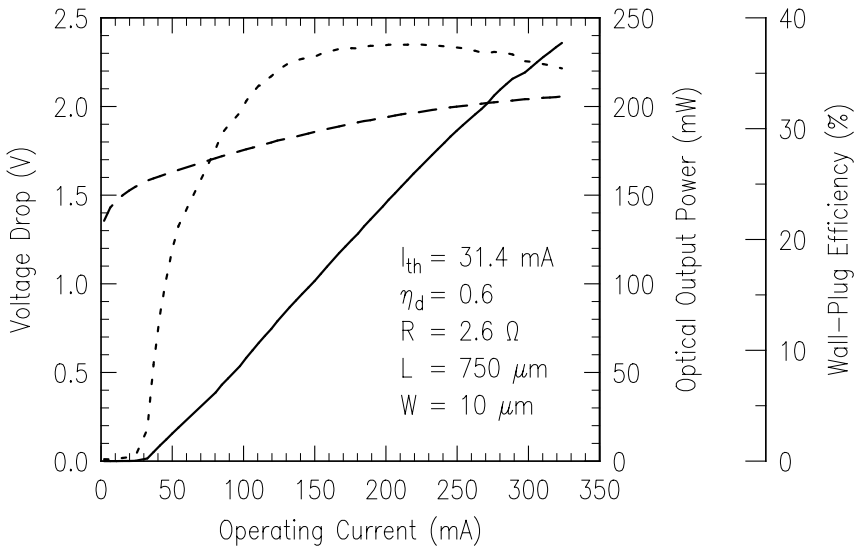

Fig. 6. The CW output characteristic (solid line), *IV* characteristic (dashed line) and wall-plug efficiency (dotted line) of a $750 \cdot 10\,\mu\text{m}^2$ large laser. The device shows a maximum output power of 240 mW and a maximum wall-plug efficiency of 38 %. The laser is measured as cleaved in CW operation without mounting on a heat sink.

References

[1] R. Jäger, M. Grabherr, C. Jung, R. Michalzik, G. Reiner, B. Weigl and K. J. Ebeling, "57 % Wallplug efficiency oxide-confined 850 nm wavelength GaAs VCSELs," *Electron. Lett.*, vol. 33, no. 4, pp. 330-331, February 1997.

[2] M. Grabherr, B. Weigl, G. Reiner, R. Michalzik, M. Miller, and K. J. Ebeling, "High power top-surface emitting oxide confined vertical-cavity laser diodes," *Electron. Lett.*, vol. 32, no. 18, pp. 1723-1724, August 1996.

[3] S. J. Caracci, F. A. Kish, N. Holonyak, Jr., and S. A. Maranowski, "High-performance planar native-oxide buried-mesa index-guided AlGaAs-GaAs quantum well heterostructure lasers," *Appl. Phys. Lett.*, vol. 61, pp. 321-323, 1992.

[4] S. A. Maranowski, A. R. Sugg, E. I. Chen, and N. Holonyak, Jr., "Native oxide top- and bottom-confined narrow stripe p-n $Al_yGa_{1-y}As$-GaAs-$In_xGa_{1-x}As$ quantum well heterostructure laser," *Appl. Phys. Lett.*, vol. 63, pp. 1660-1662, 1993.

[5] Y. Cheng, G. M. Yang, M. H. MacDougal, and P. D. Dapkus, "Low-threshold native-oxide confined narrow-stripe folded-cavity surface-emitting InGaAs-GaAs lasers," *Photon. Technol. Lett.*, vol. 7, pp. 1391-1393, 1995.

[6] S. Adachi, "GaAs, AlAs, and $Al_xGa_{1-x}As$: material parameters for use in research and device applications," *J. Appl. Phys.*, vol. 58, pp. R1-R29, 1985.

Fabrication of Vertical Facets in AlGaAs Using Chemically-Assisted Ion-Beam Etching

Franz Eberhard and Eckard Deichsel

We have investigated a chemically-assisted ion-beam etching process for the fabrication of vertical and smooth facets in AlGaAs. The optimization of the process parameters leads to a stable and reproducible etching process. A tri-level resist provides high mechanical and chemical resistivity. Additionally, its vertical profile avoids lateral mask erosion.

1. Introduction

Dry-etching processes are highly desirable in semiconductor manufacturing because they offer many advantages compared to wet-chemical etching. Compatibility with automated VLSI processing and the ability of anisotropic patterning down to a width of a few nanometers may be the most important advantages [1].

In contrast to other dry etching techniques, chemically-assisted ion-beam etching (CAIBE) shows a high decoupling of physical and chemical etching mechanisms and therefore offers the possibility to control anisotropy and etch profile [2]. The physical component is determined by the bombardment of the substrate with inert Ar ions which causes a physical removal of material. Chemical etching provides reactive attack of the substrate, forming volatile products.

For the fabrication of the high-quality vertical laser facets reported in this paper, a CAIBE system equipped with an electron-cyclotron-resonance source and load lock is used. The sample stage is temperature controlled in the range of -25 °C to 125 °C. In addition, the stage can be rotated and tilted. A computer-operated gas-handling system is used to control accurately the Ar, Cl_2, and BCl_3 flows. The base pressure of the turbo molecular pumped stainless steel chamber is below $5 \cdot 10^{-8}$ mbar. A residual gas analysis shows two main peaks caused by water vapour and hydrogen chloride. For unselective etching of AlGaAs over GaAs such a low moisture content is highly desirable [2].

To achieve smooth and vertical facets, the influences of the etch mask and the process parameters on etch rate, facet angle and roughness are investigated.

2. Etch Mask

For the fabrication of vertical dry-etched mirrors there are strict requirements regarding the etch mask. A standard AZ photoresist is not stable enough for chemically-assisted ion-beam etching. Etching with high temperatures is not possible and vertical mask erosion leads to slanting facets, which is shown in Fig. 1.

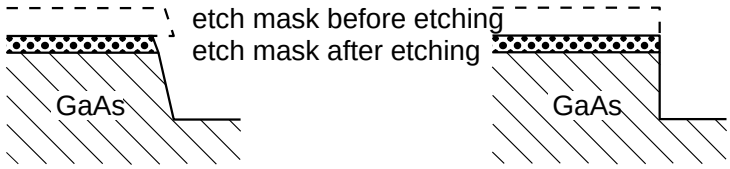

Fig. 1. Influence of mask erosion on facet angle. A slanted etch mask facet causes lateral mask erosion, showed on the left hand side. The right picture shows only erosion in vertical direction.

Only a stable etch mask with smooth and vertical facets provides good conditions for the dry etching of vertical facets in GaAs. A tri-level resist fulfils the requirements for mechanical and chemical resistance, and a vertical profile. The layer sequence and pattern transfer is shown in Fig. 2.

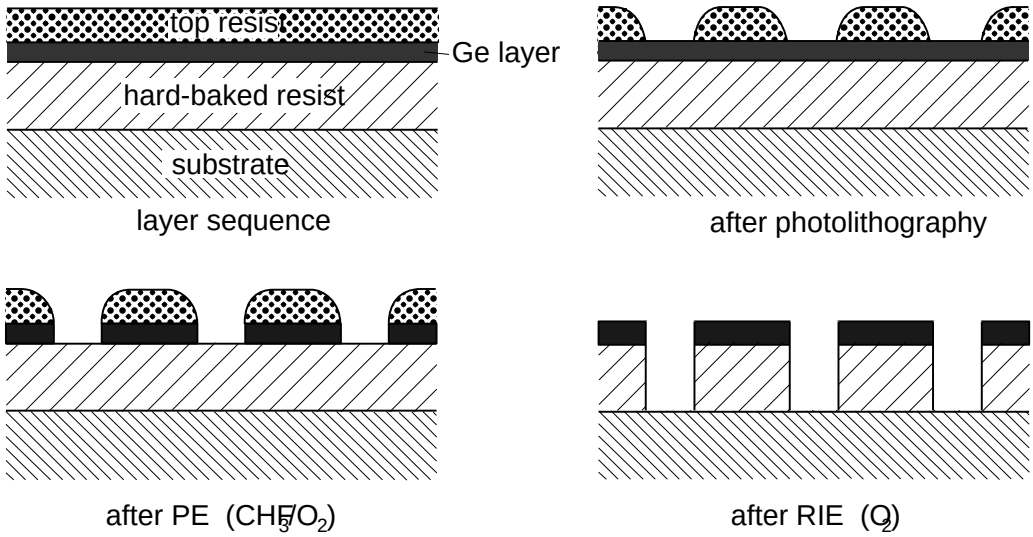

Fig. 2. Schematic of tri-level-resist.

The hard-baked (180 °C, 30 min) AZ 4533 bottom layer is covered with a 50-nm-thick Ge intermediate layer. The AZ 1512 imaging layer is structured by standard photolithography. Using CHF_3/O_2 plasma etching (PE) and O_2 reactive ion etching (RIE) for pattern transfer into the intermediate and bottom layers, respectively, the remaining hard baked resist has smooth and vertical facets. Other advantages are the high temperature stability and the good reproducibility.

3. Optimization of the Etch Process

The control of anisotropy and etch profile in dry etching of GaAs can be easily achieved by changing the physical and chemical components. The physical component, which is

determined by the ion-beam energy, current density, and tilt angle has to be chosen properly. Non-perpendicular incidence of the ions onto the substrate leads to direct impingement of ions onto the facet surface, which causes ion damage. High ion energies are also a source for ion damage.

For this experiments, an ion energy of 400 eV and a perpendicular incidence of the Ar ions has been used. All test samples consist of <100> orientated GaAs substrates and have been etched for 30 min with chlorine as reactive gas.

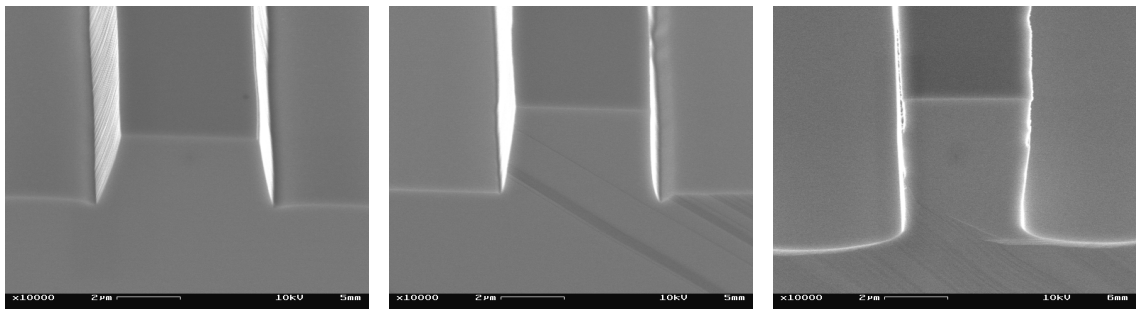

Fig. 3. Facet slopes for different substrate temperatures T = -25, 50, 125 °C.

The control of the profile has been achieved by adjusting the chemical component. As shown in Fig. 3, the slope of the facets changes for different substrate temperatures. A constant chlorine flow of 4 sccm has been used. At a temperature of -25 °C, the facets are positively sloped and change to negative slope as the temperature increases to 125 °C. At a substrate temperature of about 60 °C, the sidewalls are vertical. By changing the gas flow, the slope of the facets are also changed. Vertical facets can only be achieved by accurate control of temperature and gas flow, which can be seen in Fig. 4.

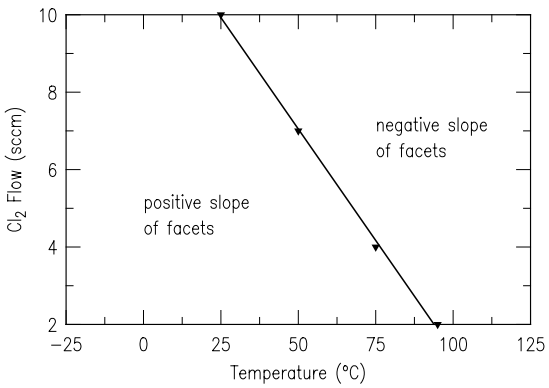

Fig. 4. Substrate temperatures and chlorine flows for vertical facets.

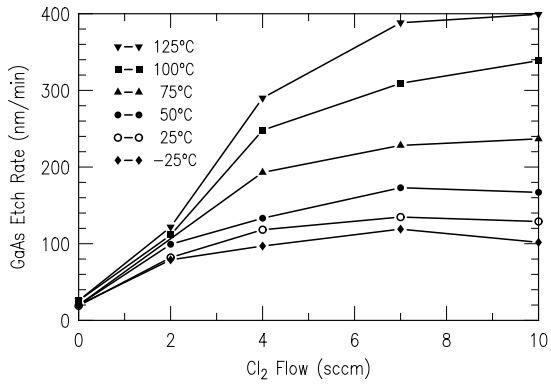

Fig. 5. Dependence of GaAs etch rate on chlorine flow for different substrate temperatures.

The temperature and reactive gas flow also effect the etch rate. An increase in one of them causes an accelerated material removal as shown in Fig. 5. Only at high chlorine flows above 7 sccm, a saturation in etch rate occurs for low substrate temperatures. This is due to the reduced mean free path of the Ar ions at high pressures in the chamber.

Results from the optimization experiments in GaAs have been used to dry etch AlGaAs/InGaAs laser structures. No changes in etch rate or in profile has been recognized. A dry-etched laser facet, fabricated with a chlorine flow of 4 sccm and a substrate temperature of 60 °C can be seen in Fig. 6. A tri-level resist has been used as the masking layer. The upper part of the 7-μm-high facet is very smooth, only in the lower part of the facet roughness can be observed.

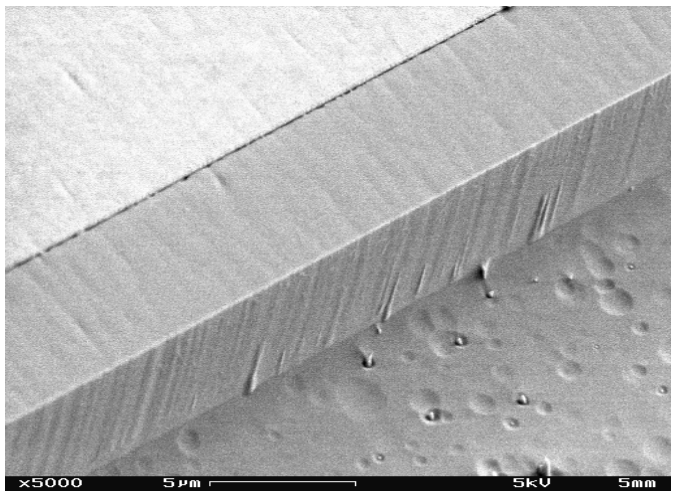

Fig. 6. Dry-etched laser facet.

Dry etching experiments using reactive gas mixtures of Cl_2 and BCl_3 have been also performed but no beneficial effects have been detected.

References

[1] D.M. Manos and D.L. Flamm, *Plasma etching*, Academic Press, 1989

[2] P. Buchmann, H.P. Dietrich, G. Sasso and P. Vettiger, "Chemically assisted ion beam etching process for high quality laser mirrors", *Microelectron. Eng.*, vol. 9, pp. 485–489, 1989.

Fabrication and Characterization of Broad-Area Lasers with Dry Etched Mirrors

Franz Eberhard and Eckard Deichsel

Using chemically assisted ion beam etching we have fabricated AlGaAs/InGaAs broad area lasers with dry etched mirrors. Optical output powers up to 400 mW per facet at room temperature under continuous wave operation have been measured. The results are comparable to lasers with cleaved facets made of the same wafer material. Monolithically-integrated monitor diodes show a linear responsivity to the optical output power of the laser. This advanced technology is a basic concept for future applications.

1. Introduction

Lasers with dry-etched facets have many advantages compared to conventionally fabricated lasers. Optoelectronic integration becomes possible. A simple example is the integration of a monitor photo diode for controlling the optical output power of the laser during operation. Another advantage is the ability of full wafer processing and testing that allows fabrication and characterization of lasers without separating the chips, leading to VLSI-type automation [1]. Therefore, the manipulation of the cleaved laser bars and chips, for example for the mirror coating, can be reduced to a minimum. Finally, the orientation and shape of the mirrors is no longer dependent on the crystal orientation. This enables new laser designs including unstable resonators and curved mirrors.

On the other hand, there are strict requirements for the dry-etched facets. Vertical, flat, smooth and damage-free laser mirrors are necessary for good device performance. Tilted facets or corrugation of mirror surfaces lead to increased threshold currents, reduced efficiencies and far-field distortions. Only an optimized etching process can fulfil these requirements.

2. Fabrication

The layer sequence of the laser is a MBE-grown graded-index separate-confinement heterostructure (GRINSCH). The active region consists of two 8-nm-thick strained $In_{0.2}Ga_{0.8}As$ quantum wells. The p- and n-dopants are Be and Si, respectively. In Fig. 1 the fabrication steps are schematically shown.

The lateral structure of the gain-guided broad-area laser is defined by wet-chemical etching of the highly p-doped surface layer. These structures are covered with a Si_3N_4-passivation

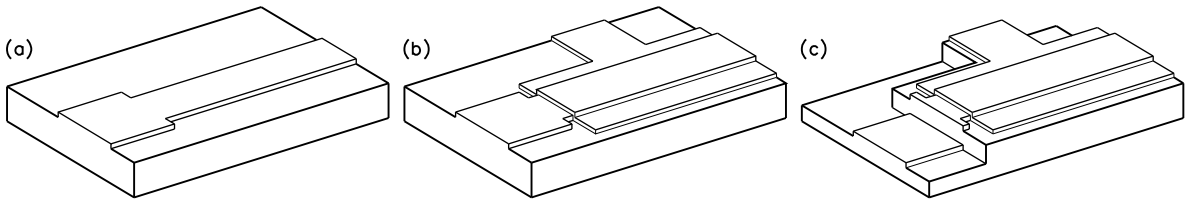

Fig. 1. Fabrication process of lasers with dry etched mirrors: (a) wet chemical etching of the ridge and deposition of the Si_3N_4 passivation, (b) evaporation of the p-contact metallization and (c) dry etching of the mirror using CAIBE.

layer deposited by ion beam-sputter deposition and a subsequent lift off. The p contact is formed by Ti/Pt/Au metallization. These first steps are similar to the fabrication of cleaved lasers. Deep mirror grooves of approximately $7\,\mu$m are formed by chemically-assisted ion-beam etching (CAIBE) [2]. A tri-level resist is used as etch mask. Vertical, flat and smooth facets are achieved at a substrate temperature of 60 °C, an ion energy of 400 eV, and chlorine and argon flows of 4 sccm.

For easier cleaving and improved heat removal, the wafer is thinned to a thickness of approximately $150\,\mu$m. The n contact is formed by evaporating and alloying a Ge/Au/Ni/Au metallization. The last step is the cleaving of the sample into single chips.

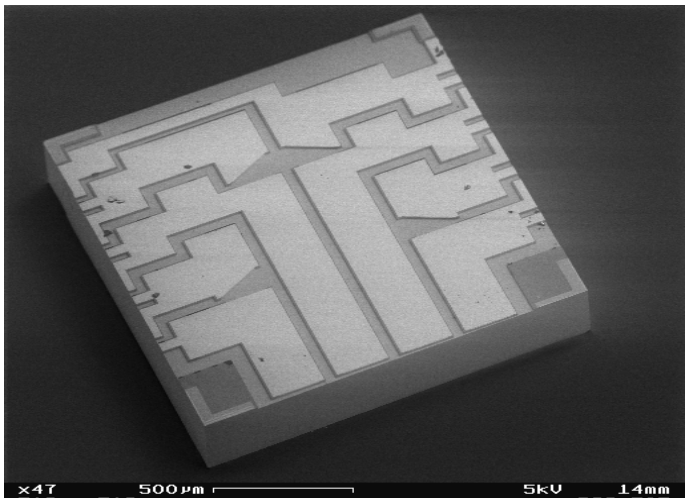

Fig. 2. SEM micrograph of a laser chip with dry etched facets.

Fig. 2 shows a single chip with 4 broad-area lasers and the integrated photo diodes. The light-emitting facets are orientated to the front of the chip. The two central lasers have an area of $1000\,\mu\text{m} \times 100\,\mu$m, the length of the two outer lasers is $500\,\mu$m. To avoid reflection back into the lasers, the facets of the photo diodes are slanted. On the right and left sides of the chip, bond pads with an area of $200\,\mu\text{m} \times 200\,\mu$m are located.

To remove the heat due to dissipated power, the laser chips are glued junction-side up by a two-component epoxy on a copper heat sink. By observing the wavelength shifts with increasing heat sink temperature and dissipated power, we have measured a thermal resistance of about 60 K/W for the small devices. The thermal resistance can be further reduced by galvanic deposition of a thick gold layer used as heat spreader.

3. Characterization

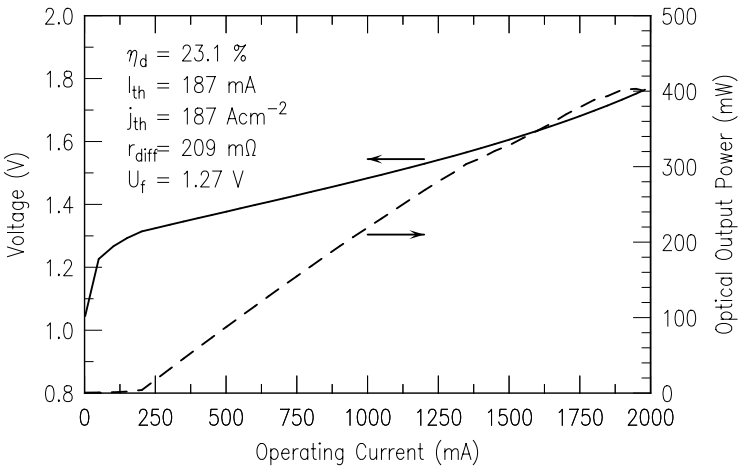

Fig. 3. *IV* characteristic and optical output power of a 1000 μm $\times$ 100 μm broad-area laser with dry-etched facets under cw operation.

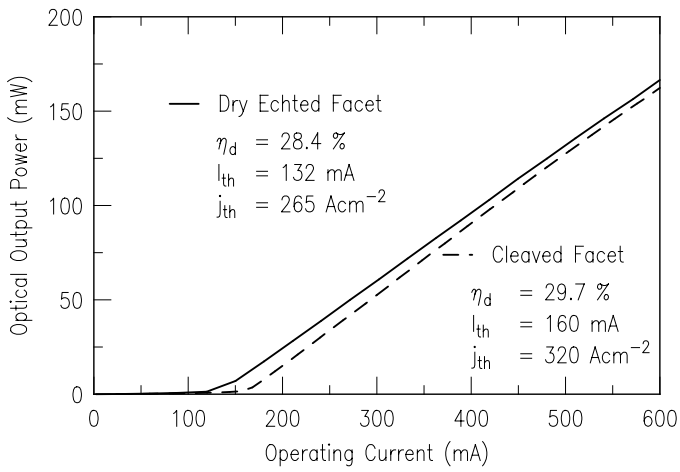

Fig. 4. Optical output power of a 500 μm $\times$ 100 μm broad-area laser with cleaved and dry-etched facets.

Fig. 3 shows the cw characteristics of a $1000\,\mu\text{m} \times 100\,\mu\text{m}$ uncoated device at room temperature. An optical output power of 400 mW per facet at a current of 2 A measured with an integrating-sphere is achieved. The threshold current density and the differential quantum efficiency are $j_{\text{th}} = 187\,\text{Acm}^{-2}$ and $\eta_{\text{d}} = 23.1\,\%$, respectively. The output power is limited by thermal roll over.

Fig. 4 shows the comparison of optical output powers of lasers with cleaved and dry etched facets. Both lasers are made of the same wafer and have a size of $500\,\mu\text{m} \times 100\,\mu\text{m}$. Their characteristics are approximately the same. These results suggest, that this dry etching process is suitable for laser fabrication.

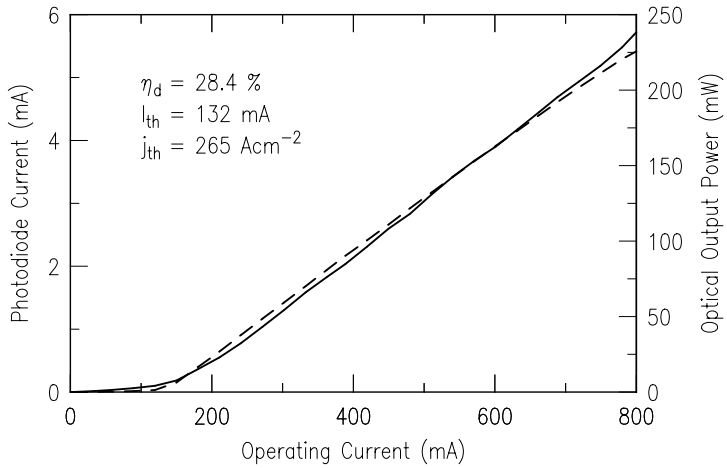

Fig. 5. Comparison of optical output power (solid line) and current of the integrated monitor diode (dashed line).

The integrated monitor diode can be used to control the optical output power of the laser during operation. Fig. 5 shows the dependence of the measured monitor diode current on the operating current of the laser. For this measurement, the photo diode has been reverse biased. The monitor diode current I_{ph} increases linearly with optical output power P_{opt} according to $I_{\text{ph}} = 0.024\,\frac{\text{A}}{\text{W}} \cdot P_{\text{opt}}$.

References

[1] P. Vettiger et al., "Full-wafer technology - a new approach to large-scale laser fabrication and integration", *IEEE Quantum Electron.*, vol. 27, pp. 1319–1331, 1991.

[2] F. Eberhard and E. Deichsel, "Fabrication of vertical facets in GaAs using chemically assisted ion beam etching", *Annual report 1997, Dept. of Optoelectronics, University of Ulm*, pp. 12–15, 1997.

High-Quality Single-Layer Antireflection Coating

Günter Jost and Ulrich Martin

Antireflection (AR) coatings are a key technology for many different semiconductor devices. We report on a high-quality SiON single-layer AR coating generated in an ion-beam sputter depostion system. The critical parameters of the sputter process and the optimization of the technology with respect to reproducibility and accuracy are discussed.

1. Introduction

AR coatings for semiconductor lasers are required for a wide range of applications. Semiconductor lasers with AR coatings on one output facet can be used for spectroscopy when combined with a grating as external reflector, since they are continuously tunable over a wavelength range of more than 25 nm. For laser amplifiers, AR coatings of extremly high quality on both facets are important to achieve high output power and near-diffraction-limited emission. These coatings have to provide a number of properties e.g. chemical and mechanical stability, good adhesion, low mechanical stress, high transparency at the useable wavelength and excellent behavior with respect to lifetime and catastrophic optical mirror damage (COMD). The coating can be composed of a number of thin optical films with different refractive indices or by using only one optical layer which is adapted to the material of the device surface. The most widely reported are Al_2O_3, SiO_2, and Si_3N_4. For our high precision AR-coating we use an ion-beam sputter deposition system with a silicon target. The slow deposition rate and the possibility of tailoring the film indices by adjusting the oxygen flux, allows the deposition of films with refractive indices between 1.6 and 2. Reflectivities around 10^{-4} need specified parameters of the ion-beam sputter deposition system with extremly high accuracy. So, we developed a measurement technique to characterize such an AR coating. The reflectivity R of a single structure with the thickness d and the refractive index n at vacuum wavelength λ on a substrate with the refractive index n_s is described by the well known formular

$$R = \frac{(1-n_s)^2\cos^2(\delta) + (\frac{n_s}{n} - n)^2\sin^2(\delta)}{(1+n_s)^2\cos^2(\delta) + (\frac{n_s}{n} + n)^2\sin^2(\delta)} \tag{1}$$

$$\delta = 2\pi\frac{nd}{\lambda} \tag{2}$$

.

With a film thickness around $d = \frac{\lambda}{4n}$ and an adapted refractive index of $n = \sqrt{n_s}$ the theoretical reflectivity can be reduced to zero [1]. For practical semiconductor amplifiers

the reflectivity should be in the range of 10^{-4}. This allows tolerances around 1 % in thickness and refractive index of the coated layer with respect to the theoretical values of a Gaussian beam with small spot size [2].

2. Ion Beam Sputter Deposition

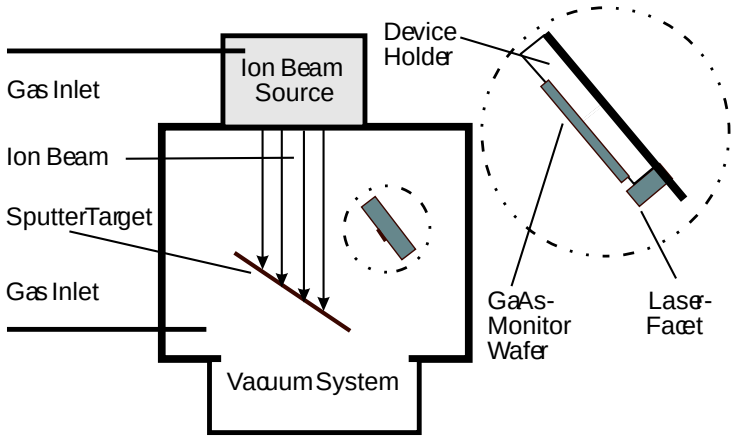

Fig. 1. Sputter deposition system for high-quality AR coatings.

To produce an antireflection coating, we use an ion-beam sputter deposition system. Fig. 1 illustrates the assembly of our system. The system contains an ion source, a sputter target, a device holder with a shutter system, a oxygen inlet, and a vacuum pumping system. The ion beam which is created by a Kaufmann Ion Source, strikes the surface of the target. This creates an ejection of atoms and molecules from the surface of the target material which is known as sputtering. These sputtered particles can deposit on the device. Above the gas inlet, the partial background pressure can be regulated. This has an effect on the composition of the deposit film. So the refractive index of the coated film is changed. The main problem to create films with an exact thickness is the deposition rate. It depends on many parameters like ion energy, temperature of the target and the device, sputter yield, and, never the less, on the background pressure during the process. The composition of the coating can be varied in a wide range, for this reason an exact thickness measurement by a quartz system is impossible. High temperatures also prevent any kind of in situ measurement during the sputter process. But never the less it is possible to adjust an exact film thickness with the sputter time because of the low deposition rate. For calibration, it is necessary to deposit a coating with the same refractive index and thickness onto a polished GaAs surface before performing the deposition onto the real laser facet. After measurement the optical length of this coating, which is explained later, the process time can be determinated. By this way, tolerances below 1 % can be obtained.

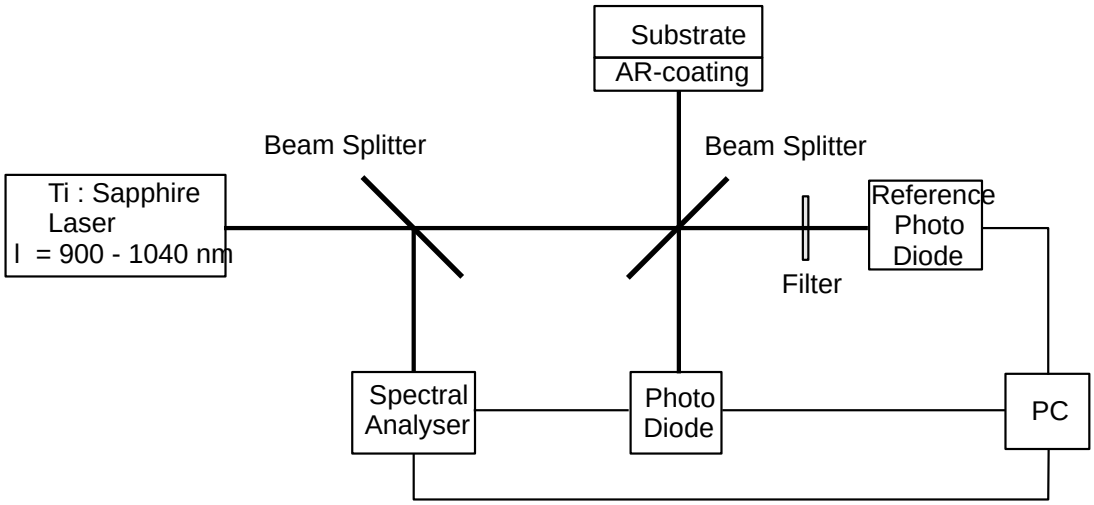

Fig. 2. AR coating characterisation setup with tunable titanium-sapphire laser.

3. Characterization of AR-coating on GaAs-substrate

To aquire the correct parameters for the ion-beam sputter deposition system it is important to measure the refractive index and the minimum wavelength with high accuracy as explained in Section 1. Therefore, we established a setup, which is depicted in Fig. 2. As optical source we use a tunable titanium-sapphire laser with an optical wavelength range from 900 nm to 1060 nm. Two identical photodiodes with the same wavelength sensitivity record the reference power and the reflected intensity of the AR coating for different wavelengths. Due to the high output power and the small spectral linewidth of the titan-sapphire laser it is possible to analize low reflectivities.

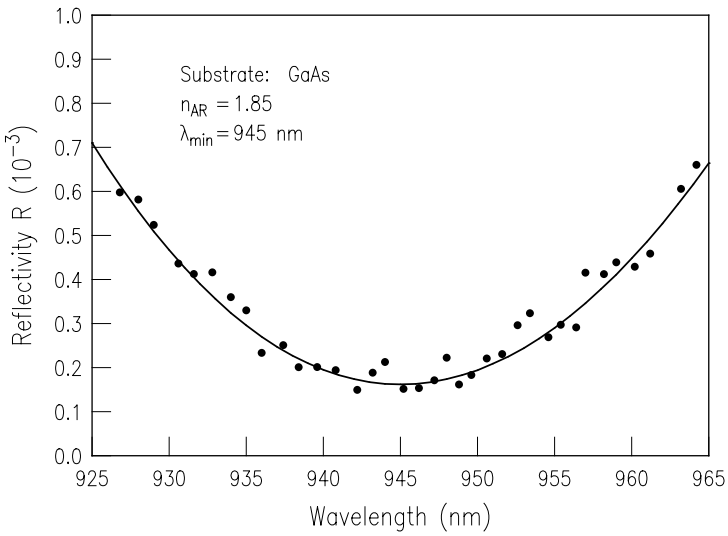

Fig. 3. SiON AR coating on GaAs with a refractive index of 1.85 and an minimum wavelength of 945 nm.

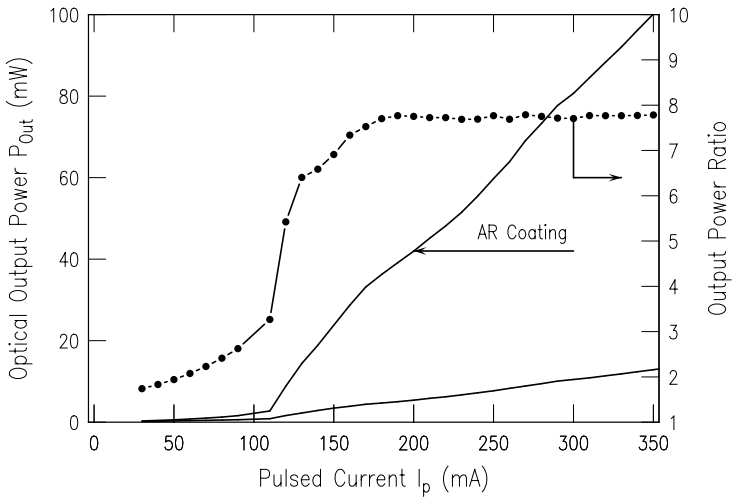

Fig. 4. Optical output characteristic and output-power ratio of the AR coating for a 20-μm broad-area laser.

The intensity reflection versus wavelength for a typical AR coating on GaAs substrate is shown in Fig. 3. The minimum wavelength is around 945 nm und the minimum reflectivity is approximately $2 \cdot 10^{-4}$. The measured values agree very well with the theoretical values for a refrative index of 1.85 and a minimum wavelength of 945 nm at normal incidence. This kind of measurement is much more accurate than ellipsometric measurements at a fixed wavelength. With this method, it is possible to calibrate the ion-beam deposition system. So we are able to fabricate reproducible AR coatings between 900 nm and 1060 nm. Fig. 4 shows the *P-I* curve under pulsed conditions for a 20-μm broad-area laser with a cavity length of 500μm and an AR coating on one output facet. The pulsed operation of the device prevents thermal disturbances and changes of the output power for unmounted lasers. The optical output power from the cleaved facet is much lower than the output from the AR-coated facet. For the cleaved facet, we assumed an reflectivity of 29.2 %. A major difference to broad-area laser diodes without AR coating is the gradual transition of amplified spontaneous emission and stimulated emission. As a result the emission wavelength bandwidth decreases with increasing current. Due to the wavelength dependence of the AR coating we have an continuous change of the output-power ratio to a constant value of 7.2 at the point of totally-stimulated emission. By this way it is possible to analize the quality of the AR coating and we obtain a new definition of the laser threshold especially for devices with high quality AR coatings.

References

[1] H.A. Macleod, *Thin-film optical filters, 2nd Edition.* Bristol: Adam Hilger Ltd, 1986.

[2] G. Eisenstein, "Theoretical design of single-layer antireflection coatings on laser facets", *AT&T Bell Labs. Tech. J.*, vol. 63, pp. 357–364, 1984.

Gas Source Molecular Beam Epitaxy of InAlGaP/InGaP MQW-Lasers

Matthias Golling and Hin Yiu Anthony Chung

Visible light emitting laser diodes are of great interest these days. We grew InGaP, InAlP and InAlGaP on GaAs using Gas Source MBE. X-ray diffraction and, for AlGaP, photoluminescence measurements indicate good crystal quality. MQW samples and stripe lasers were fabricated and showed threshold current densities down to 1.25 kA/cm^2 *under pulsed conditions.*

1. Introduction

Laser diodes emitting in the visible wavelength range of 600 to 700 nm are very promising devices for commercial use. Important applications for these lasers are the pumping of solid state lasers and the replacement of He-Ne-Lasers emitting at 635 nm. Red laser diodes are of practical interest in the field of medicine, for industrial instrumentation and optical data storage.
Another attractive application is its usage as light source in optical communication networks. Optical communication for distances up to several hundred meters is expected to be used widely in the near future for Local Area Networks and in vehicles. Nowadays, long-distance optical data transmission in the 1.3 and 1.55 μm range is very reliable and popular. Unfortunately, these systems do not match the requirements for short distance data transmission, mainly because of their high price. For short distances, inexpensive polymer plastic fibers can be used. These fibers have a local absorption minimum near 650 nm. As a material for light sources in this wavelength range, InGaP/InAlGaP lattice matched to GaAs is a very suitable material system.

2. Epitaxial Growth

Epitaxial growth of phosphides on GaAs substrate is carried out in a Gas Source Molecular Beam Epitaxy (GSMBE). The Group-III-Elements Indium, Aluminum and Gallium and the dopants Silicon and Beryllium are provided elementally in effusion cells. The hydrides arsine (AsH_3) and phosphine (PH_3), cracked at $T = 900^oC$ in one common High Temperature Injector, serve as Group-V-precursors. As substrate, (100)-GaAs of epi-ready quality is used for all samples. The growth temperature of the indium-containing layers is $T = 500^oC$, measured by a pyrometer. The growth rates vary from 600 to 1250 nm/h, depending on the composition required.

3. Material Characterization

X-ray diffraction is used to investigate the lattice matching of the epi-layers which we use in our laser structures. According to the rocking curve results, we have succeeded in growing InGaP, InAlP and InAlGaP with a lattice mismatch to GaAs of less than $5E-4$, which is small enough for the layer compositions we need. In Fig. 1, a room temperature photoluminescence (PL) spectrum of such InGaP/InAlGaP MQWs is shown. At 676 nm wavelength, a sharp and intense PL-peak with a FWHM of 34 meV is observed indicating that the optical quality of our MQWs is excellent.

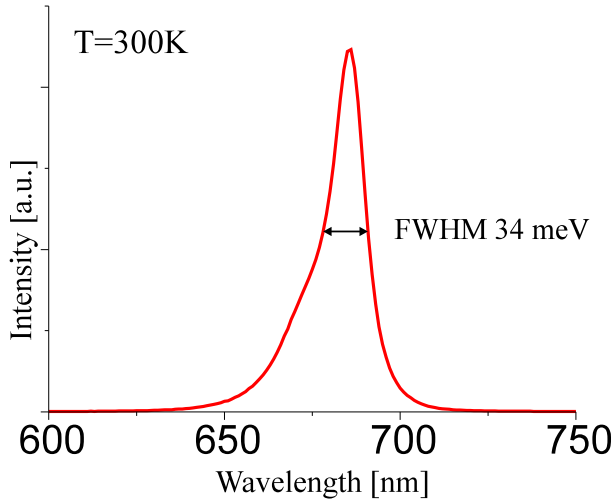

Fig. 1. Photoluminescence spectrogram of MQW structure.

4. Laser diodes with MQW Active Layer

The laser structures which we have studied is shown in Fig. 2. It consists of two 1 μm thick InAlP cladding layers which are doped by Si and Be, respectively. The optical confinement layers are 140 nm InAlGaP. The active zone, sandwiched between the two InAlGaP confinement layers, is made of 3 periods of InGaP/InAlGaP quantum wells. Laser stripes with a width up to 200 μm were processed and cleaved. The output power versus current characteristics of a device with a length of 600 μm, taken under pulsed condition, is shown in Fig. 3. The threshold current density was determined to be 1.25 $kA\ cm^{-2}$. The differential quantum efficiency η_d, obtained with these device dimensions, was 42 %. Laser stripes with a length of 300 μm and a width of 100 μm showed an even higher η_d of 55.5 %.

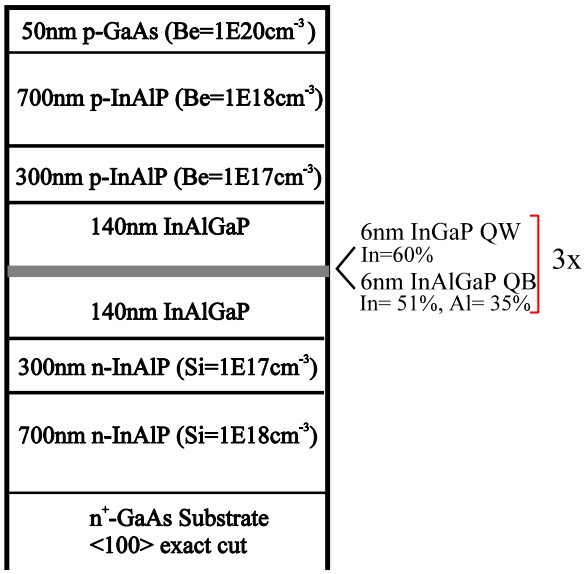

Fig. 2. Epitaxial structure of MQW laser.

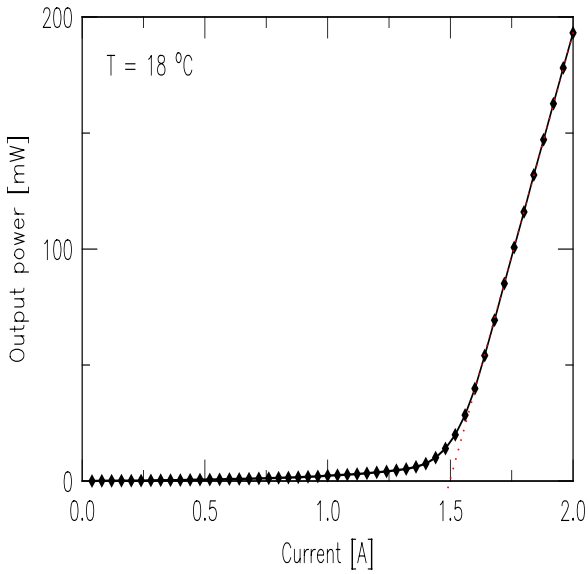

Fig. 3. I-P curve of MQW Laser.

5. Summary

We have successfully grown ternary and quaternary phosphides on exact cut GaAs substrate using GSMBE. Photoluminescence and X-ray measurements indicate the good quality of both bulk material and MQW samples.
MQW stripe lasers have been fabricated. We observed threshold current densities of 1.2 $kA\ cm^{-2}$ under pulsed conditions and differential quantum efficiencies up to η_d = 55.5 %.

Efficient Single-Mode Oxide Confined GaAs VCSELs Emitting in the 850 nm Wavelength Regime

Roland Jäger

Single- and Multi-mode Vertical-Cavity Surface-Emitting Lasers (VCSELs) with 3 unstrained GaAs quantum wells and emission wavelengths around 850 nm have been fabricated using molecular beam epitaxy for crystal growth. Wet chemical etching and subsequent selective oxidation are applied for current confinement. The influence of oxide layer position on lateral index guiding is studied in detail in order to increase maximum single-mode output power. A device of 3 μm active diameter and reduced index guiding shows maximum single-mode output power of 2.25 mW with a side mode suppression ratio of more than 30 dB for high efficiency oxidized VCSELs.

1. Introduction

Vertical-cavity surface-emitting lasers (VCSELs) [1] are most attractive light sources for optical interconnects, especially for parallel data links [2], [3]. Using selective oxidation for fabrication [4], wallplug efficiencies and output powers of multi-mode VCSELs have been increased up to 57 % [P-10] and 180 mW [5], respectively. Due to the large refractive index step induced by the oxide aperture transverse single-mode emission can be maintained only in very small active diameter devices. Selective oxidation offers the possibility to reliably fabricate active diameters of even less than 3 μm. Maximum single-mode power of such VCSELs emitting at 980 nm wavelength has already been increased up to 2.7 mW [6] applying a 30 nm thin oxide layer, which is to be compared with 4.4 mW single-mode output power obtained in proton implanted devices [1] at 950 nm wavelength.
In this paper we study single-mode and nearly single-mode oxide confined high efficiency VCSELs emitting at shorter wavelengths. Clear evidence is given for the increase of single-mode power at 850 nm wavelength by placing the oxide layer in the vicinity of a node in the standing wave pattern. Mode control is obtained by varying the aperture diameter and for the first time the longitudinal position of the confinement layer. Increased single-mode output power of up to 2.25 mW is observed for weakened optical guiding.

2. Device Structure and Processing

Devices investigated, schematically shown in Fig. 1, consist of carbon doped p-type $Al_{0.9}Ga_{0.1}As/Al_{0.2}Ga_{0.8}As$ and silicon doped n-type $AlAs/Al_{0.2}Ga_{0.8}As$ Bragg reflectors

with 26 and 33.5 pairs of quarter wavelength thick layers, respectively, that surround the three active 8 nm thick GaAs quantum wells and the cladding layers. For lateral current

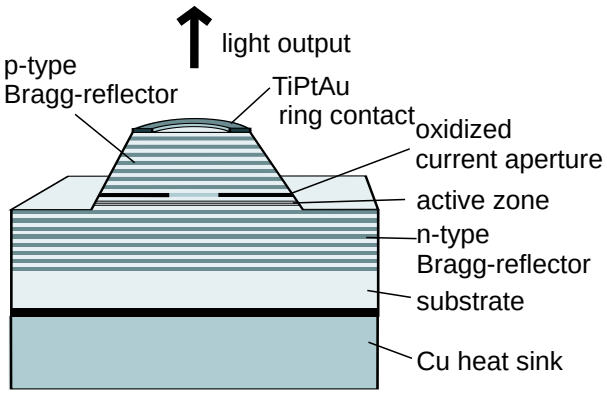

Fig. 1. Oxidized VCSEL mounted junction up on a copper heat sink.

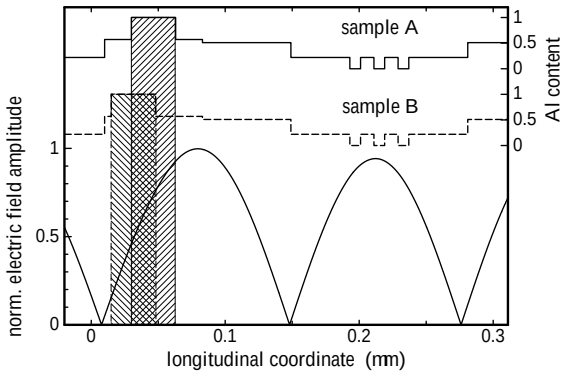

Fig. 2. Different positions of the AlAs layer in the standing wave pattern of samples A and B.

and optical confinement, a single 30 nm thick AlAs layer is placed in the first quarter wavelength layer above the active zone and subsequently oxidized at 400 °C in a nitrogen/water vapor atmosphere after wet chemical etching of mesas with diameters from 38 to 58 μm. Linear dependence of oxide depth with time allows controllable definition of various active diameters. Evaporation of TiPtAu ring contacts on the top side and a GeNiAu contact on the bottom side completes processing. The devices are attached junction up to copper heat sinks using silver paste. Devices are operated without applying active cooling.

The oxide aperture provides both, current and optical confinement. The refractive index of approximately 1.6 [8] of the Al_xO_y formed during lateral oxidation of the AlAs layer introduces a comparatively large refractive index discontinuity to the surrounding semiconductor material. The resulting optical waveguiding is inferred from a longitudinal effective index method [9]. Due to this model the lateral effective index distribution is proportional to the difference of the longitudinal resonance wavelengths in the inner and outer part of the structure. Using a single 30 nm comparatively thin oxide layer reduces optical waveguiding as well as losses due to scattering [10]. Shifting the oxide layer towards a node of the standing wave pattern as indicated in Fig. 2 decreases the overlap of the oxide layer and the electrical field intensity and thus further weakens optical waveguiding. For the high efficiency devices investigated we find constant wavelength spacings between transverse modes independent of driving current indicating that thermally induced waveguiding can be neglected. In addition to using near and far field properties we use the size dependent transverse mode spacing given by [11] to determine effective active diameters of the devices. We have investigated two nominally identical wafers (A and B) with slightly different positions of the AlAs layer, as illustrated in Fig. 2. For sample B the longitudinal position is shifted 15 nm towards the node of the electrical field. Evaluations of the resonance conditions in the inner and outer part of the VCSEL

structure lead to a reduction of the effective refractive index step from $\Delta n = 1.9 \cdot 10^{-2}$ (sample A) to $\Delta n = 9.2 \cdot 10^{-3}$ (sample B).

3. Measurements

Using saturated oxidation conditions and precise temperature control we have been able to reproducibly generate circular oxide apertures of arbitrary size with a precision of 1 μm. Fig. 3 presents output characteristics of 4 μm active diameter VCSELs of type A and B and Fig. 4 shows the corresponding output spectra, measured with a spectrum analyzer with minimum resolution of nominally 0.1 nm. The fundamental LP_{01} mode is linearly

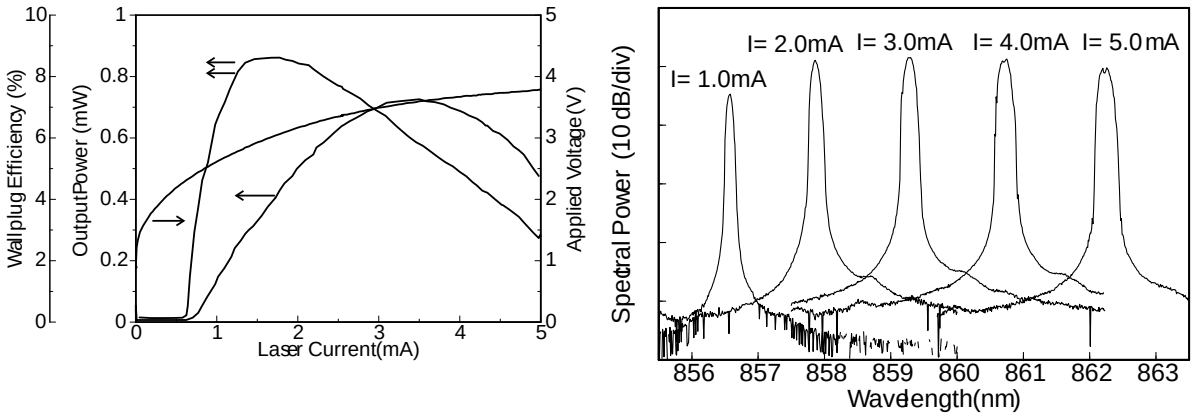

Fig. 3. Output characteristics of 4 μm active diameter VCSELs from samples A and B.

polarized. Higher order transverse modes LP_{11} and LP_{21} split into two orthogonal polarizations. Fundamental mode LP_{01} and the shorter wavelength LP_{11} component have the same polarization. As the modal behavior sensitively depends on the device size, great care has to be taken for a fair comparison between devices from different wafers. Besides near field and far field pattern widths the wavelength spacing between fundamental and first order higher transverse mode indicates the effective size. The corresponding spacings in the spectra of Fig. 4 are 0.48 nm and 0.43 nm for devices A and B, respectively. These values are constant up to driving currents of 1.6 mA (sample A) and 2.2 mA (sample B), indicating that thermally induced guiding can be neglected compared to the dominating index guiding. Difference in current ranges showing constant mode spacings is due to differing intrinsic temperatures caused by small variations in applied voltages and output powers. Temperature rises at 1.6 mA are 5.6 K for sample A and 4.8 K for sample B. Thermal resistances are 2.8 K/mW and 3.0 K/mW for samples A and B, respectively. Mode spacing is getting larger by further increase of dissipated power and reaches 0.52 nm and 0.48 nm at 2.4 mA laser current. The mode spacing is approximately inversely proportional to the active area [11]. It can thus be inferred that VCSEL B with weaker index guiding is of similar active size, but certainly not smaller than device A having stronger optical confinement. Similar size is also confirmed by threshold currents of about 600 μA

at threshold voltages of 1.6 V for both devices. Differing distances from the aperture to the quantum wells and thus different current spreading can be neglected since the longitudinal position of the aperture is only varied by 15 nm. For sample B single-mode emission

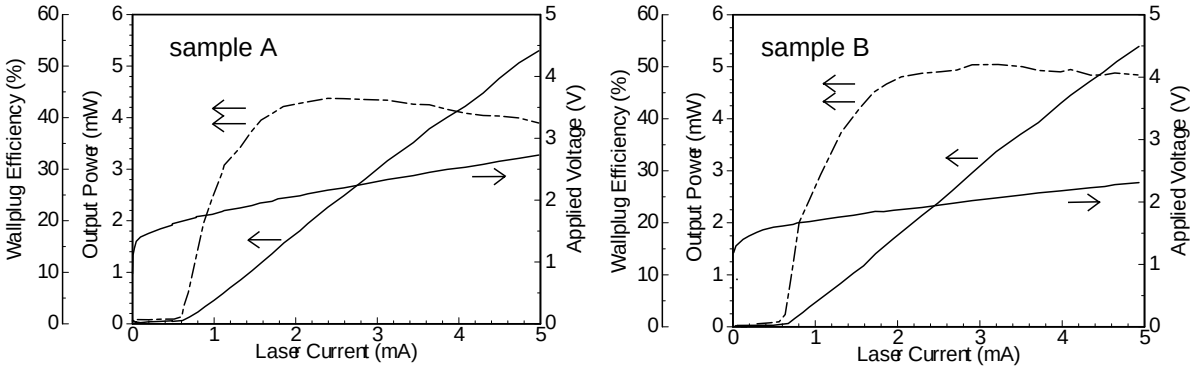

Fig. 4. Spectra of the stronger (Sample A) and weaker (Sample B) guided 4 μm devices.

with a side mode suppression ratio (SMSR) of more than 30 dB up to a driving current of 1.6 mA is observed, whereas devices from sample A with higher effective index step show 25 dB maximum SMSR just above threshold. This result is not necessarily expected as scattering losses of higher order modes are also reduced in weakly confining cavities. It seems, however, that loss reduction is most effective for the fundamental mode. Maximum single-mode output power for sample B is 1.25 mW at a laser current of 1.6 mA and an applied voltage of 1.8 V resulting in a wallplug efficiency at maximum single-mode power of 43 %. Maximum wallplug efficiency is 51 % and increases even up to 57 % in slightly larger devices [4].

To achieve single-mode operation over the whole operating range with maximum output power smaller devices of 3 μm active diameter have been fabricated from wafer B with reduced index guiding.

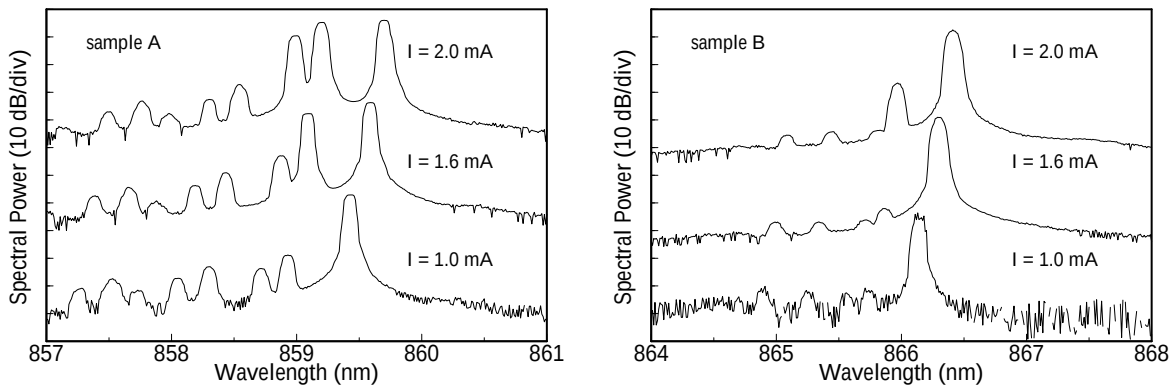

Fig. 5. Optimized output characteristics and spectra of a weakly guiding 3 μm VCSEL operating single-mode with 30 dB SMSR up to 11 times threshold (I_{th} = 310 μA).

The output characteristics and corresponding spectra depicted in Fig. 5 show single-mode operation with a SMSR of about 35 dB. Maximum single-mode output power is 2.25 mW near thermal rollover at a laser current of 3.4 mA. Threshold current is 300 μA and threshold voltage is 1.80 V. To achieve 1 mW output power 1.6 mA laser current has to be applied, resulting in 25 % power conversion efficiency. Differential resistance of 450 Ω and thermal resistance of 3.5 K/mW are typical values for a 3 μm active diameter device.

4. Conclusion

In conclusion, we have improved the single-mode behavior of selectively oxidized VCSELs emitting at 850 nm wavelength by reducing optical confinement. Maximum single-mode output power is 2.25 mW for 3 μm active diameter and maximum single-mode wallplug efficiency is 43 % at 1.25 mW for slightly larger devices.

References

[1] K. Iga, F. Koyama, and S. Kinoshita, "Surface emitting semiconductor lasers", *IEEE J. Quantum Electron.*, vol. 24, pp. 1845-1855, 1988.

[2] C.J. Chang-Hasnain, J.P. Harbison, C.-E. Zah, M.W. Maeda, L.T. Florez, N.G. Stoffel, and T.-P. Lee, "Multiple wavelength tunable surface-emitting laser arrays", *IEEE J. Quantum Electron.*, vol. 27, pp. 1368-1376, 1991.

[3] E. Zeeb, B. Möller, G. Reiner, M. Ries, T. Hackbarth, and K.J. Ebeling, "Planar proton implanted VCSELs and fiber coupled 2-D VCSEL arrays", *IEEE J. Sel. Top. Quantum Electron.*, vol. 1, pp. 616-623, 1995.

[4] D.L. Huffaker, D.G. Deppe, and K. Kumar, "Native-oxide defined ring contact for low threshold vertical-cavity lasers", *Appl. Phys. Lett.*, vol. 65, pp. 97-98, 1994.

[5] M. Grabherr, B. Weigl, G. Reiner, R. Michalzik, M. Miller, and K.J. Ebeling, "High power top-surface emitting oxide confined vertical-cavity laserdiodes", *Electron. Lett.*, vol. 32, pp. 1723-1724, 1996.

[6] B. Weigl, M. Grabherr, R. Michalzik, G. Reiner, and K.J. Ebeling "High power single-mode selectively oxidized vertical-cavity surface-emitting lasers", *IEEE Photon. Technol. Lett.*, vol. 8, pp. 971-973, 1996.

[7] K.L. Lear, R.P. Schneider, K.D. Choquette, S.P. Kilcoyne, J.J. Figiel, and J.C. Zolper, "Vertical cavity surface emitting lasers with 21 % efficiency by metalorganic vapor phase epitaxy" *IEEE Photon. Technol. Lett.*, vol. 6, pp. 1053-1055, 1994.

[8] M.H. MacDougal, H. Zhao, P.D. Dapkus, M. Ziari, and W.H. Steier, "Wide-bandwidth distributed Bragg reflectors using oxide/GaAs multilayers", *Electron. Lett.*, vol. 30, pp. 1147-1148, 1994.

[9] G.R. Hadley, "Effective index model for vertical-cavity surface-emitting lasers", *Opt. Lett.*, vol. 20, pp. 1483-1485, 1995.

[10] B.J. Thibeault, E.R. Hegblom, P.D. Floyd, R. Naone, Y. Akulova, and L.A. Coldren, "Reduced optical scattering loss in vertical-cavity lasers using a thin (300 Å) oxide aperture", *IEEE Photon. Technol. Lett.*, vol. 8, pp. 593-595, 1996.

[11] R. Michalzik and K.J. Ebeling "Generalized BV diagrams for higher order transverse modes in planar vertical-cavity laser diodes", *IEEE J. Quantum Electron.*, vol. 31, pp. 1371-1379, 1995.

Highly Efficient Single-Mode Oxide Confined GaAs VCSELs

Christian Jung

We have optimized MBE grown GaAs VCSELs emitting at 840 nm wavelength for maximum single-mode output power. Devices of 3.5 µm diameter show record high single-mode cw output power of 4.8 mW and above 80 % butt-coupling efficiency into single-mode fiber. Stable single-mode operation with 3 mW optical output power over a temperature from −10 to +70° C has been demonstrated.

1. Introduction

Increasing single-mode output powers is one of the major issues in vertical-cavity surface-emitting laser (VCSEL) research. Fundamental mode oscillation is desirable for all applications requiring free-space propagation like optical reading and writing or two-dimensional interconnects. Also high performance optical links utilizing single-mode optical fibers and taking advantage of the unique coupling efficiencies of VCSELs would largely benefit from the availability of improved devices. The maximum single-mode output power of 4.4 mW was still obtained with a proton-implanted VCSEL showing strong saturation effects in the light-current characteristics [1]. Single-mode operation is more difficult to obtain with the new class of selectively oxidized VCSELs due to the inherent index guiding properties of the oxide aperture [2]. We have recently demonstrated the beneficial effects of reduced index guiding on fundamental mode stability by comparing different positions of the oxide layer in the standing wave pattern [P-6] and have achieved single-mode powers up to 2.25 mW [P-35]. Using the same technique this value has been increased to 3.5 mW [3]. In this paper, by further optimizing our devices, we present fundamental mode powers of 4.8 mW, the highest value ever obtained with a VCSEL, and demonstrate efficient coupling to single-mode fibers.

2. Device structure

The investigated top emitting VCSEL structure was grown by solid source MBE. The one-wavelength thick inner cavity contains three active GaAs-$Al_{0.2}Ga_{0.8}As$ quantum wells (QWs) designed for about 850 nm gain peak wavelength. The p- and n-doped Bragg reflectors are optimized for low voltage drop and optical loss. Details of the layer structure can be found in [P-10]. Lateral current confinement is achieved by selective wet oxidation

of a single 30 nm thick AlAs layer placed in the first quarter wavelength layer above the cavity region. This layer is shifted towards a node of the standing wave pattern to reduce the built-in effective index guiding and the optical losses [P-6]. The p-type TiPtAu ring contact on the top side is evaporated after oxidation to achieve good ohmic contacts as well as light emission through the top Bragg reflector. TiAu conducting tracks and bondpads are deposited on a polyimide insulation layer. Polyimide provides a smooth planar surface, good passivation and improves the high frequency behavior due to the small permittivity. Mechanically polishing the GaAs substrate down to 150 μm and evaporating a GeNiAu broad area contact are final process steps.

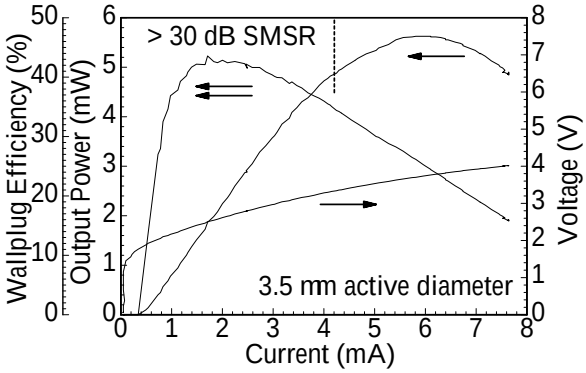

Fig. 1. Output power, applied voltage, and conversion efficiency versus laser current for an optimized single-mode VCSEL with 3.5 μm active diameter.

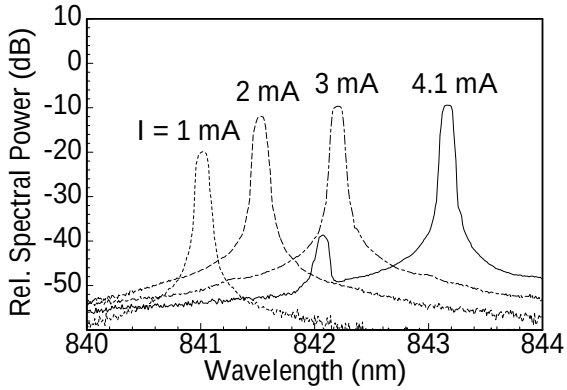

Fig. 2. Spectra of the VCSEL from Fig. 1 for different driving currents.

3. Device characteristics

The attainable single-mode power strongly depends on the diameter of the oxide aperture. In Fig. 1, the output characteristics of the most favorable, about 3.5 μm active diameter VCSEL is displayed. Threshold current and voltage are 0.5 mA and 1.8 V, respectively. Maximum single-mode output power is 4.8 mW with a side mode suppression ratio (SMSR) of about 30 dB, as can be seen from the spectra in Fig. 2. This value is obtained for a driving current of 4.1 mA with a wallplug efficiency of 35 %. The maximum conversion efficiency of 42 % is observed at 2.0 mA at an output power of 2.2 mW. The differential quantum efficiency amounts to about 95 % over a large current range above threshold. Smaller or larger diameter devices deliver reduced total or fundamental mode powers, respectively. The light output was measured using a Newport 1830C optical power meter with a calibrated silicon diode, which was directly illuminated. This equipment was cross-checked using a further detector system. The spectra were measured using a microscope objective to couple the laser emission into a 50 μm core fiber and to feed the light to an Anritsu optical spectrum analyzer.

4. Thermal behavior

Lasers with high wallplug efficiencies show low thermal heating and are therefore well suited for operation over a wide temperature range. Fig. 3 shows the optical output characteristics for cw operation, indicating good homogeneity in a temperature range from -10 to $+\,70\,^{\circ}\mathrm{C}$.

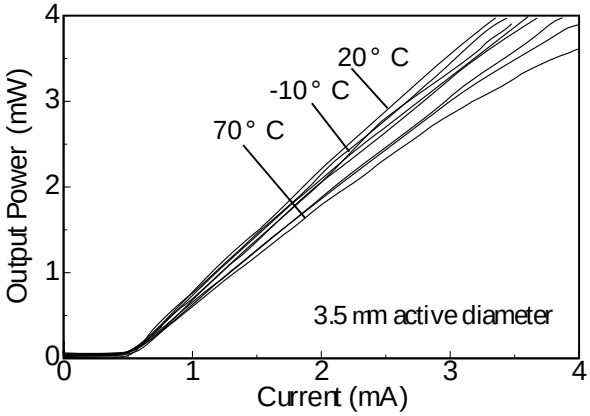

Fig. 3. Light output power versus current for a $3.5\,\mu$m single-mode GaAs VCSEL for various temperatures from -10 up to $+70\,^{\circ}\mathrm{C}$.

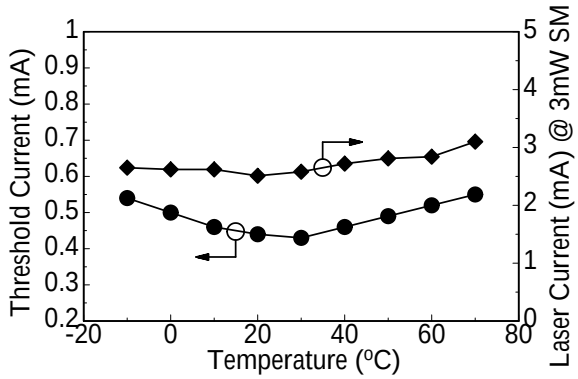

Fig. 4. Threshold current and laser current required for 3 mW single-mode output power in an industrially relevant temperature range from -10 up to $+70\,^{\circ}\mathrm{C}$.

Fig. 4 summarizes threshold current and laser current required for 3 mW single-mode output power over the whole temperature range. Within this range threshold currents vary between 440 and $550\,\mu$A, while laser currents for 3 mW optical output power range between 2.5 and 3.1 mA. These homogeneous characteristics should allow technical applications without any temperature stabilization. The emission spectra for different temperatures at 3 mW output single-mode operation are depicted in Fig. 5. The spectral shift of the emission wavelength with temperature is evaluated to 0.06 nm/K.

5. Coupling efficiency

Highly efficient coupling from VCSEL to single-mode fiber has been already demonstrated earlier for proton-implanted devices [4]. Here we show in Fig. 6 coupling efficiency of an oxide confined VCSEL into a $5\,\mu$m core diameter single-mode (SM) fiber as a function of the lateral displacement Δx. Measurement was done for butt-coupling to an uncoated fiber without using an index-matching fluid. A lateral alignment tolerance of $3.7\,\mu$m is obtained from the FWHM of the coupling curve. The peak efficiency of slightly above 80 % corresponds to a maximum single-mode power of about 3.9 mW in the fiber, making the device attractive also for larger distance data transmission.

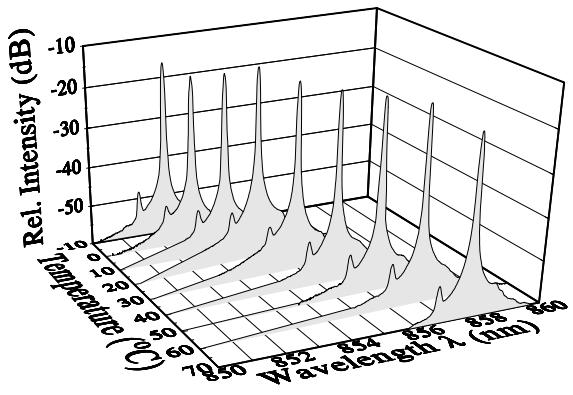

Fig. 5. Emission spectra of the VCSEL from Fig. 3 in a temperature range from −10 to +70 °C at a single-mode output power of 3 mW.

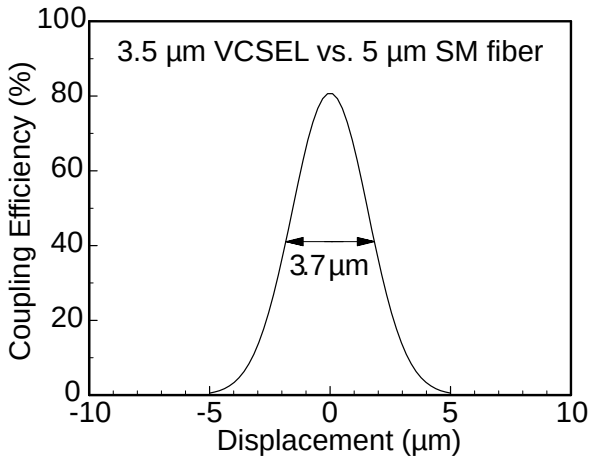

Fig. 6. Measured butt-coupling efficiency of VCSEL emission into a 5 μm core diameter single-mode fiber as a function of lateral VCSEL-fiber displacement.

For increasing lateral displacement Δx between VCSEL and fiber we expect a decay in coupling efficiency according to [5]

$$\eta = \eta_{max} \cdot \exp\left(-\frac{2\Delta x^2}{w_f^2 + w_L^2}\right) , \tag{3}$$

where w_f and w_L are the spot radii of the fiber and the VCSEL mode, respectively. Maximum coupling efficieny η_{max} is determined by Fresnel reflection, tilt, and wavefront curvature. For the 5 μm core diameter fiber of numerical aperture 0.14, the spot radius is $w_f = 2.5\,\mu$m at 840 nm wavelength. From the gaussian decay of the coupling efficiency in Fig. 6 we infer a spot radius of $w_L = 1.9\,\mu$m which seems reasonable for the VCSEL of 3.5 μm oxide aperture diameter used in the experiment.

6. Conclusion

In conclusion, we have improved the single-mode behavior of oxide confined VCSELs emitting at 840 nm wavelength by optimizing the optical confinement. Record high single-mode output power of 4.8 mW is achieved for a 3.5 μm active diameter device when the 30 nm thick oxide aperture is displaced towards the node of the standing wave pattern. Stable cw single-mode operation at 3 mW optical power is found over a temperature range from −10 up to +70 °C The butt-coupling efficiency into a 5 μm diameter single-mode fiber is 80 % resulting in 3.9 mW power in the fiber.

References

[1] K.L. Lear, R.P. Schneider, K.D. Choquette, S.P. Kilcoyne, J.J. Figiel, and J.C. Zolper, "Vertical cavity surface emitting lasers with 21 % efficiency by metalorganic vapor phase epitaxy", *IEEE Photon. Technol. Lett.*, vol. 6, pp. 1053–1055, 1994.

[2] G.R. Hadley, "Effective index model for vertical cavity surface emitting lasers", *Opt. Lett.*, vol. 20, pp. 1483–1485, 1995.

[3] K.D. Choquette, H.Q. Hou, G.R. Hadley, and K.M. Geib, "High power single transverse mode selectively oxidized VCSELs", in Proc. *1997 Summer Top. Meet. on Vertical-Cavity Lasers.* Montreal, Quebec, Canada, Aug. 1997.

[4] K. Tai, G. Hasnain, J.D. Wynn, R.J. Fischer, Y.H. Wang, B. Weir, J. Gamelin, and A.Y. Cho, "90 % coupling of top surface emitting GaAs/AlGaAs quantum well laser output into 8 μm diameter core silica fiber", *Electron. Lett.*, vol. 26, pp. 1628–1629, 1990.

[5] W. van Etten, J. van der Plaats, *Fundamentals of Optical Fiber Communications.*, New York: Prentice Hall, 1991, Chapter 11.

Bias-Free 2.5 Gb/s Data Transmission Using GaAs VCSELs at 835 nm Emission Wavelength

Peter Schnitzer

GaAs based selectively oxidized VCSELs are investigated as light sources for optical interconnection. Bias-free data transmission at 2.5 Gb/s with a BER of less than 10^{-11} *is reported for transmission over 500 m of graded index multimode fiber.*

1. Introduction

The use of selective oxidation for current confinement in vertical cavity surface emitting lasers (VCSELs) has recently led to devices with very high wallplug efficiencies of up to 57 % [1]. Extremely low threshold currents of less than 100 μA have already been demonstrated [2]. Transmission of data rates up to 10 Gb/s with proton implanted InGaAs VCSELs [3] as well as 16.3 GHz modulation of oxidized InGaAs VCSELs [4] and bias-free 1 Gb/s data transmission with oxidized InGaAs [5] and GaAs [6] VCSELs make these devices ideally suited as transmitters in optical interconnects. Here we demonstrate for the first time bias-free 2.5 Gb/s non-return-to-zero (NRZ) pseudo-random bit sequence (PRBS) transmission with $2^{31}-1$ word length using polyimide passivated GaAs VCSELs. The bit error rate (BER) remains below 10^{-11} after transmission over 500 m of graded index 50 μm core diameter fiber.

2. Device Structure and Output Characteristics

Fig. 1 illustrates the general layer structure of the selectively oxidized VCSEL employed in the transmission experiments. The multilayer system is grown by solid source molecular beam epitaxy on n-GaAs substrate. For emission near 850 nm wavelength the one-wavelength thick inner cavity contains three, each 8 nm thick GaAs quantum wells (QWs) separated by 10 nm $Al_{0.2}Ga_{0.8}As$ barriers. Quarter-wavelength $Al_{0.5}Ga_{0.5}As$ cladding layers are introduced on both sides of the active region to improve longitudinal carrier confinement. Top and bottom mirrors consist of $Al_{0.9}Ga_{0.1}As$-$Al_{0.2}Ga_{0.8}As$ and AlAs-$Al_{0.2}Ga_{0.8}As$ quarter-wavelength Bragg stacks, respectively. Single-step grading with 5 nm thick intermediate $Al_{0.5}Ga_{0.5}As$ layers at the heterointerfaces is used to reduce electrical series resistance. Current is supplied through the carbon p-doped top and silicon n-doped bottom reflectors, where modulation and δ-doping is required for high performance devices. Current confinement is achieved by selective lateral oxidation of a 30 nm thick extra AlAs

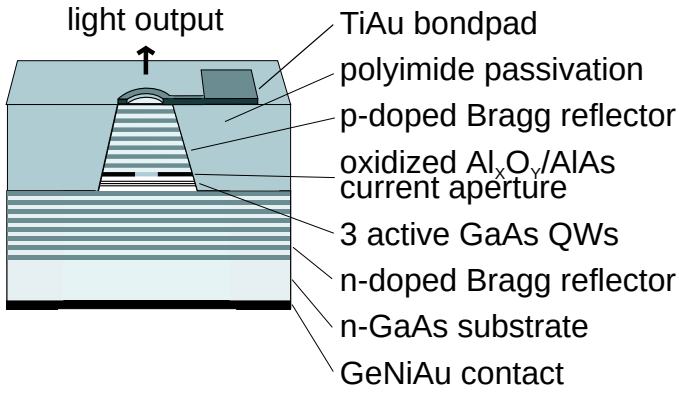

Fig. 1. Cross-sectional view of a selectively oxidized, polyimide passivated GaAs VCSEL.

layer placed directly above the top cladding layer. Prior to oxidation a broad area mesa is produced by wet chemical etching. After 2.2 μm thick polyimide passivation a TiAu bondpad is evaporated.

The output characteristics of the 4 μm active diameter VCSEL used for the transmission experiments are given in Fig. 2. Threshold current and voltage are 0.4 mA and 1.65 V, respectively. The threshold voltage is just 170 mV higher than the photon energy limit of 1.48 V at 835 nm emission wavelength. The output power is 1.25 mW at a driving current of 5 mA. Both, biased and bias-free operation show multimode emission centered at 837 nm as illustrated in Fig. 3.

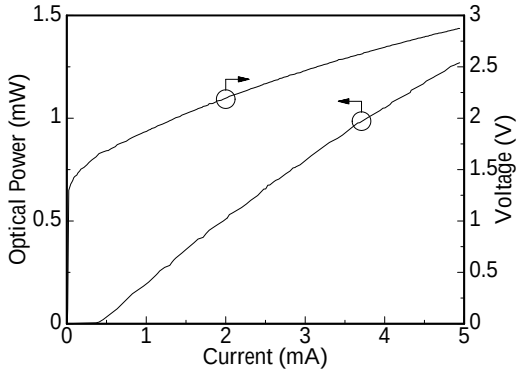

Fig. 2. Output characteristics of 4 μm selectively oxidized GaAs VCSEL.

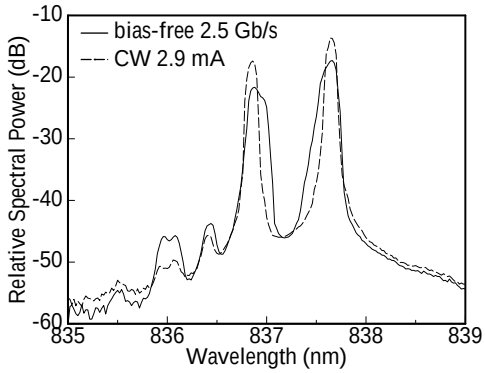

Fig. 3. Emission spectra for CW and bias-free 2.5 Gb/s modulation.

3. Experimental Setup

The setup for the transmission experiments is shown in Fig. 4. The laser is wire bonded to an SMA socket to keep feeding lines as short as possible. For data transmission experiments the laser is either directly driven by a pattern generator with a pseudo-random bit

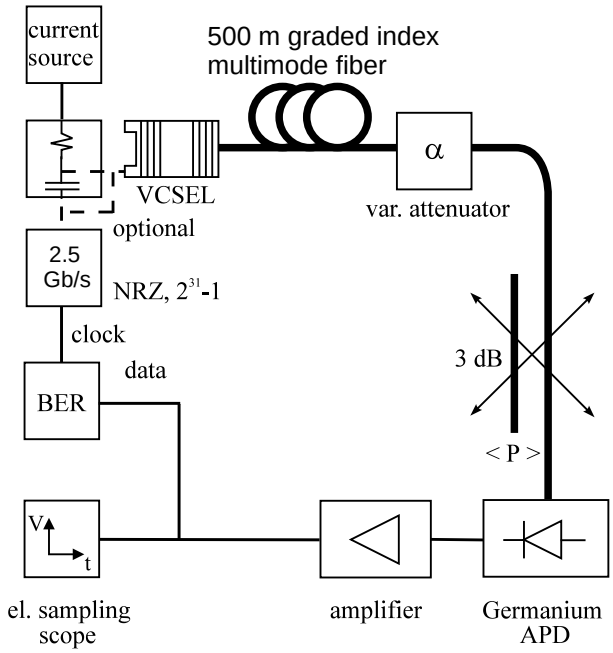

Fig. 4. Experimental setup for the data transmission experiments.

sequence (PRBS) at 2.5 Gb/s NRZ data rate with $V_{pp} = 2$ V without any additional bias, or a bias current of 2.9 mA and 2.5 Gb/s modulation with $V_{pp} = 0.5$ V are combined in a bias-tee and fed to the VCSEL. Output power is launched in a butt-coupled graded index multimode fiber with 50 μm core diameter and 500 m length. The transmitted signal is passed through a variable attenuator and detected with a 2 GHz bandwidth Germanium avalanche photodiode (APD). The preamplified bit sequence is monitored with an electrical sampling oscilloscope and analyzed with a bit error rate (BER) detector.

4. Data Transmission

Low threshold devices are crucial for bias-free data transmission in order to minimize the turn-on delay. Fig. 5 shows the eye diagrams for biased and bias-free 2.5 Gb/s PRBS NRZ modulation for back-to-back testing and transmission over 500 m multimode fiber. All eyes are wide open and symmetric. For non-biased modulation we observe a turn-on delay of $\tau_d \approx 100$ ps and a broadened turn-on rise trace due to intersymbol interference. The results of the transmission experiments are summarized in Fig. 6, where triangles denote biased 2.5 Gb/s PRBS back-to-back testing, rhombs denote bias-free back-to-back testing, squares denote biased transmission over 500 m of multimode fiber, and circles denote bias-free transmission over 500 m of multimode fiber. The bit-error rate of 2.5 Gb/s remains better than 10^{-11} for biased as well as for bias-free operation and for back-to-back testing as well as for transmission over 500 m of graded index fiber. The received optical power necessary for a bit-error rate of $< 10^{-11}$ is as low as -26.4 dBm for biased back-to-back testing and -24.5 dBm for bias-free back-to-back testing while 500 m transmission

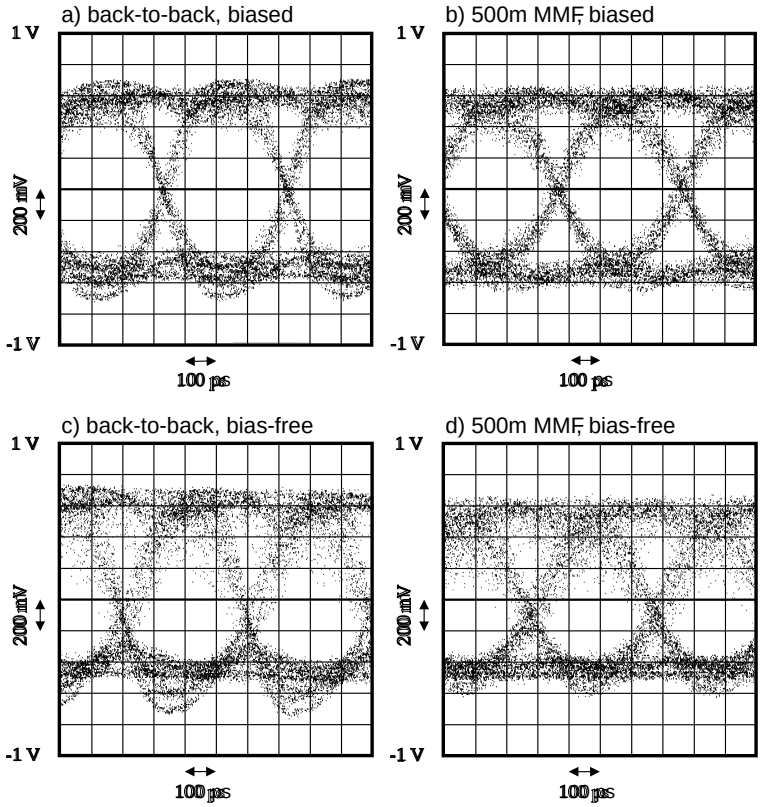

Fig. 5. Eye diagrams recorded at 2.5 Gb/s PRBS data rate and $2^{31}-1$ word length for a) biased back-to-back testing, b) biased transmission over 500 m of multimode fiber, c) bias-free back-to-back testing and d) bias-free transmission over 500 m of multimode fiber.

requires a received optical power of -22.5 dBm and -20.6 dBm for biased and bias-free operation, respectively. The power penalty of 1.9 dB for biased and bias-free operation is independent of the fiber length almost independent of the BER. The power penalty for 2.5 Gb/s transmission over 500 m of multimode fiber compared to back-to-back testing is 3.9 dB for biased and bias-free operation.

5. Conclusion

We have for the first time successfully demonstrated bias-free data transmission with $2^{31}-1$ PRBS signals at 2.5 Gb/s data rate using a high performance selectively oxidized GaAs VCSEL source. A BER of 10^{-11} is obtained for a received power of -22.5 dBm for biased and -20.6 dBm for bias-free transmission over 500 m of graded index multimode fiber. Bias-free operation greatly facilitates optical interconnection systems but the achievable bit rate is limited by the turn-on delay of the VCSEL. The turn-on delay of the VCSEL studied is less than 100 ps for pulses of 2 V applied without any bias. The results obtained seem particularly useful for massively parallel data transmission with VCSEL transmitter arrays.

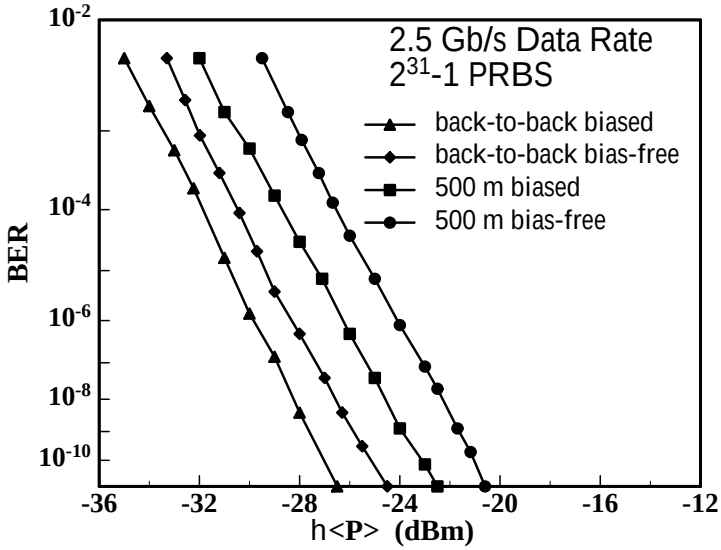

Fig. 6. Bit-error rate measurement at 2.5 Gb/s and $2^{31} - 1$ word length.

References

[1] R. Jäger, M. Grabherr, C. Jung, R. Michalzik, G. Reiner, B. Weigl, and K.J. Ebeling, "57 % wallplug efficiency oxide-confined 850 nm wavelength VCSELs", *Electron. Lett.*, vol. 33, pp. 330–331, 1997.

[2] Y. Hayashi, T. Mukaihara, N. Hatori, N. Ohnoki, A. Matsutani, F. Koyama, and K. Iga, "Lasing characteristics of low-threshold oxide confinement InGaAs-GaAlAs vertical-cavity surface-emitting lasers", *IEEE Photon. Technol. Lett.*, vol. 7, pp. 1324–1326, 1995.

[3] U. Fiedler, G. Reiner, P. Schnitzer, and K.J. Ebeling, "Top-surface emitting laser diodes for 10 Gb/s data transmission", *IEEE Photon. Technol. Lett.,* vol. 8, pp. 746–748, 1996.

[4] K.L. Lear, A. Mar, K.D. Choquette, S.P. Kilcoyne, R.P. Schneider Jr., and K.M. Geib, "High-frequency modulation of oxide-confined vertical cavity surface emitting lasers", *Electron. Lett.,* vol. 32, pp. 457–458, 1996.

[5] P. Schnitzer, U. Fiedler, G. Reiner, B. Weigl, W. Zick, and K.J. Ebeling, "Bias-free 1 Gbit/s data rate transmission using top vertical-cavity surface-emitting laser diodes", *IEEE Photon. Technol. Lett.,* vol. 5, pp. 693–695, 1997.

[6] P. Schnitzer, U. Fiedler, M. Grabherr, C. Jung, G. Reiner, W. Zick, and K.J. Ebeling, "Bias-free 1 Gbit/s data transmission using single-mode GaAs VCSELs at $\lambda = 835$ nm", *Electron. Lett.*, vol. 32, pp. 2145–2146, 1996.

Oxide Confined 2D VCSEL Arrays for High-Density Inter/Intra-Chip Interconnects

Roger King

We have designed and fabricated vertical-cavity surface-emitting laser (VCSEL) arrays with 4 × 8 elements intended to be used as transmitters in short-distance parallel optical interconnects. In order to meet the requirements of two-dimensional (2D), high-speed optical links, each of the 32 laser diodes is supplied with two individual top contacts. The metalization scheme allows flip-chip mounting of the array modules junction-side down on silicon complementary metal oxide semiconductor (CMOS) chips. The driving characteristics of all arrays are fully compatible to advanced 3.3 V CMOS technology. Using these arrays, we have measured small-signal modulation bandwidths exceeding 10 GHz and transmitted pseudo random data at 8 Gbit/s per channel over 500 m graded index multimode fiber. This corresponds to a data transmission rate of 256 Gbit/s per array of 1 × 2 mm^2 footprint area.

1. Introduction

Due to continuous progress in very-large-scale integrated circuit (VLSI) technology in terms of integration density and clock rate, enormous computing bandwidths will be available to electronic microchip and multichip systems. This development creates a great demand for high-bandwidth, high-density interconnects which conventional electrical interconnection technologies are expected not to be able to fulfill [1], neither on system-to-system, nor chip-to-chip or chip level. In order to overcome the interconnection bottleneck, new interconnection technologies have to be developed, where optoelectronic interconnects may offer attractive solutions.

The requirements of future integrated circuits (ICs) and multichip modules can only be fulfilled using optical interconnects if the optics fit into the chip architecture. This means that overall I/O rates in the Tbit/s range should be made available by using massively parallel interconnects, each operating in the Gbit/s range, rather than using a small number of channels. The 2D array approach avoids multiplexing the electrical signals to a high bandwidth on few channels and therefore such parallel optical interconnects should be competitive with advanced electrical interconnect schemes in terms of performance and cost. Designing optical interconnections around 2D input and 2D output arrays does also open up new possibilities for designing faster parallel computing algorithms and systems.

The inherent possibility of forming 2D arrays, high-speed modulation [2], and high-speed data transmission capabilities [P-24] even under bias-free operating conditions [P-32] make

the VCSEL the transmitter of choice for parallel optical interconnects. Due to high efficiency operation at low driving currents [P-35], VCSEL transmitters can significantly reduce thermal problems when using optical interconnections combined with today's high speed ICs.

2. Design and Fabrication

The top view of a whole array is shown in Fig. 1. Mounting the arrays junction-side down is done straightforward as all electrical contacts are on the top-side, whereas the light is emitted through the substrate. Each unit cell of 250 $\times$ 250 μm^2 size contains the VCSEL with its p-contact as well as an n-contact going down to the n$^+$-GaAs substrate through a plated via hole. Both contacts are connected by tracks to remote solder bump pads.

Fig. 2 shows a schematic cross section through the VCSEL and its remote p-contact pad. The epitaxial layers are grown on n$^+$-GaAs substrate with a solid-source molecular beam epitaxy (MBE) system. Three $In_{0.2}Ga_{0.8}As/GaAs$ quantum wells for emission wavelengths of around 980 nm are surrounded by quarter-wave AlGaAs spacer layers to form the one-wavelength long inner cavity. This optical cavity is sandwiched between an upper p-doped and a lower n-doped distributed Bragg reflector. A 30 nm thin AlAs layer is incorporated in the first $\lambda/4$ layer above the inner cavity for selective lateral oxidation [P-35].

Mesas are etched in the epitaxial material and the surface is planarized by polyimide. Current is supplied through a full p-contact and is confined by a dielectric aperture, obtained by selective wet oxidation of the AlAs layer. The n-contact is brought to the surface by a plated gold via in the polyimide, shown in Fig. 3. Both, the VCSEL as well as the plated via are connected with tracks to remote bond pads. A non-wettable dielectric layer serves to restrict the solder flow during a subsequent flip-chip bond process.

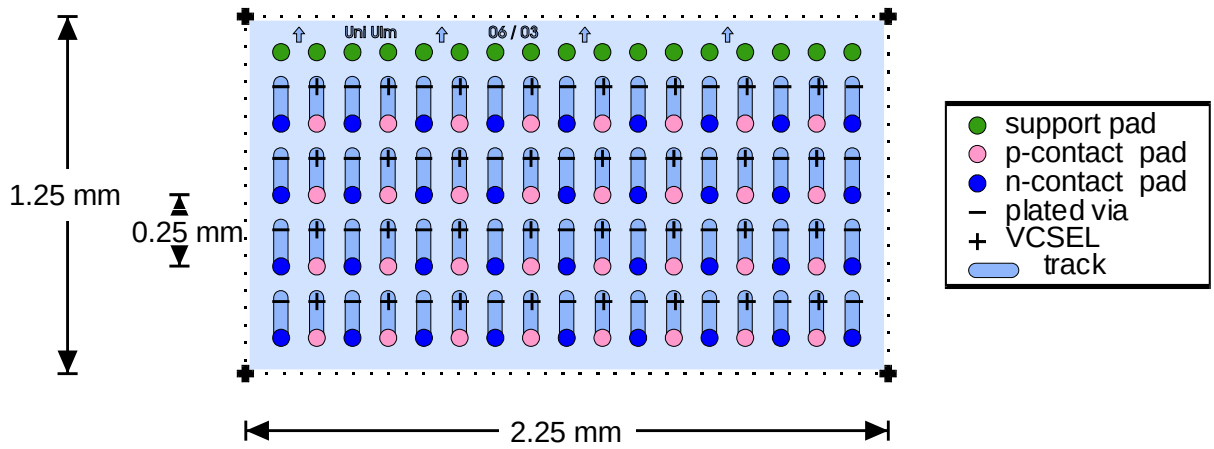

Fig. 1. Top view of the 4 $\times$ 8 VCSEL array with a device pitch of 250 μm. All electrical contacts are located on the top-side, whereas light is emitted through the transparent GaAs substrate.

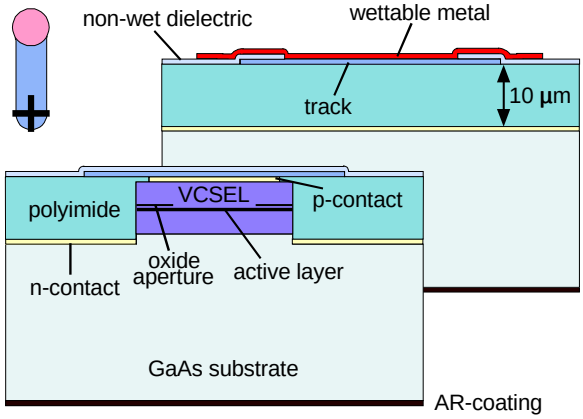

Fig. 2. Cross-sectional view through a VCSEL and the corresponding remote bond pad.

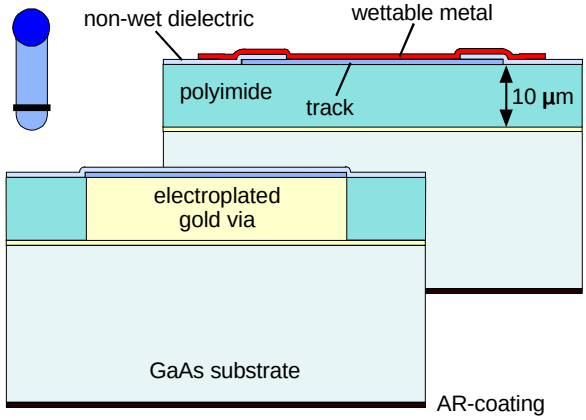

Fig. 3. Cross-sectional view of a ground contact.

3. Continuous Wave Characteristics

Bottom emitting VCSEL arrays with active diameters of 3 μm and 6 μm have been characterized. As Fig. 4 shows, all devices of the arrays do work and have maximum conversion efficiencies from electrical to optical power better than 20 %.

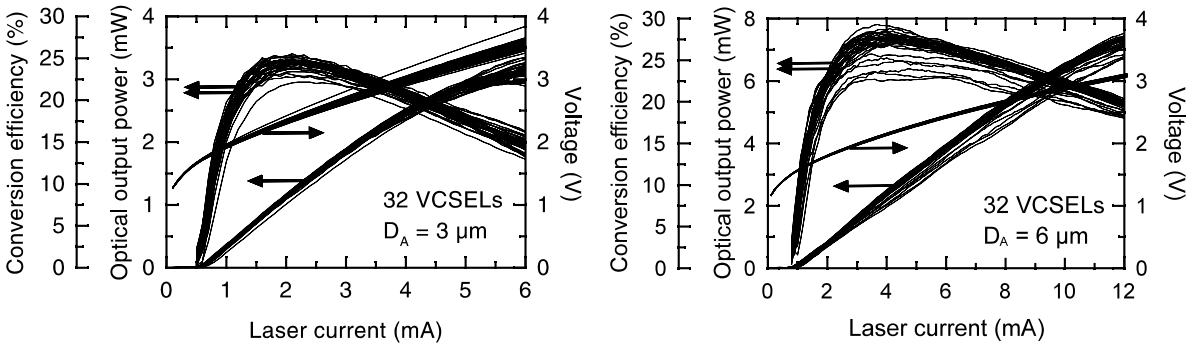

Fig. 4. Optical and electrical characteristics of 4 × 8 VCSEL arrays with 3 μm and 6 μm diameter oxide apertures.

Optical and electrical characteristics across the arrays are rather homogeneous. Because of their small active diameters the 3 μm VCSELs emit a single mode whereas the 6 μm devices emit several transverse modes. The emission wavelength is around 1000 nm. In multimode fiber systems it is preferable to use multi-transverse-mode VCSELs in order to avoid high bit error rate (BER) floors caused by modal noise [3]. BER floors are found if the electrical noise in the receiver is dominated by detected optical noise, such that increasing the emitted optical power does not result in better BER.

Although optical receivers should operate error-free at much lower signal levels, optical links with high channel attenuation or high fan-out may require transmitters with output

powers up to 1 mW. Even at this output level the driving voltages of the arrays are fully compatible with advanced 3.3 V CMOS technology. As for the array with circular oxide apertures of 3 μm we have measured threshold currents of 0.6 mA and threshold voltages of 1.7 V. The differential quantum efficiencies are 64 %. These lasers exhibit single-mode emission with better than 30 dB side mode suppression up to 5.5 mA driving current corresponding to 3 mW output power.

4. Modulation Characteristics

For large signal digital modulation experiments a $2^{11}-1$ word length pseudo-random bit sequence (PRBS) was transmitted at 8 Gbit/s over 500 m of multimode fiber. After amplification in two stages the detected electrical signal was fed to a sampling oscilloscope or a bit error detector. The results of the transmission experiments are summarized in Fig. 5, where full circles denote back-to-back testing. It also shows the eye diagram at a BER of 10^{-11}. The eye is symmetric, wide open, and without considerable relaxation oscillations. The received optical power for a BER of 10^{-11} is -8.5 dBm for fiber transmission which is similar to values observed during a 10 Gbit/s experiment with proton-implanted VCSELs [4]. In this experiment the data rate was limited to 8 Gbit/s by the available pattern generator. To measure the modulation characteristics, the laser diode was directly contacted with a microwave probe tip. Bias current and modulation signal with 0.5 V_{pp} were combined in a bias-tee and the modulated light was detected with a 10 GHz bandwidth photodiode. Using this setup, bandwidths of around 10 GHz at a bias current of 8 mA were measured with all 32 lasers.

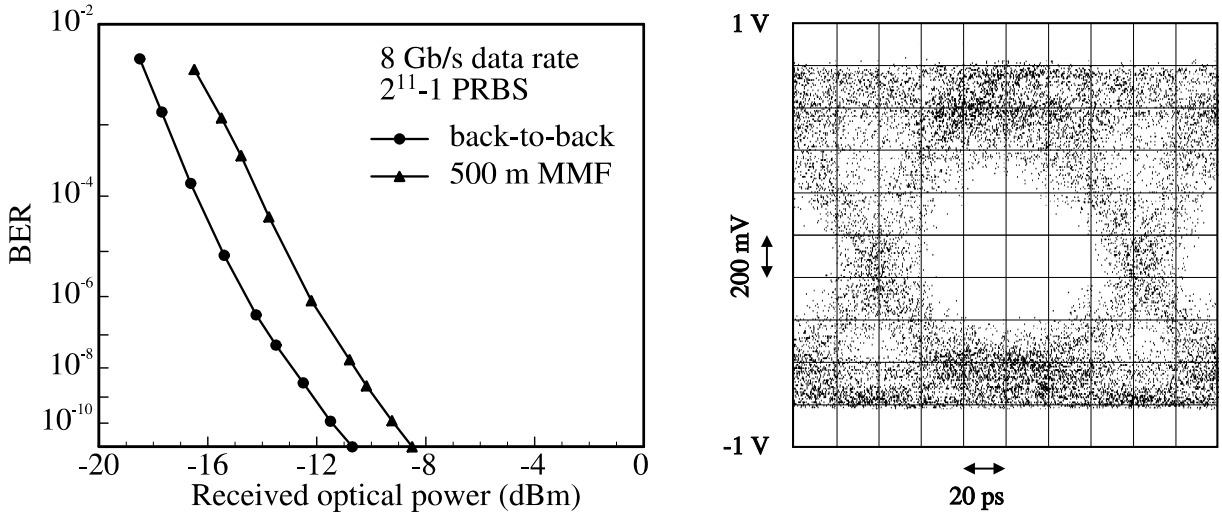

Fig. 5. BER measurement at 8 Gbit/s with $2^{11}-1$ PRBS using a 6 μm diameter VCSEL for transmission over 500 m of 50 μm core diameter graded index multimode fiber.

5. Conclusion

In summary, we have demonstrated flip-chip bondable VCSEL arrays which are ideally suited for transmitter action in parallel optical interconnects, both in terms of packaging and performance. Hybrid inter/intra-chip optoelectronic interconnects in microelectronic integrated systems may help to overcome the bottlenecks to further performance increases and miniaturization arising from conventional electrical interconnects. Measurements of top-surface contacted, bottom-surface emitting vertical cavity lasers have shown single-mode output powers as high as 3 mW, threshold currents as low as 600 μA, modulation bandwidths in excess of 10 GHz, and 8 Gbit/s data rates. The total transmission capability of a 4×8 VCSEL array with 250 μm pitch is 256 Gbit/s resulting in an information flow density of 12.8 Tbit/s/cm^2. The devices used are fully compatible with advanced 3.3 V CMOS technology.

References

[1] Semiconductor Industry Association, *The national technology roadmap for semiconductors*, 1993-1994.

[2] K. L. Lear, V. M. Hietala, H. Q. Hou, M. Ochiai, J. J. Banas, B. E. Hammons, J. C. Zolper, and S. P. Kilcoyne, "Small and large signal modulation of 850 nm oxide-confined vertical cavity surface emitting lasers," in *Advances in vertical cavity surface emitting lasers*, C. Chang-Hasnain, ed., *OSA TOPS,* vol. 15, pp. 69–74, 1997.

[3] K. H. Hahn, M. R. Tan, Y. M. Houng, and S. Y. Wang, "Large area multitransverse-mode VCSELs for modal noise reduction in multimode fibre systems," *Electron. Lett.,* vol. 29, pp. 1482–1483, 1993.

[4] U. Fiedler, G. Reiner, P. Schnitzer, and K. J. Ebeling, "Top-surface emitting vertical-cavity laser diodes for 10 Gbit/s data transmission," *IEEE Photon. Technol. Lett.,* vol. 8, pp. 746–748, 1996.

CW-Operation of a Diode Cascade InGaAs Quantum Well VCSEL

Wolfgang Schmid

A diode cascade vertical cavity surface emitting laser with two active pn-junctions connected in series is demonstrated, operating in cw mode up to 175 K. Differential quantum efficiency clearly exceeds 100 % and a maximum output power of 40 mW is obtained.

1. Introduction

Vertical cavity surface emitting laser diodes (VCSELs) of low threshold current below 100 μA [1], high wallplug efficiency above 50 % [P-35], and high-speed modulation capabilities [2] have been reported in the InGaAs-GaAs or GaAs-AlGaAs material systems mainly for optical interconnect applications. On the other hand, in external cavity configurations or in cases where high quality mirrors are not available, the extremely low roundtrip gain of electrically pumped VCSELs is a distinct disadvantage. Periodic gain structures [3] or lasers with two active layers [4] have been proposed to overcome this problem, but could be demonstrated with only limited success. In the present study we investigate diode cascade structures containing two active multiple quantum well layers connected by a modulation doped backward tunnel diode. This approach of applying several diodes in series may potentially lead to a threshold current close to the transparency current and provide high differential gain but requires an enlarged operating voltage depending on the number of pn-junctions employed.

2. Device Structure

A schematic of the MBE grown diode cascade VCSEL is shown in Fig. 1. The p- and n-type mirrors consist of conventional epitaxial AlGaAs-GaAs Bragg reflectors. The active region contains two pn-junctions in series, each of which comprises three undoped 8 nm thick $In_{0.2}Ga_{0.8}As$ quantum wells (QWs) separated by 10 nm thick GaAs barriers and embedded in $Al_{0.4}Ga_{0.6}As$ claddings. The pnpn-structure requires a backward driven pn-diode with reasonably low voltages which is realized as a tunneling junction using high doping concentrations of $n = 5 \cdot 10^{18} cm^{-3}$ (Si) and $p = 5 \cdot 10^{19} cm^{-3}$ (C) within 10 nm thick AlGaAs layers. As indicated in Fig. 1, the active quantum wells are placed in antinodes of the standing wave pattern, whereas the reverse biased junction is located in the vicinity of a field null to reduce free-carrier absorption. Current confinement is achieved by wet

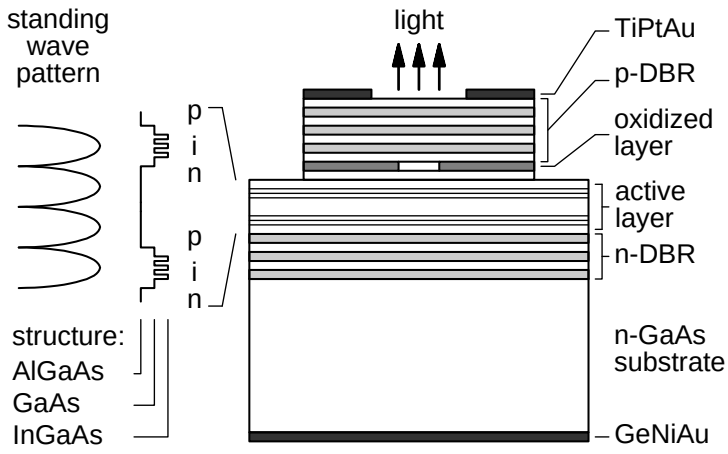

Fig. 1. Structure of a diode cascade VCSEL. The active layer consists of two sets each with 3 $In_{0.2}Ga_{0.8}As$ QWs. The backward diode between the InGaAs stacks is placed in the node of the standing wave pattern to reduce absorption.

chemical mesa etching and subsequent selective oxidation of a 30 nm thin AlAs layer incorporated in the first Bragg pair above the active region. A ring contact deposited on the mesa allows for top surface emission.

3. Operation Characteristics

The output power and voltage versus current characteristics in Fig. 2 are measured for a diode cascade VCSEL with 16 μm oxide aperture at a heat sink temperature of 95 K

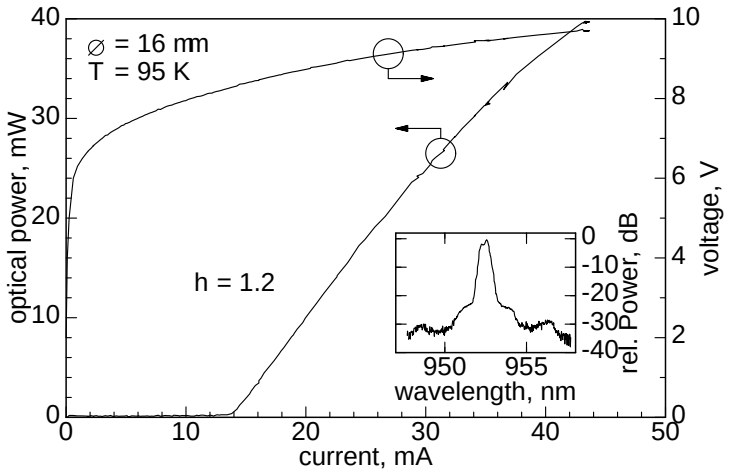

Fig. 2. CW-output characteristics of a diode cascade VCSEL with an oxide aperture of 16 μm. The inset shows the emission spectrum of the device.

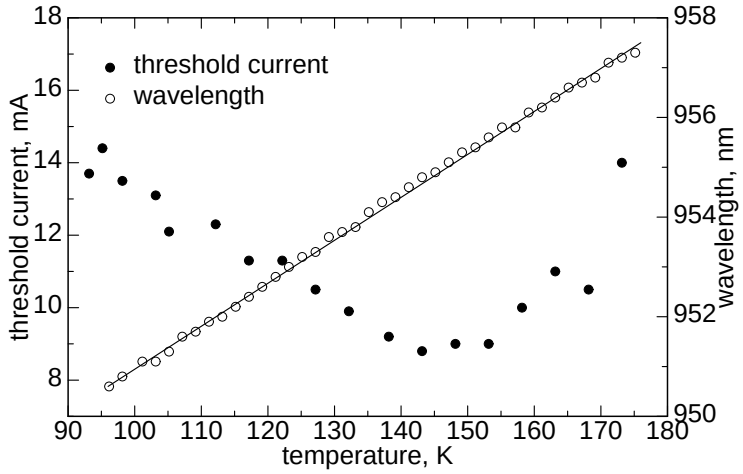

Fig. 3. Temperature dependence of threshold current and emission wavelength in cw-operation.

where the highest differential quantum efficiency of 1.2 is observed. Cascaded photon generation in the two pn-junctions is responsible for the differential quantum efficiency larger than 100 %. For a current of 43 mA the output power reaches 40 mW. The threshold voltage of about 7 V is still large compared to twice the bandgap voltage and is to be attributed to the non-negligible breakdown voltage of the backward driven tunnel diode. As depicted in the inset, the emission is centered at 953 nm wavelength and has a broad linewidth of about 1 nm. Fig. 3 shows the temperature dependence of the emission wavelength, which is given by the cavity resonance, leading to a shift of 0.084 nm/K similar to conventional VCSELs. Temperature dependent threshold current is also indicated in Fig. 3. A minimum threshold current of less than 9 mA is found at a heat sink temperature of about 150 K, when the gain peak of the QWs is aligned to the cavity resonance at 952 nm wavelength. The relatively large threshold current density of 4.5 kA/cm^2 might result from absorption in the highly doped backward junction as well as insufficient pumping of the QW stack near the substrate due to current spreading. Diode cascade VCSELs of smaller or larger active diameters show reduced maximum operating temperatures due to high voltages combined with increased resistances and current densities or operating currents, respectively.

The far field of the 16 μm diameter diode cascade VCSEL is illustrated in Fig. 4 and shows a full width at half maximum of only 6.2° compared to 9.7° of a conventional MQW VCSEL of identical aperture size. Near field broadening resulting from current distribution might be responsible for this effect, but further investigations are required for clarification.

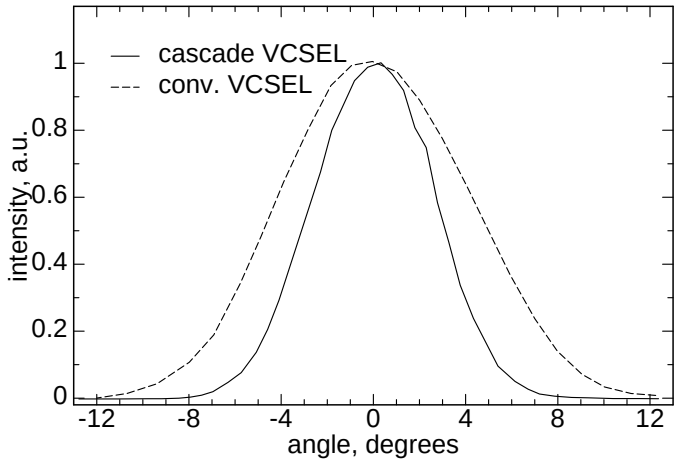

Fig. 4. Far field pattern of the diode cascade VCSEL compared to a conventional weakly index guided VCSEL with the same aperture diameter of 16 μm.

4. Summary

In conclusion, we have proposed and fabricated first diode cascade quantum well VCSELs. Although the devices still suffer from a high voltage drop and absorption at the backward diode, a cw output power of 40 mW as well as a differential quantum efficiency of 120 % is achieved, indicating successful implementation of the cascade concept. Future work should be devoted to the optimization of the backward junction and a better current confinement for the QW active layers.

References

[1] D. Huffaker, L.A. Graham, H. Deng, and D.G. Deppe, "Sub-40 μA continuous-wave lasing in an oxidized vertical-cavity surface-emitting laser with dielectric mirrors", *IEEE Photon. Technol. Lett.*, vol. 8, pp. 974–976, 1996.

[2] K.L. Lear, V.M. Hietala, H.Q. Hou, M. Ochiai, J.J. Banas, B.E. Hammons, J.C. Zolper, and S.P. Kilcoyne, "Small and large signal modulation of 850 nm oxide-confined vertical cavity surface emitting lasers", *OSA Tops*, vol. 15: Advances in vertical cavity surface emitting lasers, pp. 69–74, 1997.

[3] S.W. Corzine, R.S. Geels, J.W. Scott, R.-H. Yan, and L.A. Coldren, "Design of Fabry-Perot surface-emitting lasers with a periodic gain structure", *IEEE J. Quantum Electron.*, vol. 25, pp. 1513–1524, 1989.

[4] Y. Kotaki, S. Uchiyama, and K. Iga, "GaInAs/InP surface emitting laser with two active layers", in Proc. *Conf. on Solid State Devices and Materials*, Kobe, Japan, pp. 133–136, 1984.

Bottom Emitting VCSELs for High cw Optical Output Power

Martin Grabherr and Michael Miller

Bottom emitting VCSELs operating in the 980 nm wavelength regime have been designed for high cw optical output power. Devices of 200 µm active diameter and optimized performance reach 350 mW maximum output power when mounted on heat sink. 50 µm size lasers produce 100 mW at 25 % electrical to optical power conversion efficiency. Thermal properties and size dependent basic characteristics are investigated in detail.

1. Introduction

VCSELs have become highly efficient laser sources for optical data transmission, mainly due to reduced series resistances in Bragg reflectors and optimized current confinement. Current apertures formed by selective oxidation [1] have shown to be indispensable to achieve power conversion efficiencies above 50 % [2], [P-10]. The output power range of oxidized devices typically ranges from about 1 mW up to a few 10 mW. Higher output powers of 113 mW [4] and 180 mW [5] have already been reported for larger diameter devices, ultimately aiming at applications like solid-state laser pumping, printing, or material treatment. In this paper, investigations on size dependent electro-optical as well as thermal characteristics of bottom emitting devices are presented, clearly demonstrating the capability of VCSELs to achieve high optical output powers at still reasonably high conversion efficiencies.

2. Device Structure and Processing

A schematic cross-section of the investigated VCSEL structures is displayed in Fig. 1. The highly reflective p-type Bragg stack is built of 30 pairs of $Al_{0.9}Ga_{0.1}As/GaAs$ layers, where in its first layer a single 30 nm thin AlAs sublayer is placed to form the current aperture. To reduce the series resistance of the thick multilayer stack, Carbon as p-type dopant is employed using extra modulation doping near interfaces to decrease the voltage drop without increasing absorption losses. The n-type Silicon doped Bragg reflector is composed of only 24 pairs of the same material composition. The active zone consists of 3 InGaAs quantum wells embedded in GaAs barriers and surrounded by AlGaAs claddings to build the one wavelength thick inner cavity. Growth of the entire structure is accomplished by solid source MBE. Before oxidizing the current aperture, mesas with diameters

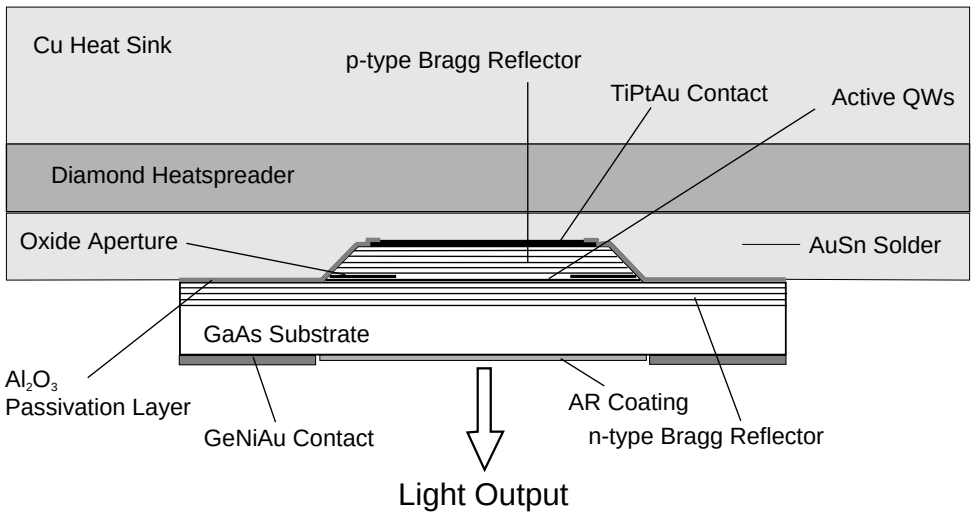

Fig. 1. Bottom emitting VCSEL soldered junction down on diamond heat spreader.

of 100 up to 250 μm are wet chemically etched down to the depth of the AlAs layer. The oxide ring of 25 μm width is formed in a water/Nitrogen atmosphere at 410 ^{o}C process temperature. After evaporating the p-type TiPtAu-contact on top of the mesa, a Si_3N_4 passivation layer is deposited on the upper side to avoid short circuits when soldering the devices on heat sinks. After polishing the substrate to a thickness of 180 μm in order to reduce absorption losses, an anti-reflection (AR) coating of $Si_xO_yN_z$ is deposited. Transmission lithography is used to define the n-type GeNiAu substrate contacts. Single devices are separated by cleaving and then soldered with AuSn on metallized diamond heat sinks, providing thermal conductivities of larger than 1100 W/(K m) for effective heat spreading. Using 5 μm thick solder, the attachment is mechanically stable and good thermal and electrical conductivity is obtained. The diamond size is 2×2 mm^2 and the chip size 300×300 μm^2. For heat sinking the diamond is attached with silver paste on a copper submount.

3. Measurements and Results

Fig. 2 shows light output power characteristics and conversion efficiencies for VCSELs of various diameters from 20 to 200 μm. Solid lines correspond to devices mounted on not actively cooled heat sinks, whereas dashed lines describe unmounted lasers. Output power increases linearly above threshold and rolls over for higher driving currents due to self-heating. VCSELs of 20 μm size exhibit similar behavior for mounted and unmounted operation, since small devices benefit from low electrical power consumption and high conversion efficiency. Reduced thermal resistances of heat sinked devices lead to higher output power of mounted compared to unmounted devices of 50 μm and 100 μm active diameter, where unmounted VCSELs show saturation of maximum output power, as observed before for bottom emitting VCSELs [6]. Due to strong internal heating, even

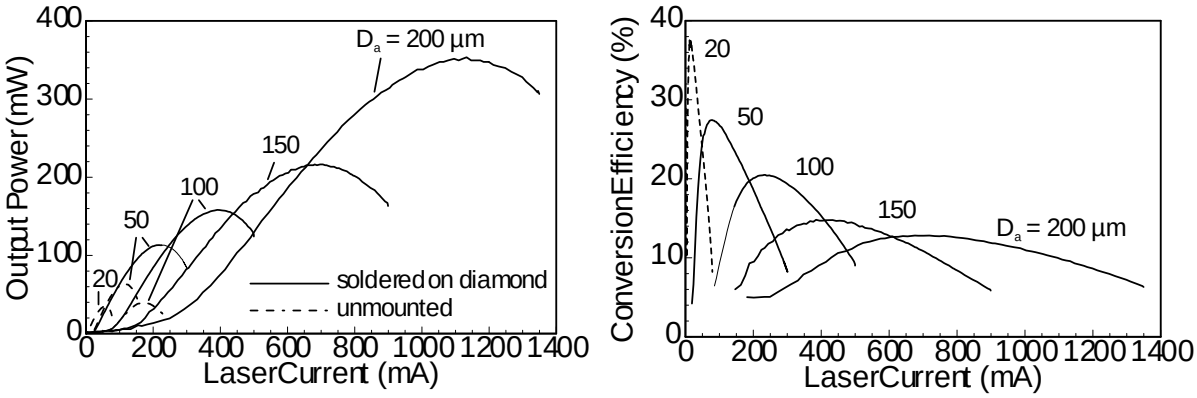

Fig. 2. CW output powers (left) and conversion efficiencies (right) of bottom emitting single devices with active diameters from 20 to 200 μm at room temperature. Solid and dashed lines correspond to mounted and unmounted devices, respectively.

suppression of cw laser emission is found for unmounted devices of 150 μm and 200 μm diameter, whereas soldered devices still show further increased maximum output power and no saturation is anticipated for even larger active areas. With diameters increasing from 20 to 200 μm near threshold, differential quantum efficiencies decrease from 80 % to 44 %. Similarly, as seen in the right hand part of Fig. 2, conversion efficiency decreases with increasing active diameter, which is additionally caused by the differential resistance. Maximum conversion efficiency of 20 μm lasers is 37 % but just 13 % for 200 μm diameter devices. Reduced efficiencies are mainly caused by increased heating but may also partly be due to amplified spontaneous emission (ASE) of laterally guided in-plane modes. Compared to VCSELs with bulk active material [7] the influence of ASE in the quantum well devices investigated is much weaker due to the smaller confinement factors.The maximum output power of 350 mW obtained for the 200 μm diameter device is the highest cw output power for an electrically pumped solitary VCSEL reported so far. The power is measured using a calibrated power meter (Newport 1830 C) with broad area photodetector. Maximum power is observed at 1100 mA driving current and 3.2 V driving voltage where an extra voltage drop of 0.2 V is included which is due to non-perfect soldering on the submount. Nevertheless the conversion efficiency at maximum power is still 10 %. Higher conversion efficiency combined with moderate output power is observed for smaller devices. It is worth to note that VCSELs of 50 μm diameter emit 100 mW at 25 % conversion efficiency. Radiation patterns and spectra are rather similar for the device sizes studied. An optical spetrum is shown in Fig. 3 for a 200 μm diameter device driven at 700 mA laser current. Transverse multimode emssion is centered at 980 nm wavelength with a spectral width of about 2 nm. Far field radiation patterns plotted in Fig. 4 for a VCSEL of 150 μm diameter typically show FWHM angles of less than 20^o. Fig. 5 presents a detailed study of threshold current, differential resistance, and thermal resistance dependencies on active diameter. Maximum output powers and maximum conversion efficiencies extracted from Fig. 2 are also included. Differential resistances decrease proportionally to $D^{1.7}$ indicating residual inhomogeneities in current supply from outer contact regions. Threshold currents

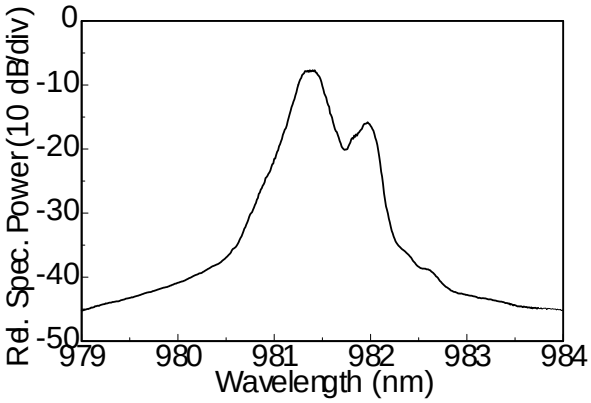

Fig. 3. Spectrum of a 200 μm diameter device at 700 mA laser current.

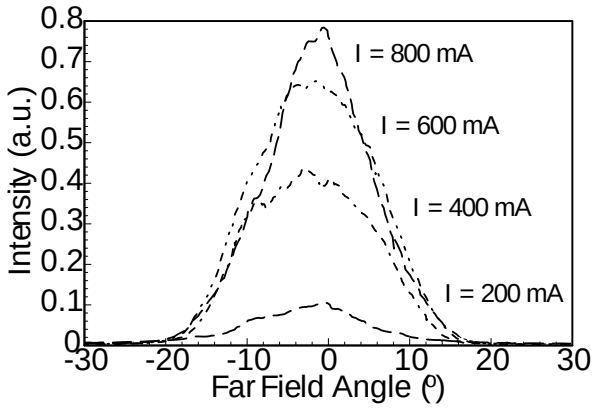

Fig. 4. Far field patterns for different laser currents of a 150 μm active diameter VCSEL.

increase linearly with active area, giving a constant threshold current density of about 850 A/cm^2 independent of device size. Thermal resistances R_{th}, determined from the mode red shift with increasing dissipated power and the red shift with growing heat sink temperature vary inversely proportional to the active diameter D in good agreement with simple analytical estimations according to [8]

$$R_{th} = (2\lambda_c D)^{-1} \ , \tag{4}$$

where the experimentally obtained thermal conductivity is $\lambda_c \approx 44\,\mathrm{W/(K{\cdot}m)}$ and is thus close to that of bulk material. Thermal resistance data given in Fig. 5 are measured for unmounted devices but are a factor of about 3 lower for soldered lasers.

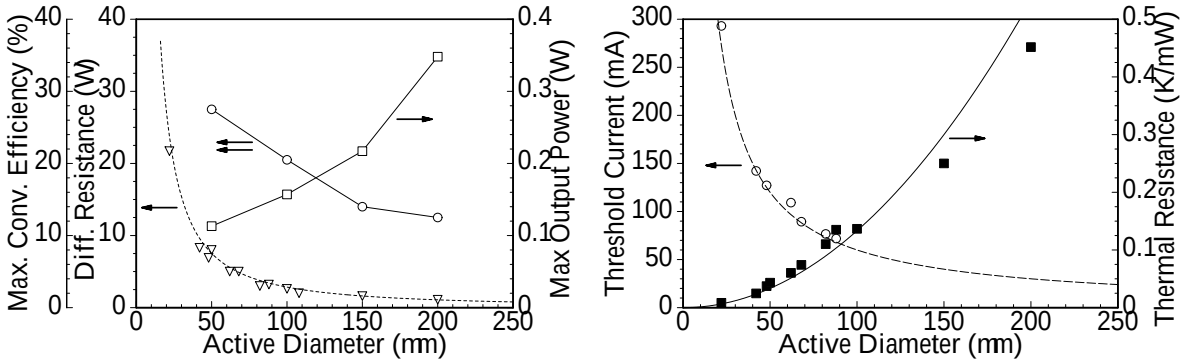

Fig. 5. Differential resistance, maximum cw output power and conversion efficiency versus active diameter of mounted bottom emitting VCSELs (left) and size dependence of threshold current and thermal resistance of unmounted devices (right).

4. Conclusion

Bottom emitting VCSELs have been fabricated that show record output powers when applying appropriate heat sinking. 350 mW for a single 200 μm device is obtained at a corresponding conversion efficiency of 10 %. An output power of 100 mW at 25 % conversion efficiency is demonstrated for a 50 μm device. Size dependent investigations show no saturation of maximum output power with increasing size, but due to further decreasing efficiencies, larger devices do not seem prospective. From the investigated scaling behavior of differential and thermal resistances it is concluded that cw output powers above 1 W at reasonably high conversion efficiencies might be attainable by using densely packed two-dimensional VCSEL arrays with small size individual devices.

References

[1] D.L. Huffaker, D.G. Deppe, and K. Kumar, "Native-oxide defined ring contact for low threshold vertical-cavity lasers", *Appl. Phys. Lett.*, vol. 65, pp. 97–98, 1994.

[2] K.L. Lear, K.D. Choquette, R.P. Schneider, Jr., S.P. Kilcoyne, and K.M Geib, "Selectively oxidised vertical-cavity surface-emitting lasers with 50 % power conversion efficiency", *Electron. Lett.*, vol. 31, pp. 208–209, 1995.

[3] R. Jäger, M. Grabherr, C. Jung, R. Michalzik, G. Reiner, B. Weigl, and K.J. Ebeling, "57 % wallplug efficiency oxide-confined 850 nm wavelength GaAs VCSELs", *Electron. Lett.*, vol. 33, pp. 330–331, 1997.

[4] F.H. Peters, M.G. Peters, D.B. Young, J.W. Scott, B.J. Thibeault, S.W. Corzine, and L.A. Coldren, "High power vertical-cavity surface-emitting lasers", *Electron. Lett.*, vol. 29, pp. 200–201, 1993.

[5] M. Grabherr, B. Weigl, G. Reiner, R. Michalzik, M. Miller, and K.J. Ebeling, "High power top-surface emitting oxide confined vertical-cavity lasers", *Electron. Lett.*, vol. 32, pp. 1723–1724, 1996.

[6] T. Wipiejewski, M.G. Peters, B.J. Thibeault, D.B. Young, and L.A. Coldren, "Size-dependent output power saturation of vertical-cavity surface-emitting laser diodes", *IEEE Photon. Technol. Lett.*, vol. 8, pp. 10–12, 1996.

[7] K. Iga, F. Koyama, and S. Kinoshita, "Surface emitting semiconductor lasers", *IEEE J. Quantum Electron.*, vol. 24, pp. 1845–1855, 1988.

[8] W. Nakwaski and M. Osinski, "Thermal resistance of top-surface emitting vertical-cavity semiconductor lasers and monolithic two-dimensional arrays", *Electron. Lett.*, vol. 28, pp. 572–574, 1992.

Oxide Confined Vertical-Cavity Semiconductor Optical Amplifier for 980 nm Wavelength

Dieter Wiedenmann

An electrically pumped surface-normal optical amplifier with high gain and low amplified spontaneous emission is demonstrated. The device can be operated either as an amplifier or as an amplifying modulator with a modulation bandwidth exceeding 1 Gb/s.

Surface-emission devices are considered to be of great importance for future high-density two-dimensional optical processing architectures and optical fiber networks. Vertical-cavity surface emitting lasers have already matured as light sources, and large 2-D arrays have been demonstrated [1].

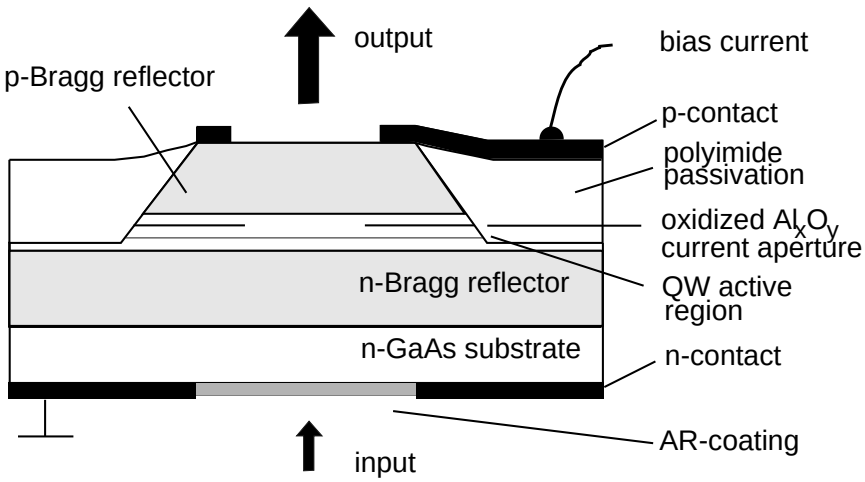

Fig. 1. Schematic of selectively oxidized VCSOA.

These devices offer high-speed current modulation for multi-Gb/s data generation [2], ultralow power consumption and simple mounting technology. Other advantages include high coupling efficiency to optical fibers and polarization insensitive gain. In earlier work we have already demonstrated a proton-implanted Vertical-Cavity Semiconductor Optical Amplifier (VCSOA) [3]. Although this device had a high gain, the saturation output power was rather low and amplified spontaneous emission very high. Here we have used the selective oxidation process for current confinement, which is meanwhile successfully incorporated into VCSEL fabrication. Fig. 1 illustrates the layer structure of a VCSOA for operation in transmission mode. It is grown by molecular beam epitaxy on n-GaAs substrate and contains a three InGaAs quantum well active region designed for 980 nm

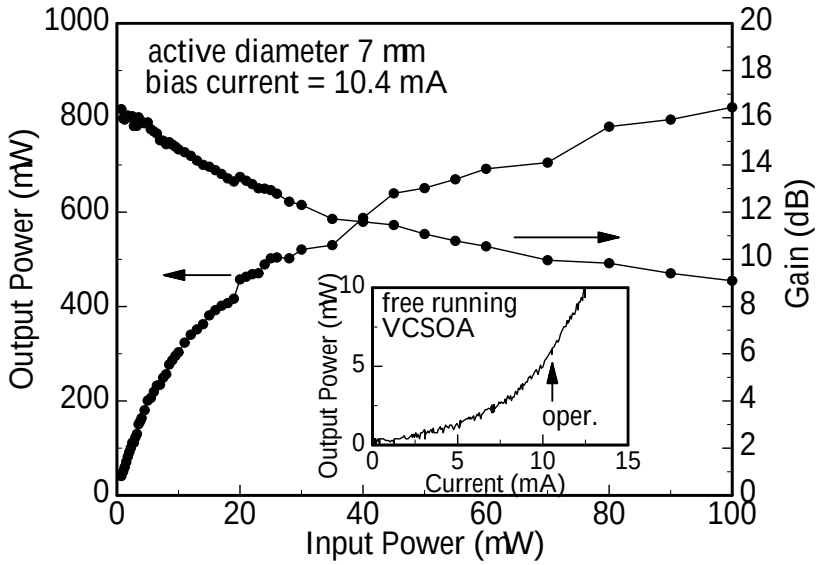

Fig. 2. Output power and gain of 7 μm VCSOA as a function of input power. The inset shows the amplifier output from the top facet at free running operation.

gain peak wavelength. The p- and n-doped reflectors consist of $Al_{0.8}Ga_{0.2}As$-GaAs Bragg stacks with 20 and 24.5 mirror pairs, respectively. Device fabrication is very similar as reported for vertical-cavity lasers [P-35]. The substrate is antireflection coated to prevent far distance reflections from the semiconductor-air interface. The reflectivity of both mirrors is calculated to be 98.3 %. In Fig. 2, the output power and amplifier net gain as a

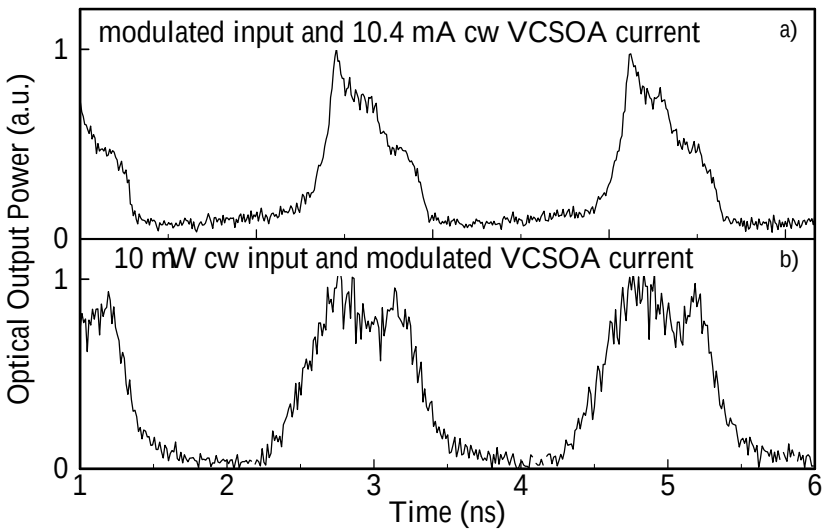

Fig. 3. Temporal output of the device in operation as an amplifier a) and modulator b) at 1 Gb/s NRZ input.

function of input power of a 7 μm diameter oxide aperture device is displayed. The inset

shows the optical output of the free running amplifier versus bias current. A bias current of 10.4 mA was selected for operation, giving a spontaneous optical output of 6 μW per facet of the free running device. As input we either use a beam from a cw Ti:sapphire laser or a vertical-cavity laser, both emitting in the fundamental transverse mode. Input and output ports are as indicated in Fig. 1. High gain above 16 dB is achieved for small input powers. Relatively moderate saturation reduces this value to 9 dB for 100 mW input. Figs. 3 a) and b) show the temporal outputs of the device operating as an optical amplifier or an amplifying modulator, respectively. In both operation modes the output signals have almost the same extinction ratios as the optical or electrical NRZ inputs at 1 Gb/s data rate.

In conclusion, we have demonstrated an oxide confined VCSOA with distinctly improved performance. Dynamic operation at 1 Gb/s data rate shows the potential for applications in, e.g., highly parallel switching networks. The wavelength selective amplification behavior makes this device especially attractive for WDM environments.

References

[1] C.J. Chang-Hasnain, J.P. Harbinson, E.-E. Zah, M.W. Maeda, L.T. Florez, N.G. Stoffel, and T.-P. Lee, "Multiple wavelength tunable surface-emitting laser arrays", *IEEE J. Quantum Electron.*, vol. 27, pp. 1368–1376, 1991.

[2] U. Fiedler, B. Möller, G. Reiner, P. Schnitzer, and K.J. Ebeling, "10 Gbit/s data transmission using top emitting VCSELs with high side-mode suppression", *Electron. Lett.*, vol. 31, pp. 1664–1665, 1995.

[3] D. Wiedenmann, B. Möller, R. Michalzik, and K.J. Ebeling, "Performance characterisitics of vertical-cavity semiconductor laser amplifiers", *Electron. Lett.*, vol. 32, pp. 342–343, 1996.

Progress Towards Long Wavelength VCSELs

Hin Yiu Anthony Chung, Juergen Joos, Juergen Maehnss and Georgi Stareev

The main results in 1997 are the improvement of the wafer fusion technology, the development of an optimized active zone for long wavelength VCSELs, an elegant model for the understanding of cavity resonance tuning and a new double fused device that operates as LED and shows the correct resonance wavelength.

In wafer fusion we investigated the influence of fusing parameters on the photoluminescence emission. Neither the applied mechanical pressure nor the standard fusing temperature used show undesirable effects on the sample. The heterojunction at the fusing interface shows a linear behavior with the electrical resistance due to the supporting layers and negligible voltage drop.

For the active zone, strain compensated multi quantum wells with constant In/Ga ratio are investigated. They are designed to withstand the high temperature treatment under wafer fusion. Broad area lasers containing these MQWs are emitting at 1550 nm and show very low threshold current densities of around 100 A/cm^2 per well and T_0 of 50 K. Active zones for Lasers emitting at 1300 nm have also been grown and investigated in broad area lasers. They show comparable behavior to the 1550 nm devices.

A simple but elegant model for the prediction of the resonance tuning by etalon etching in VCSEL devices incorporating dielectric or semiconductor mirrors has been developed. From the theoretical data an effective resonator length is derived. The resonance is then adjusted using the effective length in a calculation for the needed etch depth (and therefore etch time). Moreover, a rough estimation of necessary mirror reflectivities and additional losses with resonance mismatch is provided by the model.

First double fused devices are successfully fabricated. Owing to contact and mirror resistance, the devices operate for the moment still as LEDs.

For more details refer to the following three articles.

Design and Modeling of Long Wavelenth Fused VCSEL Cavities

Juergen Maehnss

1. Introduction

In VCSELs the emission wavelength is strongly dependent on a proper cavity adjustment. Reflection phases of the mirrors and the cavity length determine the cavity resonance where emission can occur. In our VCSEL devices the etalon between the mirrors is adjusted by wet chemical etching. The prediction of cavity resonance sensitivity on the accuracy of the etching is necessary to get a good feeling about the etch rates and accuracy one has to utilize. The objective of our modeling work was to get rules of thumb for the dependence of resonance wavelength shift on etch depth.

2. Model

For an estimation we started from the well known basic resonance formulas of a laser. The wavelength dependence can be deduced from the phase matching formula by a simple derivative. Threshold gain follows from the amplitude condition. Additional one can get information about additional required gain in case of non optimized cavity resonance wavelength (resonance is not at the maximum of the mirror reflectivities) from the amplitude expression by the same simple derivative technique as in the phase case. Numbers are calculated for mirrors with a reflectivity above 99.5% and different index contrasts (dielectric mirrors exhibit a high index contrast, semiconductor ones a low contrast).

3. Theory

The basic laser resonance condition to be satisfied is

$$r_{top} r_{bottom} \exp\{-2\gamma L\}\Big|_{\lambda_0, L_0} = 1$$

with

$$2\gamma L = \alpha_{ext}(L - \ell) + \alpha_{ac}\ell - g\ell + i\frac{4\pi n L}{\lambda}$$

were r denotes the amplitude reflectivity, L and ℓ geometrical cavity and active zone length, n refractive index of etalon, α_{ext} and α_{ac} losses in etalon and active zone, g gain in the active zone and λ vacuum wavelength, index 0 indicates resonance conditions.

From the imaginary part (phase matching condition) the resonance wavelength is determined:

$$\phi_{top}\Big|_{\lambda_0} + \phi_{bottom}\Big|_{\lambda_0} - \frac{4\pi n L}{\lambda}\Big|_{\lambda_0, L_0} = -m2\pi\,.$$

ϕ denotes the mirror reflectivity phase. With perfectly adjusted cavities the first order mode (m = 0 or 1 depending on the phase at center wavelength) cavity length is between $\frac{\lambda_0}{4n}$ and $\frac{\lambda_0}{2n}$ in the case of one dielectric / one semiconductor mirror and two equal mirror types respectively. The Phase matching condition remains unchanged with different cavity length $L_0 + \Delta L$. Assuming small changes in cavity length the wavelength will change also on a small scale and derivative techniques are applicable:

$$0 = \frac{4\pi n L_0}{\lambda_0^2} - \frac{4\pi n}{\lambda_0}\frac{\mathrm{d}L}{\mathrm{d}\lambda} + \frac{\mathrm{d}}{\mathrm{d}\lambda}(\phi_{top} + \phi_{bottom})\Big|_{\lambda_0}\,.$$

Regarding the above expression one can simplify with $\frac{\mathrm{d}L}{\mathrm{d}\lambda} \approx \frac{\Delta L}{\Delta\lambda}$ to

$$\Delta\lambda = \Delta L \frac{\lambda_0}{L_{eff}}$$

were the well known effective length

$$L_{eff} = L_0 + \frac{\lambda_0}{2n}\frac{\lambda_0}{2\pi}\,\frac{\mathrm{d}}{\mathrm{d}\lambda}(\phi_{top} + \phi_{bottom})\Big|_{\lambda_0}$$

occurs. The values of the reflection-phase derivatives $\frac{\lambda_0}{2\pi}\,\frac{\mathrm{d}}{\mathrm{d}\lambda}\phi\Big|_{\lambda_0}$ are 5 and 0.05 for semiconductor and dielectric mirrors respectively. Assuming a resonance wavelength of 1.5 μm and a refractive index of 3 one finds for a longitudinal first order mode cavity ($L = 0.25\,\mu$m) an effective length of 2.75 μm and 0.27 μm in VCSELs with two semiconductor and two dielectric mirrors respectively.

4. Results Extracted from the Phase Condition

From the above derived results it is found, that mirrors with high index contrast and therefore relative small dependence of reflection phase on wavelength exhibit a relative weak wavelength dependence compared to those that have a big phase-wavelength dependence. The later ones stabilize the cavity mode to a certain extend.

Due to the fact that the reflection phase and amplitude are Hilbert transforms of each other it can generally be said that mirrors with large stopband width exhibit a smaller phase-wavelength dependence in the stopband than those with small stopband width. The small stopband width mirrors are preferable because of their mode stabilizing behavior.

5. Required Additional Gain

The required additional gain for a slight mismatch between cavity resonance and peak reflectivity of the mirrors can be calculated from the amplitude condition

$$g_{th} = \alpha_{ac} + \alpha_{ext}\left.\frac{L-\ell}{\ell}\right|_{L_0} - \left.\frac{1}{\ell}\ln\left\{|r_{top}||r_{bottom}|\right\}\right|_{\lambda_0}.$$

Using the averaged reflectivity $R = \sqrt{R_{top}R_{bottom}}$ in lasers with high reflecting mirrors were $\Delta R = 1 - R \ll 1$ the threshold gain can be estimated by

$$g_{th} = \alpha_{ac} + \alpha_{ext}\frac{L_0-\ell}{\ell} + \frac{\Delta R}{\ell}.$$

Neglecting losses mirror reflectivity of 99.5% results into $1600\,\mathrm{cm}^{-1}$ threshold gain with 30 nm active zone length. Utilizing a derivative of second order around the peak reflectivity (the first order derivative diminishes) one finds the following simple expression for the additional required gain at wavelength mismatch $\Delta\lambda$

$$\begin{aligned}\Delta g_{th} &\approx \left.\frac{\Delta\lambda^2}{2\ell}\frac{\mathrm{d}^2}{\mathrm{d}\lambda^2}\Delta R\right|_{\lambda_0} = -\frac{1}{\ell}\left(\frac{\Delta\lambda}{\lambda_0}\right)^2\frac{\lambda_0^2}{2}\left.\frac{\mathrm{d}^2}{\mathrm{d}\lambda^2}R\right|_{\lambda_0}\\ &\approx -\frac{1}{\ell}\left(\frac{\Delta\lambda}{\lambda_0}\right)^2\frac{\lambda_0^2}{2}\left.\frac{\mathrm{d}^2}{\mathrm{d}\lambda^2}\frac{R_{top}+R_{bottom}}{2}\right|_{\lambda_0}.\end{aligned}$$

It is worthy to note that the gain-wavelength dependence $-\frac{\lambda_0^2}{2}\left.\frac{\mathrm{d}^2}{\mathrm{d}\lambda^2}R\right|_{\lambda_0}$ is much smaller for dielectric mirrors (0.25) than for semiconductor ones (2.7) but the wavelength mismatch dependence is quadratic. This leads to a drastic increase in threshold gain with a small cavity length mismatch for the VCSEL design with dielectric mirrors. For example with a mismatch of $\Delta L = 10\,\mathrm{nm}$ the resonance wavelength shifts 55 nm in a VCSELs with dielectric mirrors resulting into an additional gain of $1\,\mathrm{cm}^{-1}$ whereas with semiconductor mirrors the wavelength shifts only 5.5 nm resulting into additional gain of $0.1\,\mathrm{cm}^{-1}$. Both values are normally negligible compared to basic value of $1600\,\mathrm{cm}^{-1}$.

6. Summary

In summary we developed a rule of thumb to estimate the effect of mismatch in the cavity length of a VCSEL device. Taking the numbers from calculated reflectivity amplitude and phase curves one finds that VCSEL structures incorporating mirrors with small stop-bandwidth are preferable from the viewpoint of mode stability for nonperfectly matched

etalon length. VCSELs structure with dielectric mirrors (large stopband width) exhibit a shift in resonance wavelength that is approximately five times the etched etalon depth whereas it is only half in those with semiconductor (small stopband width) mirrors. This leads to less critical etching techniques when semiconductor mirrors are used.

Very Low Threshold Current Density 1.3μm-InAsP/InGaAsP Strained Quantum Well GRINSCH Lasers Grown by Gas Source MBE

Hin Yiu Anthony Chung, Georgi Stareev, Juergen Joos and Juergen Maehnss.

In this article we report the successful fabrication of the first Gas Source MBE grown InAsP/InGaAsP single and multi-quantum well lasers with linearly graded InGaAsP confinement layers. X-ray diffraction experiment indicates that the crystal quality of the graded InGaAsP layers is excellent. The optical quality of the InAsP/InGaAsP quantum wells are investigated by room temperature Photoluminesence (PL) spectroscopy; An intense PL-signal with a FWHM of 31meV was observed which shows that the MQWs are of high optical quality. Laser structures containing graded confinement layers and 5, 3 and 1 quantum wells are grown and fabricated into broad-area laser diodes. Typical threshold current densities of 400A/cm^2, 270A/cm^2 and 180A/cm^2 are obtained for the lasers containing 5, 3 and single quantum wells respectively. These values are among the lowest ever achieved for 1.3μm lasers grown by any kind of MBE.

1. Introduction

Low threshold current density lasers operating at 1.3μm wavelength are of particular importance for optical data links and optical telecommunications. To meet this need, laser diodes containing active zones with large carrier and optical confinements are of great interest. Conventional 1.3μm lasers containing lattice-matched InGaAsP/InGaAsP Multi-Quantum-Wells (MQWs) active zone suffer from relatively poor carrier confinement due to the small conduction band offset between the quantum wells and quantum barriers. Therefore, the threshold current densities of those lasers are far from satisfactory. In this work, we use strained InAsP/InGaAaP MQWs instead of conventional lattice-matched InGaAsP/InGaAsP MQWs as the active zone. The benefits of using InAsP/InGaAsP MQWs include a larger conduction band offset, $\Delta E_c/\Delta E_g = 0.5$ [1] and the incorporation of compressive strain in the quantum wells. The larger conduction band offset tightly confine carriers in the quantum wells, where the compressive strain in the quantum wells helps to reduce the Auger recombination and inter-valence band absorption [2]. Linearly graded index separate confinement heterostructure (GRINSCH) provides an effective optical confinement in the active region and hence help to further reduce the threshold current density of the laser. By combining these two techniques, a drastic reduction of threshold current density can be expected.

2. Epitaxial Growth

The growth of epitaxial layers was carried out in a Riber 32 Gas Source MBE (GSMBE) system using elemental In and Ga as the group-III source materials. Pure AsH_3 and PH_3, precracked at 900^0C, were used as the group-V precurors. Be and Si were used as the p-type and n-type dopants respectively. All layers were grown on (100) InP substrates, 2^0 off towards the nearest $(1\bar{1}0)$ direction. The substrate temperature during growth was 480^0C for all layers and was measured by an Accufiber pyrometer.

3. Material Characterization

A) Crystal Quality of InGaAsP with Graded Composition

One of the main concern of using GSMBE for the growth of GRINSCH lasers is its capability of growing high quality lattice-matched InGaAsP layers with graded compositions on InP. Indeed, up to now nearly all the laser diodes containing GRINSCH were grown exclusively by MOVPE [3]. It is mainly due to the fact that in the MOVPE process, the material compositions seem to be easier to control by the precise mass flow regulators. In GSMBE, similiar advanced structures can only be realized, if the temperatures of the group-III effusion cells as well as the flow of AsH_3 and PH_3 are regulated accurately. In Fig. 1 and Fig. 2, the X-ray rocking curves of two different GSMBE-grown linearly graded InGaAsP layers are shown. The compositional graded quaternary layer in Fig. 1 starts with InGaAsP (λ=0.98μm), Q(098) and ends up with InGaAsP (λ=1.10μm), Q(110). In Fig. 2, the compositional grading of the quaternary layer is vice versa. In the two rocking curves, intense X-ray peak coming from the graded layer can be observed. In both cases, the lattice-mismatch of the graded layers are well below 1×10^{-3}. These results clearly show that graded InGaAsP layers grown by GSMBE are good enough for the realization of GRINSCH.

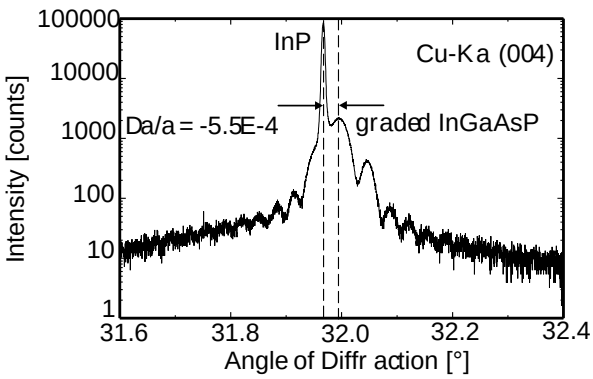

Fig. 1. X-ray rocking curve of graded InGaAsP: From Q(098) to Q(110).

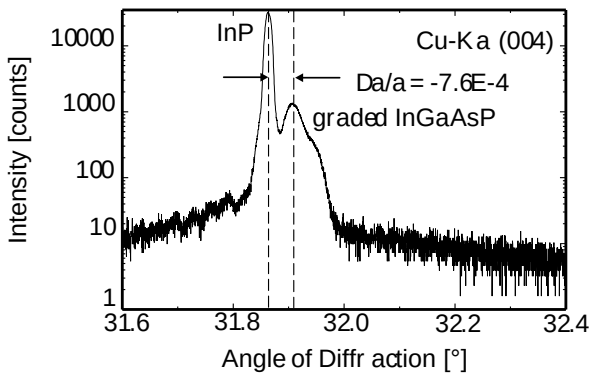

Fig. 2. X-ray rocking curve of graded InGaAsP: From Q(110) to Q(098).

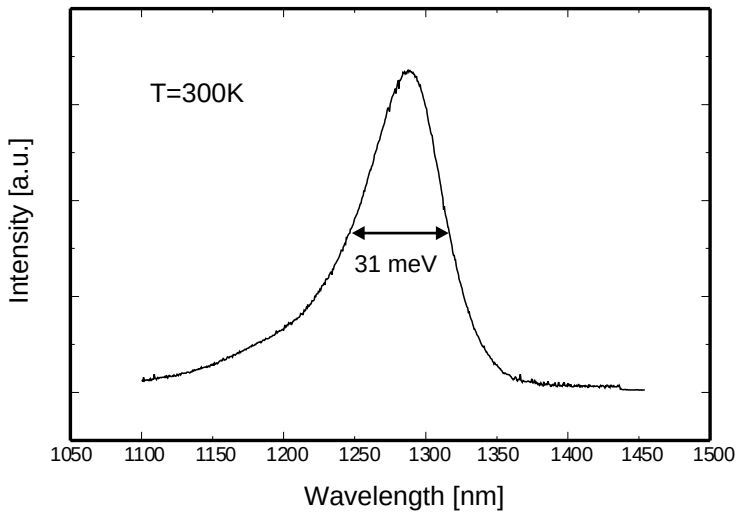

Fig. 3. Room temperature PL-spectrum of a triple InAsP/InGaAsP MQWs.

B) Optical Quality of InAsP/InGaAsP QWs

Another prerequisite for producing laser diodes with low threshold current is the ability to grow high quality quantum well active zones. The quantum well active zone used in this work consists of 8nm thick $InAs_{0.42}P_{0.58}$ QWs with a compressive strain of 1.5% and 16nm thick $In_{0.70}Ga_{0.30}As_{0.42}P_{0.58}$ QBs with a tensile strain of 1.1%. Fig. 3 shows the room temperature PL spectrum of a triple MQW structure. The high quality of the MQWs is confirmed by the intense and sharp PL peak observed at 1.295μm wavelength with a FWHM of 31meV.

4. Laser Structures: Growth and Processing

The laser structures to be discussed here is shown in Fig. 4. The structures contain five, three or one quantum wells (QWs) surrounded by two 150nm thick graded InGaAsP layers which serve as the GRINSCH. The cladding layers are 1.2μm thick Si-doped InP and 1.2μm thick Be-doped InP respectively. A 50nm thick highly Be-doped InGaAs forms the upper contact layer. After the epitaxy, Ti/Pt/Au p-contact was evaporated onto the top of the samples followed by a lift-off step. After the metal patterning, stripes with widths of 30μm to 50μm were formed by wet chemical etching. The etch-process was stopped immediately after the p-type cladding was reached. The substrate of the samples was then polished down to a thickness of 150μm. A Ge/Ni/Au layer was evaporated onto the bottom of the polished substrates to form the n-side contact. Finally, the samples was cleaved into laser bars with cavity lengths of 400μm to 1200μm.

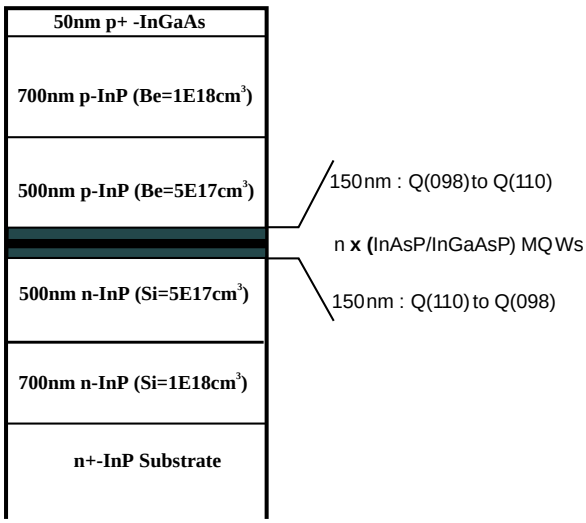

Fig. 4. Layer structure of the 1.3 μm InAsP/InGaAsP laser.

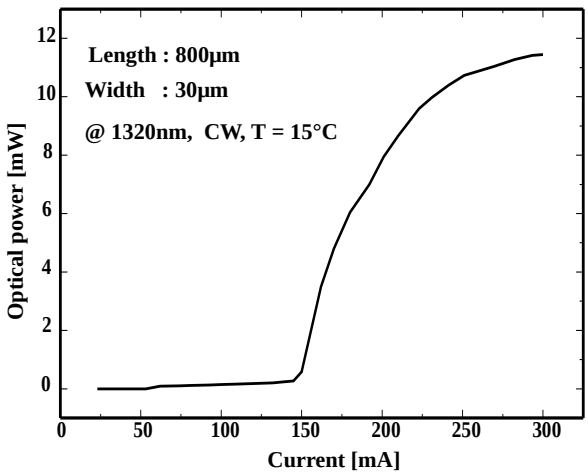

Fig. 5. Performances of laser diode containing five InAsP/InGaAsP MQWs.

5. Laser Performances

In Fig. 5 the output power vs current characteristic of a 30μm wide and 800μm long laser bar containing five QWs is shown. At room temperature the laser operates under CW condition. For laser diodes with a width of 50μm and a length of 1.2mm, the threshold current density is 400A/cm^2. It corresponds to a value of 80A/cm^2 per QW. This extremly low threshold current density per QW indicates that the laser diodes are of excellent quality. The characteristic temperature, T_0, in the temperature range between 10 and 60^{0}C is around 50K. Typical output power at double threshold current is around 20mW.

Lasers diodes containing three and single QWs are also measured. In Fig. 6 the threshold current density of lasers containing different number of QWs is ploted as a function of their corresponding number of wells. In contrast to what is usually stated [4], we observed that the threshold current density decreases monotonically even when the number of QWs is reduced under the value of five. For the three QWs lasers, the threshold current density is 270A/cm^2. A value as low as 180A/cm^2 is measured in the single QW lasers. This value is amoung the lowest ever achieved for 1.3μm lasers grown by any kind of MBE methods [5]. In Fig. 6 the threshold current density of the single QW laser is ploted as a function of the inverse cavity length. The transparent current density obtained from the y-intercept of this plot is 60A/cm^2.

6. Conclusion

In conclusion, we have successfully fabricated the first GSMBE grown InAsP/InGaAsP single and multi quantum well lasers with linearly graded InGaAsP confinement layers. The threshold current densities of 400A/cm^2, 270A/cm^2 and 180A/cm^2 are measured for

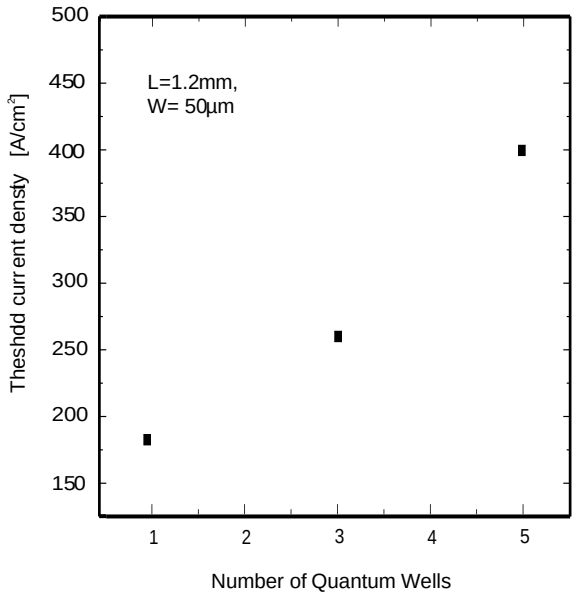

Fig. 6. Threshold current density as a function of the number of quantum wells. The cavity is 1.2 mm.

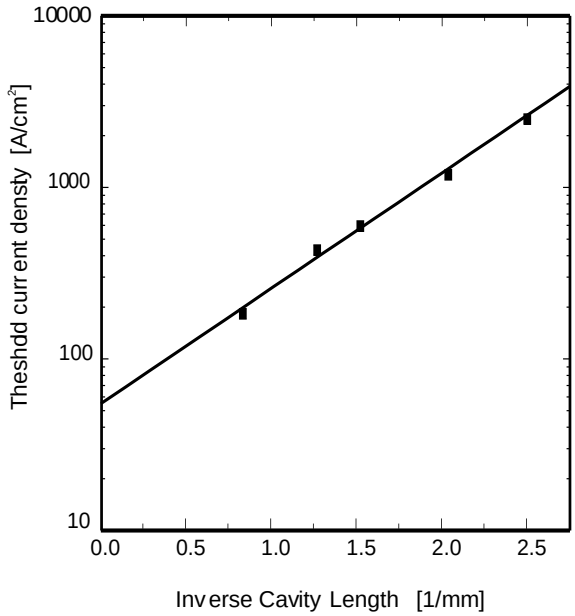

Fig. 7. Threshold current density as a function of inverse cavity length of single QW GRIN-SCH laser.

lasers containing 5, 3 and 1 quantum wells respectively. These values are amoung the lowest ever achieved for 1.3μm lasers grown by any MBE techniques.

References

[1] H. Sugiura, M. Mitzuhara, H. Oohashi, T. Hirono and K. Nakahima, *J. Crystal Growth*, vol. 147, pp. 1–7, 1995.

[2] A. Adams, *Electron. Lett.*, vol. 22, pp. 249–250, 1986.

[3] T. Tanbun-Ek, R. A. Logan, N. Olsson, H. Temkin, A. M. Sergent and K. W. Wecht, *Appl. Phys. Lett.*, vol. 57, pp. 224–226, 1990.

[4] M. Yamamoto, N. Yamamoto and J. Nakano, *IEEE J. of Quantum Electron.*, vol. 30, pp. 554–561, 1994.

[5] H. Uenohara, M. R. Gokhale, J. C. Dries and S. R. Forrest, *Electron. Letts.*, vol. 33, pp. 1263–1264, 1997.

Wafer-Fused Long-Wavelength VCSELs

Jürgen Joos

We demonstrate double-fused long-wavelength vertical-cavity surface-emitting laser devices with strain compensated InGaAsP active material and AlGaAs-GaAs Bragg reflectors. The wafer fusing process, the fabrication and the device characteristics are discussed in detail.

1. Introduction

Vertical-cavity lasers with an emission wavelength of 1.55 μm and 1.3 μm are very attractive candidates for long distance data transmission. Due to the difficulties in fabricating monolithical Bragg reflectors for the InP-based active material wafer fusion is considered as an important semiconductor technology technique. It allows combining largely mismatched semiconductor material e.g. InP and GaAs. High performance VCSELs with wafer-fused $Al_xGa_{1-x}As$-Bragg reflectors at 1.55 μm [1] as well as 1.3 μm [2] have been presented recently.

2. Wafer Fusion Process

In our 1.55 μm-VCSELs design at least one mirror is mounted by wafer fusion. We investigated the influence of fusion on photoluminescence of the active zone. Moreover the electrical resistance of a fused interface is of importance and characterized for p-p and n-n junctions between InP and GaAs.

A) Influence on Active Material

Wafer fusing is considered as critical concerning interdiffusion of epitaxial layers due to the process parameters. Especially high temperatures are suspected to worsen the active material. We have measured photoluminescence spectra of unfused InP-based material and of material which was fused on GaAs-substrates. In each case the InP substrate was removed before measurement. In both of the following figures the photoluminescence intensity is normalized to the maximum value because it changes due to adjusting inaccuracies of the setup. Fig. 1 depicts the dependence on the mechanical pressure applied in the fusing process. Evidently there is no shift of the peak wavelength even with higher pressures than the standard value of 2.6 MPa. However the FWHM (full width at half

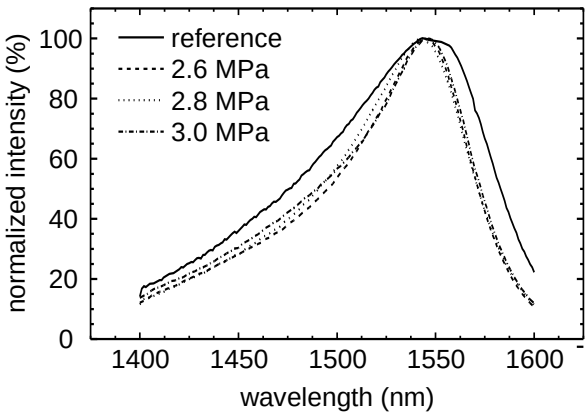

Fig. 1. Influence of applied mechanical pressure under fusing on the photoluminescence of the active quantum wells. Fusing temperature was always 650 °C.

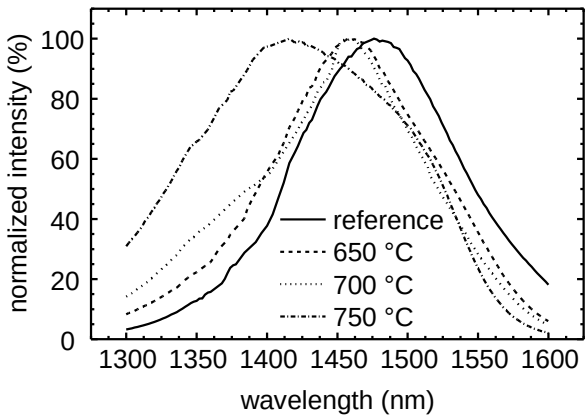

Fig. 2. Influence of different fusion temperatures on the photoluminescence linewidth the of active quantum wells. The applied pressure is 2.6 MPa. The peak offset for fusing at 650 °C and 700 °C is not typical as can be seen in Fig. 1 for fusing at 650 °C.

maximum) of reference curve which is representing the unfused sample is larger than the other ones. This might be explained by a certain inhomogeneity of the epitaxial layers which is cured at the high fusion temperatures.

Fig. 2 represents the temperature dependence. Whether the slight wavelength shift for the samples that were fused at 650 °C and 700 °C, respectively, is due to diffusion processes or lateral inhomogeneity is not too clear. But at 750 °C the PL-curve becomes broader and is shifted by about 50 nm. Summing up, it may be said that the influence of the fusing process at its standard parameters ($p = 2.6\,\mathrm{MPa}$ and $T = 650\,^{\circ}\mathrm{C}$) is negligible.

B) Electrical Resistance of Fusing Interfaces

The electrical resistance of the fusing interfaces is of great importance for the laser performance. With voltage drops of several volts at the interfaces heat is generated which has to be carried off. We have measured the electrical characteristics of fused n-InP/n-GaAs-interfaces and p-InP/p-GaAs interfaces. The measurements have been carried out by means of a four point technique in order to eliminate contact resistances. The characteristics of the samples were $p(\mathrm{GaAs}) = 2 \cdot 10^{19}\,\mathrm{cm}^{-3}$ Zn, $p(\mathrm{InP}) = 1 \cdot 10^{18}\,\mathrm{cm}^{-3}$ Be, $n(\mathrm{GaAs}) = n(\mathrm{InP}) = 1 \cdot 10^{18}\,\mathrm{cm}^{-3}$ Si. The samples were prepared as follows: After the fusing process and the removal of one substrate we have etched mesas and formed two metal contacts on the mesa as well as on the semiconductor below. As it can be seen from the following Fig. 3 the characteristics are linear for both junction types. The slope of the curves indicates mainly the series resistance in the semiconductors. This is confirmed by the higher doping of the p-GaAs which leads to a better conductivity. However the dependence of the interface resistance on doping concentrations still has to be investigated

in detail.

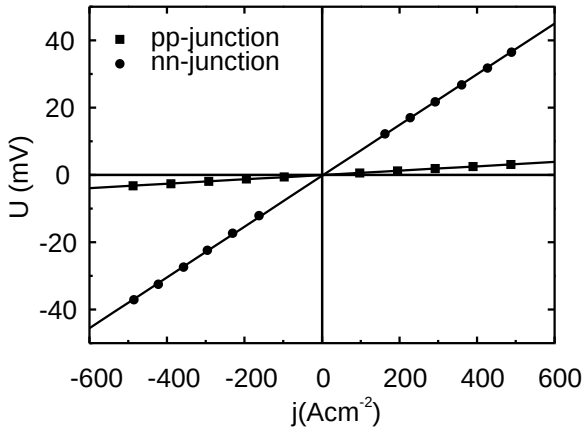

Fig. 3. Current-voltage characteristics of fused p-p and n-n junctions. No voltage offset can be seen, the slope is mainly due to the electrical resistance of the supporting materials.

3. Processing and Characterizing VCSEL Structures

There are several approaches to fabricate long-wavelength VCSELs. Two of them are sketched in Fig. 4. The first approach is a single fused VCSEL where only the bottom Bragg reflector is a semiconductor GaAs-$Al_xGa_{1-x}As$ DBR which is mounted to the InP-based active material by wafer fusing. The top reflector is a hybrid DBR, e.g. Si-Al_2O_3. The second approach is a VCSEL with two GaAs-$Al_xGa_{1-x}As$ Bragg reflectors. We mainly concentrate on double-fused VCSELs.

A) Fabrication

For the double-fused VCSEL wafer fusing of the active material and the p-GaAs-$Al_xGa_{1-x}As$ DBR is the beginning of the fabrication process. After removing the InP-substrate with an HCl-H_3PO_4 etch selectively to an InGaAsP-etch-stop layer the cavity has to be adjusted. This is carried out by step-by-step etching of the top InP-cladding and checking the reflectivity spectrum of the sample. When the adjustment is completed there has to be a resonance dip in the stop band of the DBR exactly at the maximum of the active layer photoluminescence spectrum. After the wafer-fusing of the n-GaAs-$Al_xGa_{1-x}As$ DBR the GaAs-substrate on the p-DBR side is removed for subsequent mesa etching. The substrate removal is done by a spray-etching technique with a NH_4OH-H_2O_2 mixture which is selective to an AlAs-etch-stop layer. For current confinement in the VCSEL an AlAs-layer is incorporated into the p-DBR which is provided to be oxidized laterally after mesa etching. The oxide aperture that is created by this technique has to be placed in the p-DBR because of the much lower carrier mobilities of holes resulting in

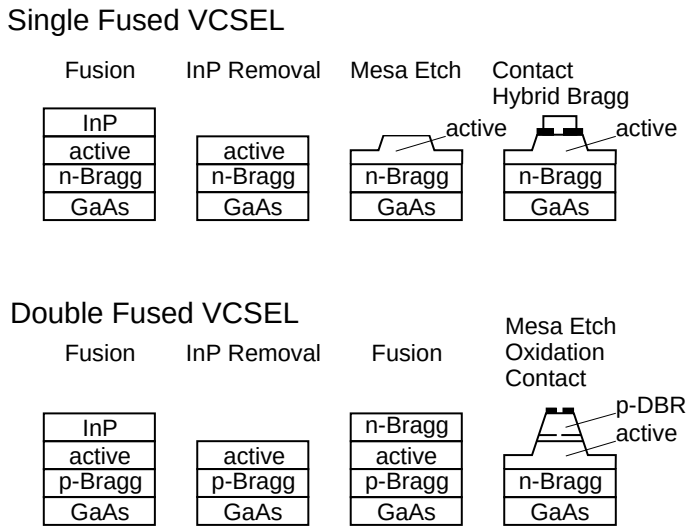

Fig. 4. Approaches for VCSELs devices. The technological steps are schematically depicted for a single and a double-fused device.

current spreading on the p-side of the sample. Mesa etching, oxidation, evaporation and structuring of the metal contacts are completing the process. First samples are processed as described above but without current confinement aperture.

B) Measurements

This section describes measurements of completed double-fused VCSEL structures without current aperture. The devices were found to exhibit LED emission under CW condition at room temperature. Fig. 5 shows the spectrum of a device with about 60 μm diameter at a driving current of 6 mA. One can find suppressed emission in the 100 nm wide region of the DBR stop band except the main resonance at about 1.54 μm wavelength. The site of the main resonance confirms the exact adjustment of the cavity length prior to the second fusing step.

In Fig. 6 the current-voltage characteristics is depicted as well as the optical power measured at a device of 75 μm under CW condition. The voltage can be explained with contact resistance, resistance at the heterointerfaces mainly in the p-DBR, which are not fully optimized, and resistance at the fused p-GaAs-p-InP-interface, which is not totally understood, yet. However the voltages are below 8 V, but no laser activity is found, even under pulsed conditions at higher current densities.

4. Summary

The photoluminescence of strain compensated quantum wells shows negligible dependence on the applied mechanical pressure needed for the fusing process. Fusing temperatures up

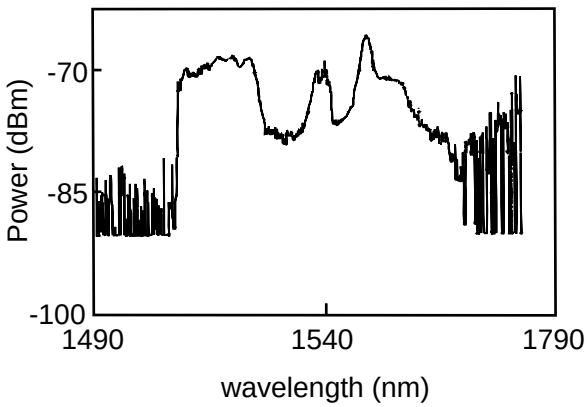

Fig. 5. CW operation of a double-fused VCSELs device. LED emission occurs in the resonance of the cavity and is suppressed in the surrounding top mirror stopband.

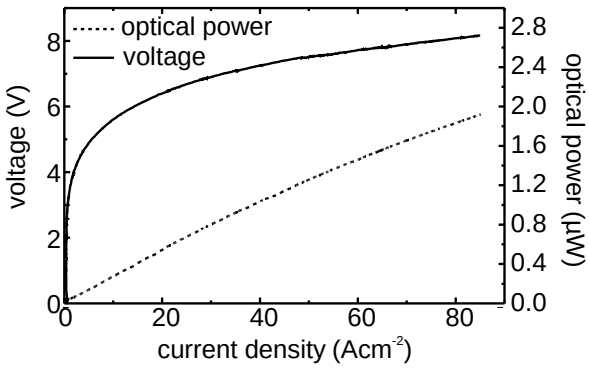

Fig. 6. Current-voltage and current light characteristics of the double-fused device. The light output indicates LED emission.

to 700 °C typically lead to slightly decreased linewidth, 750 °C gives an additional shift in peak wavelength. The fused interface between InP and GaAs exhibits ohmic behavior without any remarkable voltage drop and a series resistance that is mainly due to the resistance of the supporting layers.

Double fused VCSEL devices show emission spectra where the main resonance peak fits well to the photoluminescence of the active material. However with voltages up to 8 V the devices do not show any laser activity. The reason for this is believed to be mainly the bad current confinement due to the missing oxide aperture which will be included in future devices.

References

[1] N.M. Margalit, J. Piprek, S. Zhang, D.I. Babic, K. Streubel, R.P. Mirin, J.R. Wesselmann, and J.E Bowers, "64 °C continuous-wave operation of 1.5 μm vertical-cavity laser", *IEEE J. Sel. Top. Quant. El.*, vol. 3, pp. 359–365, 1997.

[2] Y. Qian, Z.H. Zhu, Y.H. Lo, D.L. Huffaker, D.G. Deppe, H.Q. Hou, B.E. Hammons, W. Lin, and Y.K. Tu "Low-threshold proton-implanted 1.3-μm vertical-cavity top-surface-emitting lasers with dielectric and wafer-bonded GaAs-AlAs Bragg mirrors", *IEEE Photon. Technol. Lett.*, vol 9, pp. 866–868, 1997.

Device Performance of Ultra-Violet Emitting Diodes Grown by MBE

Markus Mayer and Arthur Pelzmann

Ultra-violet emitting diodes with electroluminescence linewidths as narrow as 8 nm have successfully been grown by molecular beam epitaxy. Double-heterostructure pn- and homotype pin-diodes reveal single-peak emission at wavelengths around 371 nm. Turn-on and reverse breakdown voltages are 4 - 5 V and above 30 V, respectively.

1. Introduction

Emerging new applications for nitride based light-emitting diodes (LEDs) include luminescence conversion, where diodes are used to pump phosphors or organic dyes being encapsulated in the LED housing. Here, the light generated by electron-hole recombination is partly absorbed and re-emitted at lower energies [1]. By this down-conversion any visible color, including white light, can be achieved from blue or ultra-violet (UV) emitting *pn*-junctions. UV emitting diodes (UVEDs), however, can also be employed for optical analyses of organic molecules with their numerous absorption bands in this spectral region [2]. Focusing on above applications, we have realized ultra-violet emitting diodes employing homotype *pin*- and double-hetero (DH) *pn*-structures.

2. Structure of UVEDs

The schematics of the employed homotype and DH UVEDs are illustrated in Fig. 1. The homotype *pin*-diode consists of 800 nm Si doped *n*-GaN, followed by a 50 nm intrinsic GaN recombination layer and succeeded by 300 nm Mg doped *p*-GaN. The active layer of the DH *pn*-diode consists of 50 nm *n*-GaN, embedded in 150 nm *n*- and *p*-doped AlGaN cladding layers for carrier confinement. The electroluminescence (EL) is detected through the bottom, i.e. through the *n*-GaN and the transparent sapphire substrate. The UVEDs are grown by gas source molecular beam epitaxy using on surface cracking of ammonia [3]. Elemental Al and Si are supplied by conventional effusion cells, whereas Ga is evaporated from an EPI Sumo effusion cell and MCp_2Mg is used as Mg-source. Details of the growth procedure and luminescence properties are described elsewhere [4, 5]. The homotype devices are grown on c-plane sapphire employing a GaN nucleation layer, whereas a 2 μm thick GaN template grown by MOVPE is employed for the DH-structures. Chemically-assisted ion-beam etching (CAIBE) is performed for dry etching of 150 μm $\times$ 150 μm mesas. Ti/Au and Ni/Au metallization are utilized for *n*- and *p*-contacts.

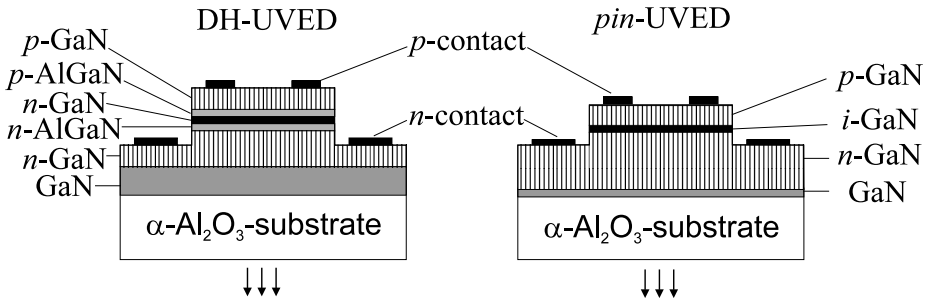

Fig. 1. Schematics of double-heterostructure *pn* and homotype *pin* UVEDs.

3. Properties of UVEDs

The room temperature EL of a homotype *pin*-junction is shown in Fig. 2 for different forward currents, revealing single-peak emission around 371 nm with linewidths as narrow as 12 nm. The energetic position is in agreement with electroluminescence, obtained from GaN homojunctions [6], indicating that electron-hole recombination takes place in the intrinsic layer. Blue emission at 430 nm from transitions related to the Mg level in *p*-GaN [7] is not observable. The abrupt decrease in luminescence on the high energy side of the spectra is attributed to internal absorption as is confirmed by transmission measurements. To confirm the influence of absorption within the Si doped *n*-GaN layer, for comparison, a transmittance spectrum of a Si doped *n*-GaN sample is included in Fig. 2. On the high energy side of the spectra the transmittance and the electroluminescence curves fall together, indicating that the originally generated luminescence is partly absorpted, thus determining intensity and line shape. Fig. 3 depicts the EL spectra obtained from the

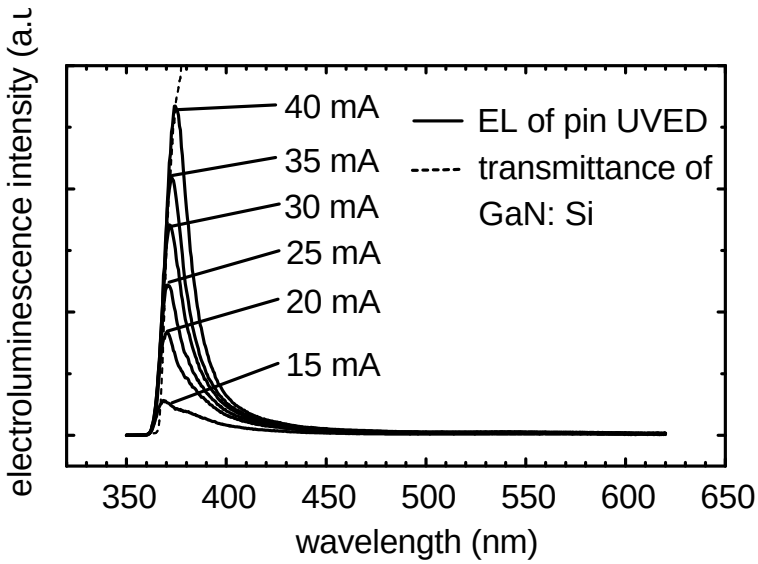

Fig. 2. Electroluminescence of a *pin*-UVED with near-bandedge emission from 370 to 374 nm and linewidths as narrow as 12 nm (300 K)

DH-UVEDs featuring single peak emission at 371 nm with a further reduced linewidth of 8 nm. The DH devices in contrast to the *pin*-diodes show no wavelength shift with increasing forward current and significant internal absorption occurs only at high currents. At 50 mA, the originally generated emission can be extrapolated with the plausible assumption that the absorption at the low-energy side of the EL spectrum is negligible and that the generated emission has a Lorentzian shape, as depicted in Fig. 4. The maximum

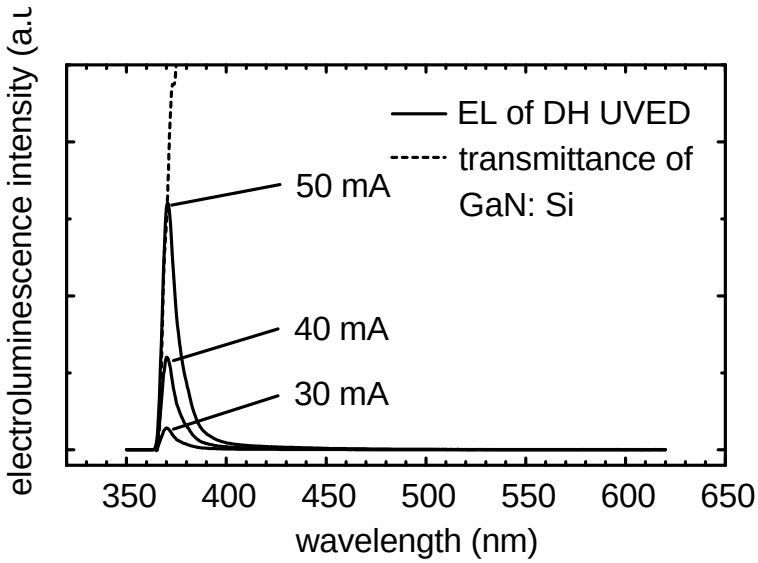

Fig. 3. Electroluminescence of a double-heterostructure UVED with near-bandedge emission at 371 nm and linewidths as narrow as 8 nm (300 K).

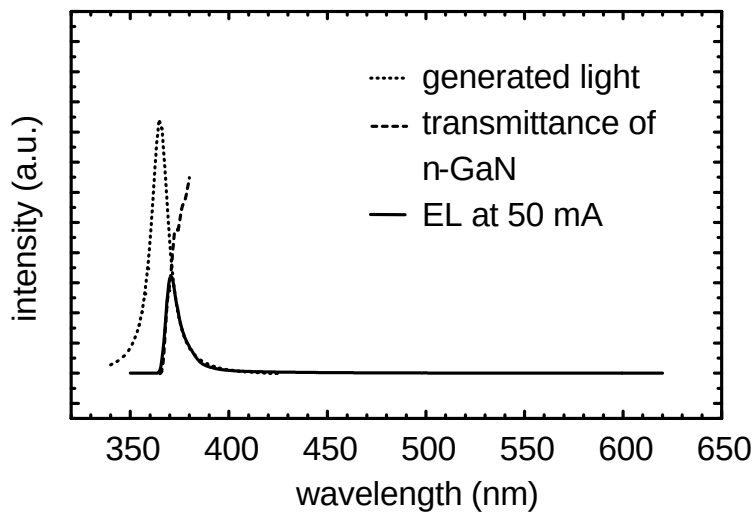

Fig. 4. Electroluminescence of a UVED, assumed light generation in the active layer and the transmission of *n*-GaN.

of the Lorentzian curve peaks close to the bandedge of GaN, between 364 - 366 nm, at energetic positions which is identical to the PL wavelength of *n*-doped GaN at 300 K. The originally generated intensity is 6 times higher than the measured one and the linewidth is still as narrow as 12 nm. Clearly, the Lorentzian curve reveals that internal absorption

within the UVEDs limits to a high degree the luminescence intensity and the device efficiency. The above shown internal absorption is also present in some EL spectra shown by Nakamura [7] and Amano [6], featuring also an abrupt decay at the high energy side. A slightly modified device design, replacing the active GaN layer with InGaN containing a small amount of In, is expected to reduce internal optical absorption.

Current-voltage characteristics of the homotype *pin*-UVEDs reveal series resistances, turn-on and reverse breakdown voltages of 250 Ω, 4 - 5 V and beyond 30 V, respectively. In the case of the DH UVEDs, the electrical characterization yields 400 Ω, 6 - 8 V and beyond 10 V, respectively.

4. Conclusion

Single-peak electroluminescence is achieved with homotype *pin*- and double-heterostructure *pn*-diodes. Homotype devices emit at 370 nm for low currents and slightly shift to 374 nm for higher currents with a linewidth of 12 nm. Double-heterostructure UVEDs reveal emission at 371 nm with a linewidth as narrow as 8 nm. The electroluminescence spectra show an abrupt decrease at the high energy sides caused by internal optical absorption within the structure. The narrow electroluminescence is encouraging for the presented homotype and double-heterostructure UVEDs and shows the potential of the metalorganic precursor MCP_2Mg as *p*-dopant in MBE. We conclude that the electrical properties of the UVEDs are still subject of improvements. An increased *p*-conductivity and a reduced sheet resistance are essentiell for increasing the optical output power.

The device efficiency can further be enhanced, employing a device design with reduced internal optical absorption. This explicitly means to slightly increase the emission wavelength by replacing the active GaN with a slightly In containing InGaN layer.

The author grateful acknowledges the financial support from the German Federal Ministry of Education, Science, Research and Technology (BMBF) under contract number 01 BM 419/9 and the Volkswagen Foundation.

References

[1] S. Nakamura and G. Fasol, *The blue laser diode, GaN based light emitters and Lasers*, Berlin, Heidelberg, New York: Springer Verlag, 1997.

[2] H.H. Perkampus, *UV-VIS Atlas of Organic Compounds*, Weinheim, New York, Basel, Cambridge: VCH Publishers, 1992.

[3] M. Kamp, M. Mayer, A. Pelzmann and K.J. Ebeling, "On surface cracking of ammonia for MBE of GaN", *Mat. Res. Soc. Proc.*, vol. 449, pp. 161-172, 1997.

[4] M. Mayer, A. Pelzmann, C. Kirchner, M. Schauler, M. Kamp, P. Unger and K.J. Ebeling, "Device performance of UV light-emitting diodes grown by MBE", *Proceedings of the Second Int. Conference on Nitride Semiconductors*, pp. 512-513, 1997.

[5] M. Mayer, A. Pelzmann, M. Kamp, K.J. Ebeling, H. Teisseyre, G. Nowak, M. Leszynski, I. Grzegory, S. Porowski, G. Karzcewski, "High quality homoepitaxial GaN grown by molecular beam epitaxy with NH_3 on surface cracking", *Jap. J. Appl. Phys.*, part. 2, vol. 36, no. 12b, L1634-L1636, 1997.

[6] H. Amano, M. Kito, K. Hiramatsu, and I. Akasaki, "P-type conduction in Mg-doped GaN treated with low-energy electron beam irradiation (LEEBI)", *Jpn. J. Appl. Phys.*, vol. 28, L2112-L2114, 1989.

[7] S. Nakamura, T. Mukai, and M. Senoh, "High-power GaN $p-n$ junction blue-light-emitting diodes", *Jpn. J. Appl. Phys.*, vol. 30, pp. 1998-2001, 1991.

MOVPE Growth of InGaN MQW LEDs

Christoph Kirchner and Arthur Pelzmann

Using low pressure Metal Organic Vapor Phase Epitaxy (MOVPE) for GaN growth, we have fabricated nitride based InGaN multi quantum-well (MQW) LED structures grown heteroepitaxially on c-plane sapphire. Blue light emission with a wavelength of 425 nm and a linewidth of 17 nm (120 meV) is obtained from fully processed devices.

1. Introduction

Recently, great interest raised in short wavelength light-emitting devices fabricated from III-V Nitride semiconductors (InAlGaN) with emission wavelengths from the UV to red spectral region. Intensive research on III-V Nitrides has paved the way to commercially available high-power blue and green LEDs [1]. Blue emitting laser diodes with InGaN multi quantum-well structures as active layers are steadily improved and now have lifetimes above 3000 hours at room temperature under CW operation [2].

2. Experimental

Epitaxial growth of GaN is performed in a horizontal, RF heated, water cooled quartz MOVPE reactor (AIXTRON AIX 200 RF), operated at low pressure. Substrate material is sapphire with (0001) orientation (c-plane). Trimethylgallium (TMGa), trimethylaluminium (TMAl), trimethylindium (TMIn) and ammonia are used as group III and group V precursors, respectively. The dopant sources are silane (SiH_4) for n-type and the organometallic source bis-cyclopentadienylmagnesium (Cp_2Mg) for p-type doping. Hydrogen is used as carrier gas. Prior to growth, the substrates are degreased in organic solvents and deionized water, loaded into the reactor and heated up 1000 °C under a steady flow of ammonia. The ammonia is used for nitridation of the sapphire substrate surface, where oxygen atoms from the sapphire surface are supposed to be exchanged against nitrogen from the ammonia to form an AlN intermediate layer [3]. Next, the substrate temperature is lowered to 550 °C and the GaN nucleation layer is deposited to a thickness of approximately 40 nm. After deposition of the nucleation layer, temperature is elevated to 1030 °C and growth of the epitaxial GaN is initiated. InGaN double-heterostructure LEDs consist of 2 μm thick Si-doped GaN, followed by the InGaN active layer. For the InGaN growth, substrate temperature is lowered to 700-800 °C. After InGaN growth, temperature is raised to 1060 °C to grow 0.5 μm p-type GaN using Cp_2Mg at a flow rate of 100 nmol/min. Former DH-LED structures contain InGaN layers with thicknesses of

60 nm as active areas [7]. With an indium mole fraction of 15 %, an emission wavelength of 400 nm can be achieved. For longer wavelength emission (blue spectral region 430 - 470nm), the indium content of the active layer must be increased.

3. Results and Discussion

While InGaN surfaces with 15 % of indium show smooth surface morphologies, InGaN bulk layers with indium contents of 20 % and above show surfaces covered with numerous metallic indium droplets. Two micrographs of InGaN surfaces, grown with different V/III ratios, are displayed in Fig. 1. It can be seen, that the number of droplets can be reduced, but they couldn't be avoided completely.

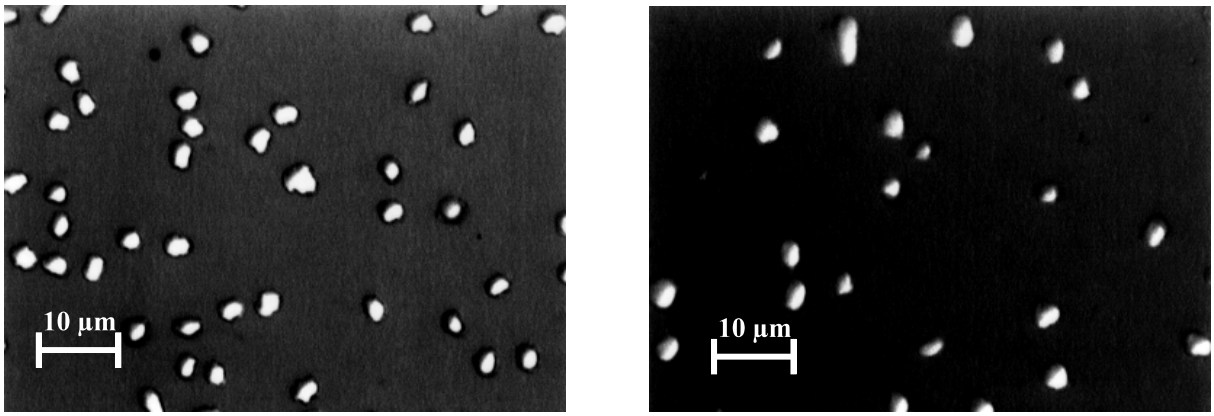

Fig. 1. Surfaces of InGaN layers grown with a V/III ratio of 6000 (left micrograph) and 8300 (right micrograph).

The high equilibrium vapor pressure of nitrogen required for InGaN growth to prevent the dissociation of the In-N bond represents a significant problem in the fabrication of In-based nitride compounds. While MOVPE growth of GaN at 1000 °C results in sufficient decomposition of ammonia on the growing surface, such a high growth temperature cannot be used with In-based compounds due to the weak In-N bonds as well as the high indium desorption from the growing surfaces. Growth of InGaN with high indium mole fractions requires high fluxes of TMIn. The presence of many indium atoms diffusing across the growing surface, coupled with the paucity of nitrogen dangling bonds due to the reduced ammonia decomposition at low growth temperatures, will result in the formation of small indium droplets. Once these droplets reach a critical size, they will become thermodynamically stable and continue to grow. These indium droplets getter other available indium atoms on the growing surface, thus competing with the process of indium incorporation in the solid InGaN phase [4]. However, there are little or no indium droplets observed in thin InGaN layers at short growth times. Therefore, if a thin GaN layer is grown on a thin InGaN layer while indium droplets are not generated or still small, it is possible to prevent the generation of large indium droplets and grow smooth

layers [5]. Thus, the InGaN bulk layer was replaced by a stack, consisting of thin InGaN and GaN layers, with the same total thickness as the bulk InGaN layer. All growth parameters, i.e. temperature, pressure, flows and V/III ratio, were kept the same as for the bulk InGaN layer. Those structures reveal improved surface morphologies shown in Fig. 2. There are only very few small metallic indium droplets. The pits in the epitaxial layer are defects, generated by initiated droplet formation. With increasing number of pairs while the single layers get thinner, the surface morphology becomes smoother, see the right picture of Fig. 2. The left picture shows 6 pairs of 8 nm, and the right picture 9 pairs of 5 nm.

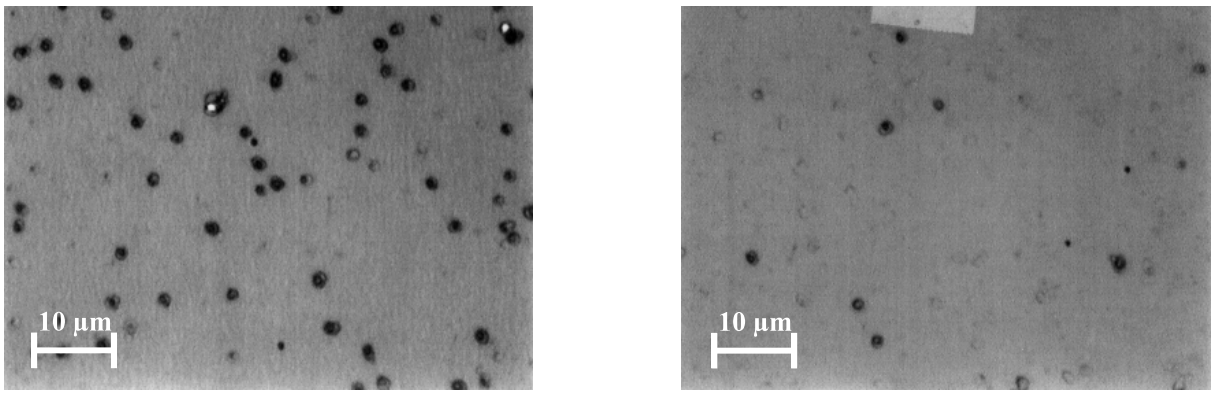

Fig. 2. Surfaces of InGaN multilayered structures with single layer thicknesses of 8 nm (left micrograph) and 5 nm (right micrograph).

To examine the microstructural properties of the InGaN/GaN multilayered structures, TEM (transmission electron microscopy) measurements were performed at the University of Erlangen (B. Jahnen, M. Albrecht and H. P. Strunk). Fig. 3 shows the TEM cross section of a InGaN/GaN multilayered structure. The single layers can be seen very well. The InGaN layers are represented by the darker areas. The different brightnesses in the InGaN areas can be explained either by In-fluctuations or by artefacts from TEM preparation. This is not yet fully cleared. The thickness of only a few nm for a single layer reveals that multi quantum-well structures were grown. Room temperature photoluminescence spectra of several InGaN MWQ structures with different well thicknesses are displayed in Fig. 4. With increasing number of layer pairs, intensity increases, while the FWHM decreases from 13.9 nm down to 11.7 nm. The indium mole fraction of those structures can be calculated from the PL peak wavelength to approx. 22%. This is more than for the bulk layers with 20%, using the same growth parameters. This can be explained by the reduced depletion of the gas phase of indium atoms over the growing surface due to reduced formation of indium droplets. Such MQW structures were embedded into GaN pn-junctions, as shown on the left picture in Fig. 5. The MQW is grown on top of a 2 μm thick GAN:Si layer with an electron concentration of $n = 10^{18}/cm^3$ and is covered by a 0.5 μm thick GaN:Mg layer with a p-type concentration of $10^{17}/cm^3$. Since the Mg is incorporated as an electrically non active Mg-H complex [6], p-type conductivity is only achieved after post-growth annealing in a nitrogen ambient at 750 °C for 15 minutes.

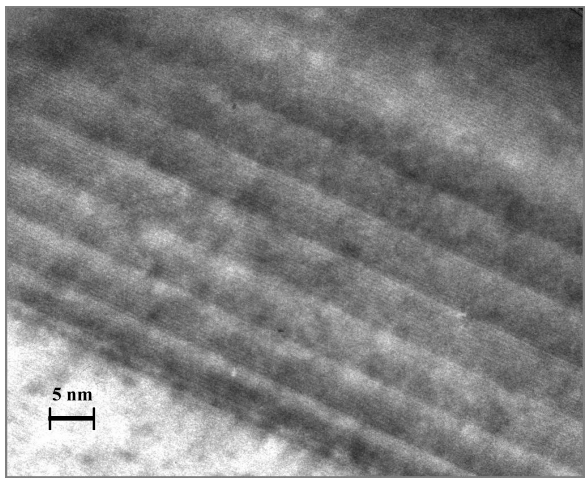

Fig. 3. TEM cross section of InGaN MQW.

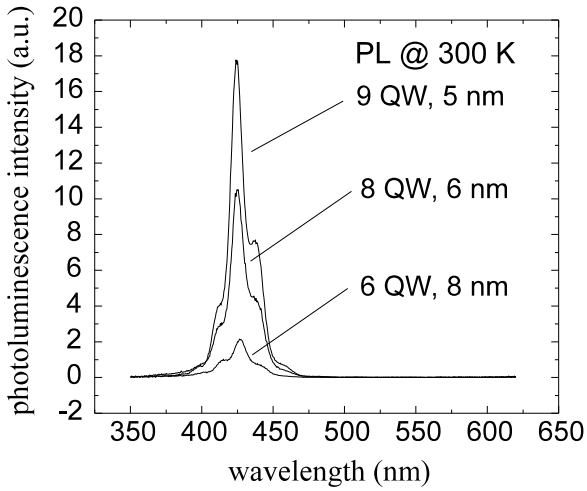

Fig. 4. PL spectra of InGaN MQWs.

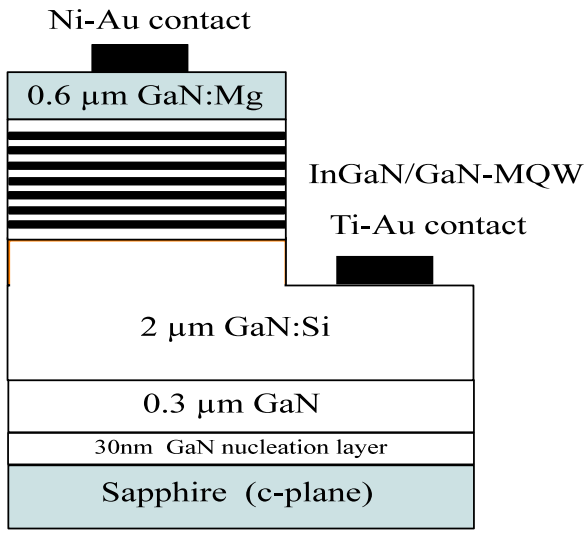

Fig. 5. Device structure of LED with InGaN/GaN MQW.

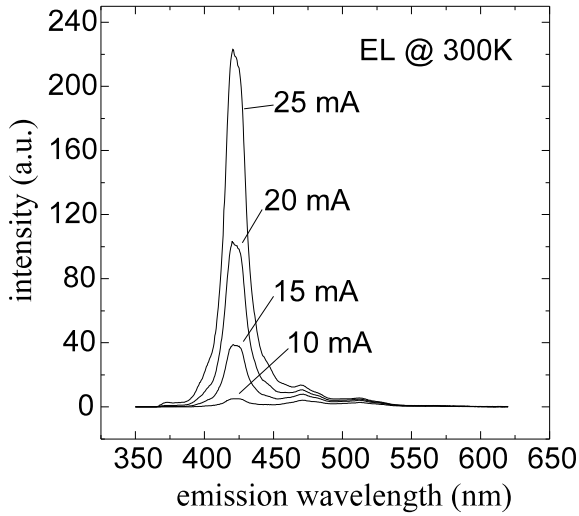

Fig. 6. Emission spectra of InGaN MQW LED for different forward currents.

The fully processed LEDs are characterized regarding their electrical and optical properties by current-voltage curves and electroluminescence (EL), respectively. Processing of the devices is described elsewhere [7]. Fig. 6 shows room temperature electroluminescence spectra of a InGaN MQW LED at various forward currents. The electroluminescence consists of a narrow single peak emission at 425 nm with a linewidth of 17 nm (120 meV). It is worth to be noticed, that the EL peak emission wavelength is the same as measured with PL. The current-voltage characteristic of a InGaN MQW LED shows a turn-on voltage of 3V. The series resistance (contact and sheet resistance) of the MQW LEDs can be calculated to 100 Ohms. A maximum output power of approx. 20 μW was measured through the bottom of the device using a calibrated photo diode, thereby neglecting

emission through the top and the edges.

4. Conclusion

MOVPE grown GaN/InGaN LED structures have been processed to blue emitting GaN LEDs. High indium containing layers without the critical Indium droplet formation were achieved by growth of InGaN/GaN multilayered structures. Single wavelength emission at 425 nm is presented with linewidths as narrow as 17 nm. Besides improvements of the epitaxial growth, i.e. optical and electrical properties, the device design (improved light outcoupling) is subject of further optimization.

References

[1] S. Nakamura, M. Senoh, N. Iwasa and S. Nagahama, "High - brightness InGaN blue, green and yellow light emitting diodes with quantum well structures", *Jpn. J. Appl. Phys.*, vol. 34, pp. L 797–L 799, 1995.

[2] S. Nakamura, M. Senoh, S. Nagahama, N. Iwasa, T. Yamada, T. Matsushita, H. Kiyoku, Y. Sugimoto, T. Kozaki, H. Umemoto, M. Sano and K. Chocho, "InGaN/GaN/AlGaN–based laser diodes with modulation-doped strained-layer superlattices", *Jpn. J. Appl. Phys.*, vol. 36, pp. L 1568–L 1571, 1997.

[3] K. Uchida, A. Watanabe, F. Yano, M. Kouguchi, T. Tanaka and S. Minagawa, "Nitridation process of sapphire substrate surface and its effect on the growth of GaN", *J. Appl. Phys*, vol. 79, pp. 3487–3489, 1996.

[4] S.M. Bedair, F.G. McIntosh, J.C. Roberts, E.L. Piner, K.S. Boutros and N.A. El–Masry, "Growth and characterization of In-based nitride compounds", *J. Crystal Growth*, vol. 178, pp. 32–44, 1997.

[5] M. Shimizu, K. Hiramatsu and N. Sawaki, "Metalorganic vapor phase epitaxy growth of $(In_xGa_{1-x}N/GaN)^n$ layered structures and reduction of indium droplets", *J. Crystal Growth*, vol. 145, pp. 209–213, 1994.

[6] S. Nakamura, N. Iwasa, M. Senoh and T. Mukai, "Hole compensation mechanism of p - type GaN films", *Jpn J. Appl. Phys.*, vol. 31, pp. 1258–1266, 1992.

[7] M. Schauler, C. Kirchner, M. Mayer, A. Pelzmann, F. Eberhard, M. Kamp, P. Unger and K. J. Ebeling, "GaN based LEDs with different recombination zones", *MRS Internet J. Nitride Semicond. Res.*, vol. 2, article 44, 1997.

Blue Light-Emitting Diodes on GaN Substrates, Growth and Characterization

Arthur Pelzmann, Christoph Kirchner and Veit Schwegler

Light-emitting diodes have been grown on GaN single crystals using metal organic vapor phase epitaxy. The homojunction devices were characterized by electroluminescence, photoluminescence and I-V measurements. Intense, single-peak electroluminescence is obtained at 420 nm wavelength, which is attributed to transitions in the p-type GaN underpinned by photoluminescence measurements. The electrical and optical device performance compares favorable to homotype pn-junctions grown on sapphire using identical conditions for growth and characterization. The homoepitaxial light-emitting diodes are twice as bright as the heteroepitaxial devices.

1. Introduction

Homoepitaxial growth of GaN has proven its tremendous potential to achieve superior material quality resulting in photoluminescence (PL) linewidths as narrow as 0.5 meV (see Fig. 1) [1] and a reduction of the dislocation densities by six orders of magnitude. These material qualities can only be attained using a substrate which is identical in crys-

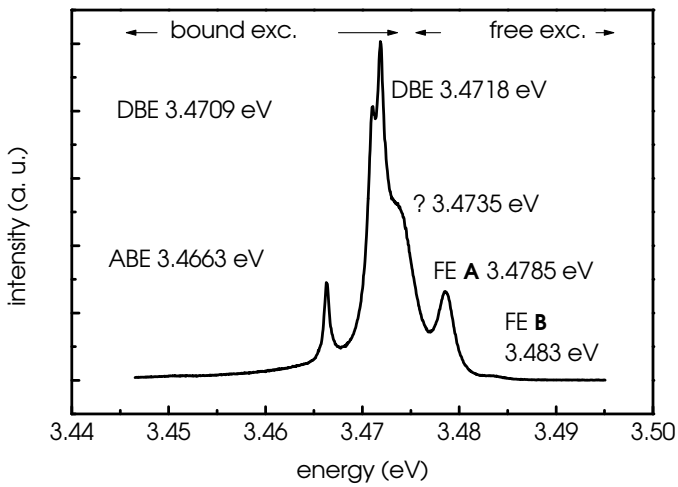

Fig. 1. Photoluminescence of a homoepitaxial GSMBE grown GaN layer at 4.2 K. The linewidth of the donor bound exciton is 0.5 meV.

tal structure, lattice constant and thermal expansion coefficient. Under above conditions,

layer-by-layer growth can be obtained, resulting in two-dimensional growth without generation of dislocations. Additional process steps such as nucleation layers, mandatory in heteroepitaxy of GaN, are no longer required. Besides the fundamental advantages of homoepitaxy, GaN substrates have a high thermal conductivity, facilitating high power applications. Since they are electrically conductive, too, they provide additional freedom for the device design (e.g. vertical current transport) and simplify the device processing. Furthermore, homoepitaxial GaN lasers allow simple facet cleaving. These outstanding properties justify the enormous endeavor conducted at several laboratories on the growth of single crystal GaN substrates [2, 3, 4]. Even when the effort for those substrates is too high for mass products such as LEDs, it might be worth for high power laser applications. Homojunction LEDs on thick GaN layers on sapphire have already been successfully realized by Detchprohm et al. [5]. For the first time, we present a study on LEDs using GaN single crystals as substrates. The GaN substrates have been grown in a high-temperature high-pressure process (fabrication at UNIPRESS in Warsaw, Poland) where the GaN is formed at N_2 pressures up to 20 kbar and at temperatures up to 1600 °C from atomic nitrogen dissolved in a Ga melt. At a growth rate of approximately 100 μm/h perpendicular to the c-plane, the wurtzite crystals are grown up to areas of 70 mm^2 at a thickness of approximately 200 μm. After growth, the nitrogen terminated side later used for epitaxy is mechanically polished. The crystal quality of the GaN substrates is excellent as indicated by x-ray rocking curve measurements [1]. Using Cu$K\alpha_1$ radiation, linewidths of 30 - 40 arcsec are obtained for the (0002) reflex. The excellent structural properties are also pointed out by very low dislocation densities ranging from 10^3 - 10^5 cm^{-2}. The optical quality however is poor, weak and broad yellow PL peaking at 534 nm and a peak at 380 nm is observable at room temperature (RT). No near-bandgap excitonic transition is visible in the RT PL (see Fig. 4 c). The yellow luminescence is consistent with a high density of point defects, probably due to gallium vacancies [6]. The peak at 380 nm is probably due to oxygen impurities in the GaN bulk crystals which are responsible for the high electron concentration of 1×10^{19}cm^{-3} [7, 8].

2. Experimental

The homoepitaxial growth of GaN was performed in a horizontal, RF heated, water cooled quartz MOVPE reactor (AIXTRON AIX 200 RF) operated at low pressures. Trimethylgallium (TMGa), ammonia (NH_3) and bis-cyclopentadienylmagnesium (Cp_2Mg) were used as Ga, N and Mg precursors, respectively. Hydrogen is used as carrier gas. The one side polished GaN substrates (approximately 6×6 mm^2 in size) were heated to 1060 ° C under a steady flow of ammonia to avoid surface degradation. Subsequently to temperature stabilization, a 0.9 μm thick p-GaN layer was deposited. During growth, the flow rates of NH_3 and TMGa were kept at 2.0 slm and 17 μmol/min. The Cp_2Mg flow rate was 90 nmol/min. After growth, thermal annealing under nitrogen ambient at 750 °C was performed to obtain p-type conduction [9]. Hall measurements of the p-type GaN are not possible due to the highly conductive GaN substrate. Therefore, the p-type conduction of the Mg-doped epitaxial layer was verified using rectification method which yields the

conductivity type, but provides no quantitative value for the hole concentration [10]. For measurements of the I-V characteristics, the n-type GaN substrate was mounted on a copper plate using silver glue as backside contact material (n-type). To contact the homoepitaxial p-GaN layer, gold needles were used. Photoluminescence measurements at RT were performed using a HeCd laser with a power density of 16 mW/mm^2 as excitation source. For EL measurements the current was pulsed to allow the usage of a lock-in amplifier. The current pulse-width for EL measurements was 0.7 ms and the duty cycle was 50 %. All EL and PL spectra were corrected, using the spectral response function of our setup to eliminate the spectral sensitivity.

3. Results and Discussion

The I-V characteristics of the homoepitaxial GaN homojunction LED is depicted in Fig. 2. The current is obviously limited by the series resistance (i.e. contact and sheet resis-

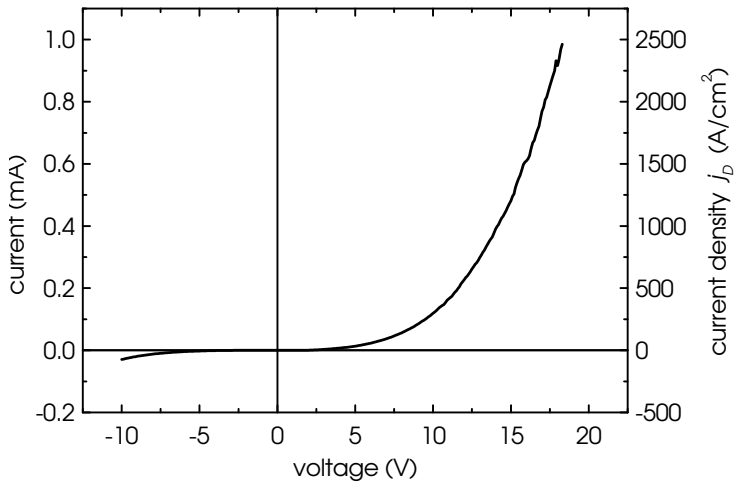

Fig. 2. I-V characteristic of the homoepitaxial GaN homojunction LED.

tances) of the device, which can be deduced to 8 kΩ from the currents at high voltages (U_D larger than a few $(nk_BT)/q$). Considering the voltage drop at the series resistance which is most likely caused by the imperfect contact (Au needle) to the p-material, a turn-on voltage of approximately 4 V can be determined. The EL of the LED shows a intense, single peak at about 420 nm wavelength with a linewidth of 60 nm for low currents (see Fig. 3). A slight peak shift with increasing current from 423 nm to 416 nm is observable probably due to band filling of the Mg acceptor band. The electron-hole recombination takes place in the p-GaN as indicated by the comparison between PL and EL depicted in Fig. 4. The peak wavelengths of the p-GaN PL and the EL are almost identical, as are the linewidths with 50 nm and 60 nm, respectively. Whereas the n-GaN substrate PL shows a broad yellow emission at 534 nm and a defect related emission peak at 380 nm wavelength, which is

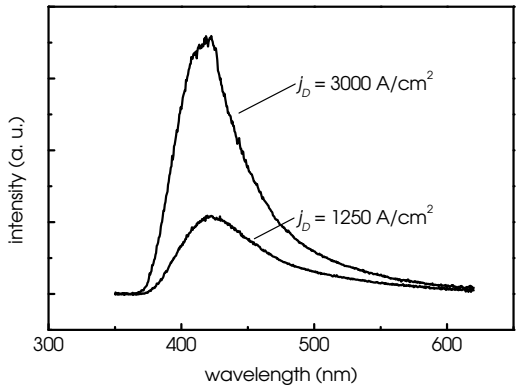

Fig. 3. Room temperature electroluminescence of a homoepitaxially grown GaN LED at different driving current densities.

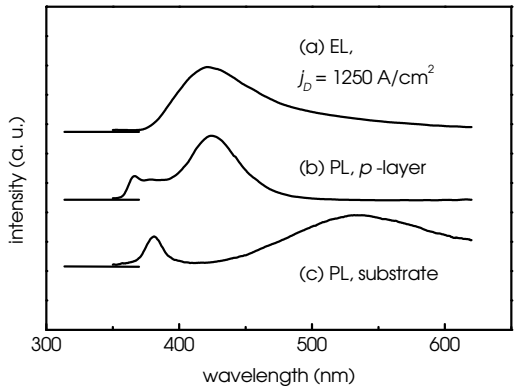

Fig. 4. Comparison between room temperature (a) electroluminescence, (b) photoluminescence of a homoepitaxial GaN LED, and (c) a photoluminescence of GaN bulk crystal. The driving current density j_D for the electroluminescence spectrum (a) is 1250 A/cm^2.

attributed to oxygen impurities. The high quality of the p-GaN is indicated by the occurrence of bandgap PL from the free A exciton at 300 K. For comparison, heteroepitaxial LEDs were grown under identical growth conditions as the homoepitaxial ones except for additional nitridation and nucleation layer steps mandatory on sapphire. As Fig. 5 shows the homoepitaxial LED is twice as bright as the heteroepitaxial LED. Obviously, the peak

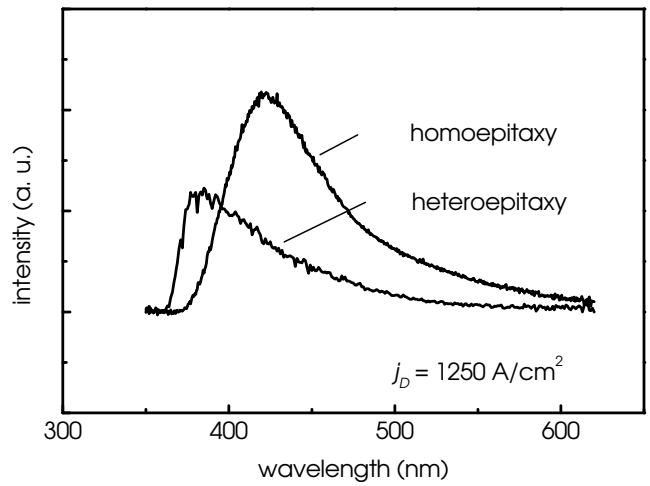

Fig. 5. Comparison of the room temperature electroluminescence of pn-junction GaN LEDs grown homoepitaxially on a bulk GaN crystal and heteroepitaxially on c-oriented sapphire.

wavelength for the heteroepitaxial GaN LED is 384 nm whereas the homoepitaxial LED peaks at 423 nm for the same driving current density j_D of 1250 A/cm^2. According to

Nakamura, under high current densities, the dominance of the EL at about 430 nm is an indicative for high hole concentrations [11]. We assume that the intense blue (420 nm) EL reveals the superiority of the homoepitaxial LED. Since homo- and heteroepitaxial LEDs were grown under nominally identical conditions, we attribute the differences to an increased incorporation of electrical active magnesium into the homoepitaxial *p*-type layer and an enhanced material quality rather than to differences caused by contaminations.

4. Summary

Summarizing these results, we presented for the first time a comprehensive study of homoepitaxial GaN LEDs grown by MOVPE on bulk GaN single crystals. The GaN single crystals were fabricated in a high-pressure high-temperature process. Single-peak blue emission at 420 nm is obtained, with a linewidth of 60 nm. The excellent quality of the homoepitaxial LEDs grown on GaN substrates is revealed by a comparison with heteroepitaxially LEDs on sapphire. The homoepitaxial device is twice as bright as the LED grown on sapphire which peaks in the ultra-violet at 380 nm. This is an indication for a higher hole concentration of the homoepitaxial device. A further significant improvement of the performance can be expected after *p*-contact optimization and growth of double heterostructure LEDs. These results are encouraging for the final objective of homoepitaxial GaN technology, the GaN based high power laser.

Acknowledgments

The authors gratefully acknowledge the financial support by the German Federal Ministry of Education, Science, Research and Technology (BMBF) under contract no. 01 BM 419 / 9 and the Volkswagen Foundation.

References

[1] M. Mayer, A. Pelzmann, M. Kamp, K.J. Ebeling, H. Teisseyre, G. Nowak, M. Leszczynski, I. Grzegory, M. Bockowski, S. Krukowski, B. Lucznik, S. Porowski, G. Karczewski, "High quality homoepitaxial GaN grown by molecular beam epitaxy with NH_3 on surface cracking", *Jpn. J. Appl. Phys.*, Part 2, vol. 36, No. 12b (1997).

[2] J. Karpinski, J. Jun and S. Porowski, "Equilibrium Pressure of N_2 over GaN and high pressure solution growth of GaN" *J. Crystal Growth*, vol. 66 (1984) 1-10.

[3] T. Detchprohm, H. Amano, K. Hiramatsu and I. Akasaki, "The growth of thick GaN film on sapphire substrate by using ZnO" *J. Crystal Growth*, vol. 128 (1993) 384-390.

[4] S. Sakai, S. Kurai, K. Nishino, K. Wada, H. Sato and Y. Naoi, "" *Mat. Res. Soc. Symp. Proc.*, vol. 449 (1997) 15-22.

[5] T. Detchprohm, K. Hiramatsu, N. Sawaki and I. Akasaki, "Metalorganic vapor phase epitaxy growth and characteristics of Mg-doped GaN using GaN substrates", *J. Crystal Growth*, vol. 145, pp. 192–196, 1994.

[6] C. G. Van De Walle and J. Neugebauer, "Theory of point defects and interfaces", *Mat. Res. Soc. Symp. Proc.*, vol. 449, pp. 861–870, 1997.

[7] P. Perlin, T. Suski, A. Polian, J. C. Chervin, E. Litwin-Staszewska, I. Grzegory, S. Porowski and J. W. Erickson, "Spatial distribution of electron concentration and strain in bulk GaN single crystals - relation to growth mechanism ", *Mat. Res. Soc. Symp. Proc.*, vol. 449, pp. 519–524, 1997.

[8] B. C. Chung and M. Gershenzon, "The influence of oxygen on the electrical and optical properties of GaN crystals grown by metalorganic vapor phase epitaxy", *J. Appl. Phys.*, vol. 72, No. 2, pp. 651-659, 1992.

[9] S. Nakamura, T. Mukai, M. Senoh and N. Iwasa, "Hole compensation mechanism of P-Type GaN films", *Jpn. J. Appl. Phys.*, vol. 31, pp. 1258–1266, 1992.

[10] W. A. Keenan, C. P. Schneider and C. A. Pillius, "Type-all system for determining semiconductor conductivity type ", *Solid State Technol.*, vol. 14, 51–56, 1971.

[11] S. Nakamura, T. Mukai and M. Senoh, "High-Power GaN P-N junction blue-light-emitting diodes", *Jpn. J. Appl. Phys.*, vol. 30, No. 12A, pp. L1998–L2001, 1991.

GaN Based LEDs with Different Recombination Zones

Markus Schauler and Arthur Pelzmann

GaN based homo- and heterotype LEDs have been fabricated and characterized which emit in the blue and ultra-violet part of the spectral range. Complete epitaxial LED layer sequences with different recombination zones have been grown using MOVPE as well as MBE. Subsequent to the material growth, chemically-assisted ion-beam etching and contact metallization are utilized to achieve full LED devices. MBE-grown homotype LEDs reveal a peak in the output light spectrum at a wavelength of 372 nm with a linewidth being as narrow as 12 nm. GaN/InGaN LEDs grown by MOVPE show visible single peak emission with linewidths of 23 nm.

1. Introduction

In recent times, there has been increasing interest in light-emitting diodes (LEDs) which emit in the visible spectral range from green to blue [1]. Such devices are key components for LED-based full-color displays that are going to become a significant market over the next years. Another interesting application will be the conversion of blue or UV radiation from GaN-based LEDs into virtually any color by phosphors or organic dyes. Particularly white LEDs are expected to gain a reasonable share of the illumination market because LEDs are smaller, much more robust, and live about 50 times longer compared to ordinary light bulbs [2].

For the presented work on GaN LEDs, two major growth techniques, molecular beam epitaxy (MBE) and metalorganic vapor phase epitaxy (MOVPE) are employed. Processing and characterization of the devices are performed under identical conditions. Differences in the device performance can therefore be attributed to the vertical structure of the LED.

2. Experimental

All GaN structures are grown on c-plane oriented sapphire. Details on the MOVPE and MBE growth processes have been reported earlier ([6],[7]). The structures in general consist of approximately 1 μm of n-type GaN topped by 0.5 μm to 1 μm of p-type GaN. For the homotype MBE-grown LED, an additional 50-nm-thin undoped recombination zone is inserted between n- and p-type material. The recombination zone for the heterotype MOVPE LED consists of a 50-nm-thick $In_{0.15}Ga_{0.85}N$ layer.

The processing steps needed to get full devices have been presented in [8].

3. Results

A typical IV characteristics of a LED is shown in Figure 1. Turn-on voltages of the devices are between 2.5 and 3 V; breakdown occurs at a reverse voltage of approximately 8 V. A series resistance of 60 Ω can be deduced from the IV characteristics, which is comparable to the values of commercially available devices. The specific contact resistance is determined using circular transmission-line structures [4]. On p-type GaN with $p \approx 1 \cdot 10^{17}\,\mathrm{cm}^{-3}$, a value of $1 \cdot 10^{-2}\,\Omega\,\mathrm{cm}^2$ for Ni/Au contacts is achieved. On n-type material with free electron concentrations of about $n \approx 1 \cdot 10^{19}\,\mathrm{cm}^{-3}$, specific contact resistances are in the $10^{-5}\,\Omega\,\mathrm{cm}^2$ range for Ti/Au contacts.

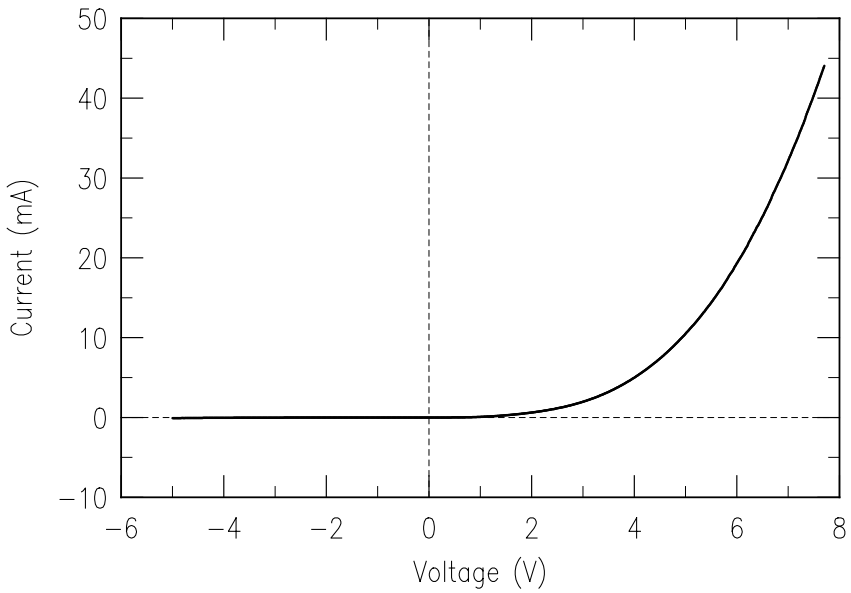

Fig. 1. IV characteristic of a homotype MOVPE-grown LED. Typical devices exhibit turn-on volages between 2.5 and 3 V, breakdown voltages of approximately 8 V, and series resistances of 60 Ω.

Homotype LEDs fabricated from MOVPE material feature emission spectra as shown in Figure 2. A relatively broad electroluminescence (EL) band with the two emission peaks gives the LED a bluish-white appearance, which additionally varies with current since the relative intensities of the peaks change. At lower current densities, the maximum intensity occurs at a wavelength of about 440 nm. Such an emission can be attributed to the Mg related transitions which is also observable in photoluminescence (PL) spectra at 300 K. At higher current densities Figure 2 reveals the dominance of the emission at 380 nm. This is in accordance to S. Nakamura's observations [5] who found a similar behavior for his homotype GaN LEDs in case of a non-perfect p-doping.

LEDs featuring a separate recombination zone behave different as can be observed in the single peak spectra shown in Figures 3 and 4. The MBE-grown homotype LED which contains the above mentioned 50-nm-thick undoped recombination zone, reveals a

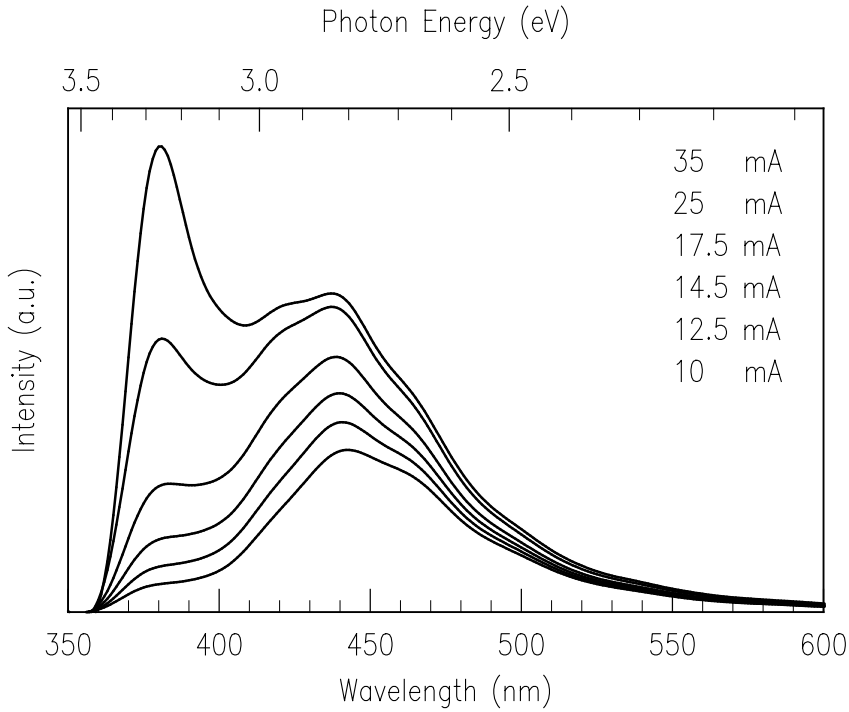

Fig. 2. Electroluminescence spectra of a homotype MOVPE-grown LED at different driving currents. Relatively broad electroluminescence ranges are observed. The peak emission at a wavelength of 440 nm (Mg related transitions) for low driving currents shift towards 380 nm for high current densities.

narrow electroluminescence linewidth with a full-width at half-maximum (FWHM) value of only 12 nm at a peak wavelength of 372 nm when operated at a driving current of 20 mA (Figure 3). A variation of the current from 25 mA to 40 mA results in a very small shift of the emission peak from 368 nm to 374 nm. No indication of Mg-induced recombination, neither at 430 nm nor at 380 nm, is observed in the EL spectra. Only one radiative transition path is prominent in this structure. From the energetic position, it can be derived that the light generation occurs in the undoped GaN region between *p*- and *n*-type material. The difference in the peak PL emission at a wavelength of 364 nm related to the free exciton transition and the EL emission peak at 368 nm is probably attributed to ohmic heating. Since the light generated in the intrinsic region of the junction is absorbed in the *p*- and *n*-doped cladding layers, the lineshape reveals a sharp decrease at the high energy side and a broader tail at the low energy side of the spectrum which also leads to a reduction in linewidth.

GaN / InGaN / GaN double heterostructure LEDs grown by MOVPE reveal emission spectra as shown in Figure 4. The device features single peak emission at a wavelength of 392 nm with a FWHM linewidth as small as 23 nm. Even at high driving current densities, an intrinsic GaN peak can barely be detected in the spectrum nor is the Mg-related long wavelength tail present. The wavelength shift caused by driving current variation

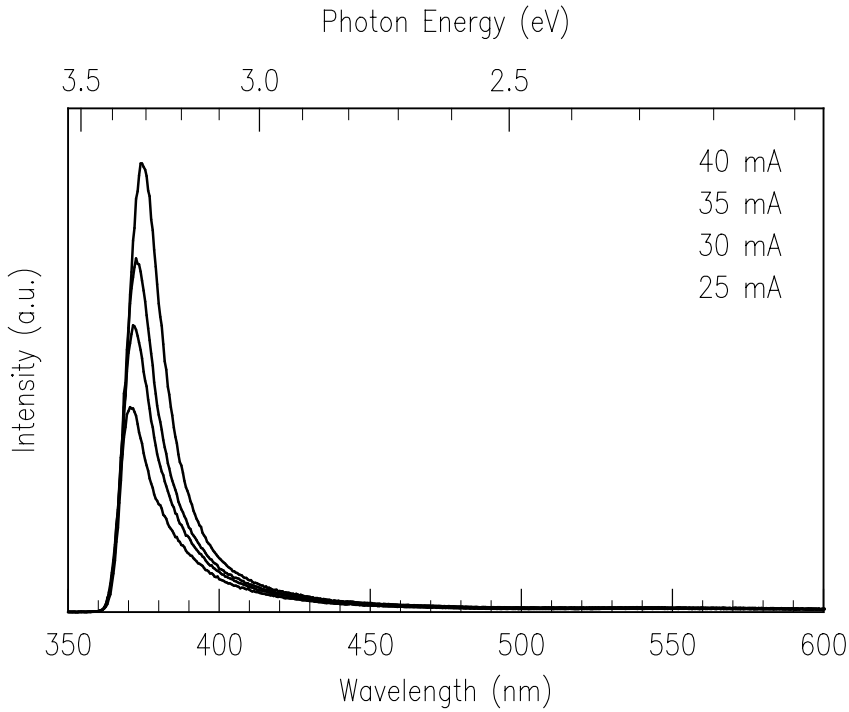

Fig. 3. Electroluminescence spectra of a homotype MBE-grown LED featuring an undoped recombination layer at different driving currents. A FWHM linewidth of only 12 nm at a peak wavelength of 372 nm is observed.

is negligible. PL measurements on a sample with an InGaN layer embedded in undoped GaN grown under identical conditions show a transitions at an emission wavelength of 401 nm, proving that recombination takes place in the InGaN layer of the LED.

A comparison of the EL spectra obtained from the different LEDs reveals striking differences which are attributed to the vertical structures rather than to the different growth techniques. The standard homotype *pn*-junction (Figure 2) is in almost every feature (lineshape, linewidth, current dependence, peak positions, etc.) similar to results obtained by Nakamura [5] for *p*-doping of about $1 \cdot 10^{17}\,\mathrm{cm}^{-3}$. With introduction of an intrinsic GaN layer (Figure 3), the transitions at 440 nm and 380 nm are no longer present, indicating that the electron-hole recombination does not occur in the Mg-doped part of the junction, but in the intrinsic region. This leads to single peak emission and a significant reduction of the linewidth, however, the structure suffers from internal absorption. Since the observed small linewidth of 12 nm is partially caused by the absorption mechanism, this feature can not be compared to results obtained with LEDs where no internal absorption occurs. Substitution of the intrinsic GaN recombination layer with InGaN provides an improved carrier confinement and avoids internal absorption (Figure 4).

The optical output power of the LEDs has been measured with a calibrated Ulbricht sphere. For the MOVPE-grown homojunction LED (Figure 2) a saturation occurs at

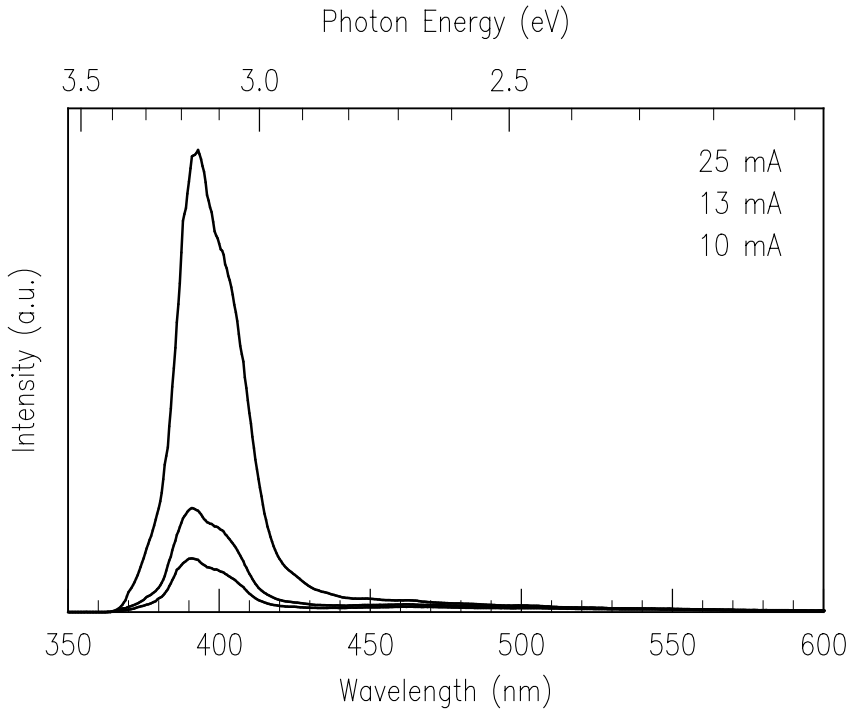

Fig. 4. Electroluminescence spectra of a heterotype MOVPE-grown InGaN/GaN LED at different driving currents. Due to the heterostructure, the emission peak is shifted towards longer wavelengths (392 nm) having a FWHM linewidth of 23 nm.

a power level of about 0.7 μW and a corresponding driving current of 30 mA. Under comparable conditions we do not observe a saturation for the MBE homojunction with recombination layer (Figure 3). However, the output power is lower (0.4 μW at 25 mA) because a significant part of the generated light is absorbed in the cladding layers.

References

[1] S. Nakamura, T. Mukai, M. Senoh, "Candela-class high-brightness InGaN/AlGaN double-heterostructure blue-light-emitting diodes", *Appl. Phys. Lett.* vol. 64, pp. 1687–1689, 1994.

[2] P. Schlotter, R. Schmidt, J. Schneider, "Luminescence conversion of blue light emitting diodes", *Appl. Phys. A* vol. 64, pp. 417–418, 1997.

[3] M. Kamp, M. Mayer, A. Pelzmann, K.J. Ebeling, "On surface cracking of ammonia for MBE growth of GaN", *Mat. Res. Soc. Symp. Proc.* vol. 449, pp. 161–172, 1997.

[4] G.K. Reeves, "Specific contact resistance using a circular transmission line model", *Solid-State Electronics* vol. 23, pp. 487–490, 1980.

[5] S. Nakamura, T. Mukai, M. Senoh, "High-power GaN p-n junction blue-light-emitting diodes", *Jpn. J. Appl. Phys.* vol. 30, pp. L1998–L2001, 1991.

[6] C. Kirchner, M. Kamp, "GaN-based light emitting diodes grown by low pressure MOVPE", *University of Ulm, Dept. of Optoelectronics*, Annual Report 1996.

[7] M. Mayer, M. Kamp, "Molecular beam epitaxy of GaN – homoepitaxial films and LEDs", *University of Ulm, Dept. of Optoelectronics*, Annual Report 1996.

[8] M. Schauler "Fabrication of GaN LEDs", *University of Ulm, Dept. of Optoelectronics*, Annual Report 1996.

Ph.D. Theses

[Ph.D.-1] Fiedler, U., *Hochbitratige optische Nachrichtenübertragung mit Vertikallaserdioden*, Ph.D. Thesis, Dept. of Optoelectronics, University of Ulm, 1997.

[Ph.D.-2] Dai, Z., *Numerical Simulation of High-Power Semiconductor Laser Amplifiers*, Ph.D. Thesis, Dept. of Optoelectronics, University of Ulm, 1997.

Diploma Theses and Semester Projects

[D-1] Förstner, Jörg, *Steuerung und Regelung der optischen Ausgangsleistung eines Titan-Saphirs zur Einkopplung in Halbleiterlaserverstärker mit definierter Leistung*, Semester Project, Dept. of Optoelectronics, University of Ulm, 1997.

[D-2] Köhler, Bernd, *Aufbau eines computergesteuerten Meßplatzes zur Analyse der Harmonischen-Generation von nichtlinearen Bauelementen*, Semester Project, Dept. of Optoelectronics, University of Ulm, 1997.

[D-3] Schreiner, Matthias, *Aufbau eines Autokorrelators zur Analyse kurzer optischer Laserimpulse im ps-Bereich*, Semester Project, Dept. of Optoelectronics, University of Ulm, 1997.

[D-4] Czwella, Dirk, *Aufbau eines Meßplatzes zur Vermessung hochreflektierender Bragg-Reflektoren für Laseranwendungen*, Semester Project, Dept. of Optoelectronics, University of Ulm, 1997.

[D-5] Mohn, Brigitta, *Strukturierung und Vermessung dielektrischer Bragg-Reflektoren für Laseranwendungen*, Semester Project, Dept. of Optoelectronics, University of Ulm, 1997.

[D-6] Ziegler, Volker, *Untersuchung der Diffusion von Zink in Galliumnitrid*, Semester Project, Dept. of Optoelectronics, University of Ulm, 1997.

[D-7] Martin, Ulrich, *Selektiv oxidierte Vertikallaserdioden für die hochfrequente Nachrichtenübertragung*, Diploma Thesis, Dept. of Optoelectronics, University of Ulm, 1997.

[D-8] Abele, Peter, *Untersuchung statischer Emissionseigenschaften an vertikalemittierenden Laserdioden mit elliptischer Geometrie*, Semester Project, Dept. of Optoelectronics, University of Ulm, 1997.

[D-9] Stangl, Markus, *Prozeßentwicklung zur Spiegelbeschichtung von Laserdioden*, Diploma Thesis, Dept. of Optoelectronics, University of Ulm, 1997.

[D-10] Schwegler, Veit Matthäus, *Optische und elektrische Charakterisierung von Galliumnitrid-Leuchtdioden*, Semester Project, Dept. of Optoelectronics, University of Ulm, 1997.

[D-11] Koerbler, Ulrich, *Untersuchung von Einschalteffekten bei Vertikallaserdioden*, Diploma Thesis, Dept. of Optoelectronics, University of Ulm, 1997.

[D-12] Miller, Michael, *Untersuchungen an oberflächenemittierenden Laserdioden mit Vertikalresonator hoher Ausgangsleistungen*, Diploma Thesis, Dept. of Optoelectronics, University of Ulm, 1997.

[D-13] Waidmann, Stephan, *Untersuchung von Plastikfasern in optischen Übertragungssystemen*, Semester Project, Dept. of Optoelectronics, University of Ulm, 1997.

[D-14] Müller, Steffen, *Herstellung und Charakterisierung eines linearen Vertikallaserdiodenarrays*, Diploma Thesis, Dept. of Optoelectronics, University of Ulm, 1997.

[D-15] Meyer, Roman, *Herstellung und Charakterisierung von trapezförmigen Lasern und Vertärkern*, Diploma Thesis, Dept. of Optoelectronics, University of Ulm, 1997.

[D-16] Splitthof, Karsten, *Untersuchung schneller Schaltvorgänge in oberflächenemittierenden Laserdioden im AlGaAs-InGaAs Materialsystem*, Diploma Thesis, Dept. of Optoelectronics, University of Ulm, 1997.

[D-17] Mistele, David, *Charakterisierung von nitridischen Verbindungshalbleitern*, Diploma Thesis, Dept. of Optoelectronics, University of Ulm, 1997.

[D-18] Rinke, Titus, *Einbrennverfahren von Siebdruckpasten zur Metallisierung von Solarzellen*, Diploma Thesis, Siemens Solar GmbH, München.

[D-19] Rabel, Matthias, *Erzeugung kurzer optischer Impulse hoher Leistung mit Vertikallaserdioden*, Semester Project, Dept. of Optoelectronics, University of Ulm, 1997.

[D-20] Riedel, Markus, *Untersuchung zur Realisierung eines faseroptischen Wellenlängenzuordnungssystems*, Semester Project, DaimlerBenz AG,Ulm.

[D-21] Deichsel, Eckhard, *Entwicklung einer Prozeßtechnologie zur Herstellung von Halbleiter-Laserdioden mit trockengeätzten Resonatorspiegeln*, Diploma Thesis, Dept. of Optoelectronics, University of Ulm, 1997.

[D-22] Schäuble, Philipp, *Charakterisierung epitaktisch abgeschiedener Polysilizium-Schichten*, Diploma Thesis, Bosch, Reutlingen.

[D-23] Mönch, Udo, *Aufbau und Charakterisierung eines linearen Laserdiodenmoduls*, Diploma Thesis, Dept. of Optoelectronics, University of Ulm, 1997.

[D-24] Thalmaier, Carmen, *Herstellung und Charakterisierung von Leistungslaserdioden mit Vertikalresonator in Array-Anordnungen*, Diploma Thesis, Dept. of Optoelectronics, University of Ulm, 1997.

[D-25] Golling, Matthias, *Wachstum und Charakterisierung von InGaP Quantenfilmen für Laserdioden*, Diploma Thesis, Dept. of Optoelectronics, University of Ulm, 1997.

[D-26] Sönmez, Ertugrul, *Optimierung von Legierkontakten auf n^+ GaAs für Halbleiterlaserdioden*, Semester Project, Dept. of Optoelectronics, University of Ulm, 1997.

[D-27] Schwegler, Veit Matthäus, *Wachstum und Charakterisierung von Galliumnitrid-Leuchtdioden*, Diploma Thesis, Dept. of Optoelectronics, University of Ulm, 1997.

[D-28] Schiehlen, Eckart, *Herstellung und Untersuchung von Diodenlaserarrays hoher Ausgangsleistung*, Diploma Thesis, Dept. of Optoelectronics, University of Ulm, 1997.

[D-29] Ecker, Irene, *Herstellung von Leuchtdioden und Laserdioden mit Vertikalresonator mittels Wafer-Fusing*, Diploma Thesis, Dept. of Optoelectronics, University of Ulm, 1997.

Talks and Seminars

[T-1] H.Y.A. Chung, D. Sowada, T. Wipiejewski, G. Stareev, and K.J. Ebeling, "Gas source molecular beam epitaxy of laser diodes with strain compensated MQWs operating at 1.5 μm and 1.3 μm", *Invited talk at the Dept. of Technical Physics*, University of Erlangen, Germany, May 1997.

[T-2] H.Y.A. Chung, G. Stareev, J. Joos, J. Maehnss, and K.J. Ebeling, "Gas source MBE of GRINSCH InAsP/InGaAsP MQW laser diodes emitting at 1.3 μm", *National MBE Workshop*, Bremen, Germany, Sept. 1997.

[T-3] H.Y.A. Chung, G. Stareev, J. Joos, J. Maehnss, and K.J. Ebeling, "Low threshold InAsP/InGaAsP quantum well GRINSCH lasers grown by GSMBE", *12. Workshop des DGKK-Arbeitskreises "Epitaxie von III/V–Halbleitern"*, Evangelische Akademie Tutzing, Germany, Dec. 1997.

[T-4] K.J. Ebeling, "Highly efficient VCSELs for optical interconnects", *Japanese–German Workshop*, Berlin, Germany, Mar. 1997.

[T-5] K.J. Ebeling, "Research on GaN at Ulm University", *Japanese–German Workshop*, Berlin, Germany, Mar. 1997.

[T-6] K.J. Ebeling, "Neue Entwicklungen in der optischen Informationstechnik", *Frühjahrsakademie '97*, Ulm University, Germany, Mar. 1997.

[T-7] K.J. Ebeling, "Potential und Chancen von Vertikallaserdioden", *Opto–Kolloquium, Siemens AG*, Regensburg, Germany, June 1997.

[T-8] K.J. Ebeling, "Laser diodes", *Laser '97, Topical Meeting on Novel Lasers, Devices and Applications*, München, Germany, June 1997.

[T-9] K.J. Ebeling, "Multimedia - Herausforderungen an die Hochtechnologie", *Tagung der Universitätskanzler*, Stadthaus Ulm, Germany, Sept. 1997.

[T-10] K.J. Ebeling, "Diodenlaser für die Kommunikation", DPG–Schule für Physik, Bad Honnef, Germany, Sept. 1997.

[T-11] K.J. Ebeling, "Halbleiter–Mikrolaser: Physikalische Eigenschaften und Anwendungen in der optischen Datenübertragng", *Symposium zur Heinrich–Hertz–Stiftungsprofessur*, University of Bonn, Germany, Oct. 1997.

[T-12] K.J. Ebeling, "High performance vertical cavity laser diodes", NEC, Tsukuba, Japan, Nov. 1997.

[T-13] K.J. Ebeling, "Chancen der Optoelektronik: Lichtquellen als Schlüsselkomponenten", *Elektrotechnisches Kolloquium*, University of Stuttgart, Germany, Nov. 1997.

[T-14] K.J. Ebeling, "Vertical cavity surface emitting laser diodes: technology, properties, applications, part I", University of Montpellier II, France, Nov. 1997.

[T-15] K.J. Ebeling, "Vertical cavity surface emitting laser diodes: technology, properties, applications, part II", University of Montpellier II, France, Nov. 1997.

[T-16] M. Golling, H.Y.A. Chung, and K.J. Ebeling, "Gas source MBE von InAlGaP/InGaP MQW Laserdioden", *12. Workshop des DGKK–Arbeitskreises "Epitaxie von III/V–Halbleitern"*, Evangelische Akademie Tutzing, Germany, Dec. 1997.

[T-17] M. Kamp, C. Kirchner, M. Mayer, A. Pelzmann, M. Schauler, P. Unger, and K.J. Ebeling, "GaN basierende Leuchtdioden: Epitaxie, Prozessierung und Charakterisierung", University Nürnberg–Erlangen, Erlangen, Germany, July 1997.

[T-18] M. Kamp, "Doping of group–III nitride semiconductors", *IUVSTA Workshop on "Growth and Processing of GaN and Related Materials"*, Hawaii, USA, Aug. 1997.

[T-19] M. Kamp, C. Kirchner, M. Mayer, A. Pelzmann, M. Schauler, P. Unger, and K.J. Ebeling, "GaN basierende Leuchtdioden: Wachstum, Prozessierung und Charakterisierung", *VW–Photonik, Symposium*, Würzburg, Germany, Oct. 1997.

[T-20] M. Kamp, M. Mayer, A. Pelzmann, C. Kirchner, and K.J. Ebeling, "Growth kinetics of group III nitrides using ammonia in MBE", *GaN Workshop*, Schloß Ringsberg, Germany, Dec. 1997.

[T-21] M. Kamp, C. Kirchner, M. Mayer, A. Pelzmann, M. Schauler, and K.J. Ebeling, "GaN basierende Leuchtdioden: Anwendungen, Grundlagen und Technologie", Forschungszentrum Jülich, Institut für Schicht- und Ionentechnik, Germany, Dec. 1997.

[T-22] C. Kirchner, A. Pelzmann, M. Schauler, M. Kamp, V. Schwegler F. Eberhard, P. Unger, and K.J. Ebeling, "MOVPE von InGaN MQW LED's", *12. Workshop des DGKK–Arbeitskreises "Epitaxie von III/V–Halbleitern"*, Evangelische Akademie Tutzing, Germany, Dec. 1997.

[T-23] C. Kirchner, M. Mayer, A. Pelzmann, M. Schauler, F. Eberhard, M. Kamp, P. Unger, and K.J. Ebeling, "GaN based LEDs by MOVPE and MBE", *Electrochemical Society Meeting*, Paris, France, 1997.

[T-24] M. Mayer, A. Pelzmann, M. Schauler, M. Kamp, and K.J. Ebeling, "MBE von Nitrid–basierenden LEDs unter Verwendung von MCp2Mg", *12. Workshop des*

DGKK–Arbeitskreises "Epitaxie von III/V–Halbleitern", Evangelische Akademie Tutzing, Germany, Dec. 1997.

[T-25] R. Michalzik, D. Wiedenmann, B. Weigl, P. Schnitzer, W. Schmid, C. Jung G. Reiner, R. Jäger, M. Grabherr, and K.J. Ebeling, "50 % conversion efficiency GaAs based VCSELs", Bell Laboratories, Lucent Technologies, Murray Hill, NJ, USA, Aug. 1997.

[T-26] R. Michalzik, M. Grabherr, R. Jäger, C. Jung, R. King, W. Schmid G. Reiner, P. Schnitzer, B. Weigl, D. Wiedenmann, and K.J. Ebeling, "Vertikallaserdioden – zukunftsträchtige Bauelemente für die optische Verbindungstechnik", *Research Forum 1997 of the German Ministry for Research and Technology*, Leipzig, Germany, Sept. 1997.

[T-27] R. Michalzik, P. Schnitzer, M. Grabherr, R. Jäger, C. Jung, W. Schmid R. King, D. Wiedenmann, B. Weigl, and K.J. Ebeling, "VCSEL research at Ulm University - An overview", Hewlett - Packard Company, Optical Communication Division, San Jose, CA, USA, Nov. 1997.

[T-28] R. Michalzik, M. Grabherr, R. Jäger, C. Jung, W. Schmid R. King, P. Schnitzer, D. Wiedenmann, B. Weigl, and K.J. Ebeling, "Recent advances in VCSEL research at Ulm University", Sandia National Laboratories, Albuquerque, NM, USA, Nov. 1997.

[T-29] M. Schauler, "Leuchtdioden auf GaN–Basis, hergestellt mit MBE und MOVPE", *Frühjahrstagung der Deutschen Physikalischen Gesellschaft*, Münster, Germany, Mar. 1997.

[T-30] M. Schauler, "GaN based LED's with different recombination zones", *EGW–2 Workshop*, Valbonne, France, June 1997.

[T-31] P. Schnitzer, "VCSELs for data transmission", University of the Philippines, Quezon City, Febr. 1997.

[T-32] P. Unger, "Halbleiterlaserdioden mit hoher optischer Ausgangsleistung", *Elektrotechnisches Kolloquium*, Gesamthochschule Kassel, Germany, Jan. 1997.

[T-33] P. Unger, "Herstellungstechnologie und Eigenschaften von Halbleiterlaserdioden für Anwendungen im Hochleistungsbereich", *Seminar der technischen Physik*, University of Würzburg, Germany, June 1997.

[T-34] D. Wiedenmann, "Hochfrequenzeigenschaften von Vertikallaserdioden", University of Marburg, Germany, Oct. 1997.

[T-35] S. Christiansen, M. Albrecht, C. Hierl, H.P. Strunk, A. Pelzmann M. Mayer, M. Kamp, and K.J. Ebeling, "The early stages of III–Nitride growth - the playground of low crystal symmetry and high strain", *Electron. Microscopy Halle*, Saale, Germany, 1997.

[T-36] I. Daumiller, A. Vescan, E. Kohn, C. Kirchner, and M. Kamp K.J. Ebeling, "Technologie von GaN Feldeffekttransistoren", *12. Workshop des DGKK–Arbeitskreises "Epitaxie von III/V–Halbleitern"*, Evangelische Akademie Tutzing, Germany, Dec. 1997.

[T-37] K. Kornitzer, M. Mayer, M. Kamp, A. Pelzmann, K. Thonke, K.J. Ebeling, and R. Sauer, "Photoleitfähigkeitsmessungen an GaN–Schichten auf Saphirsubstrat", *Frühjahrstagung der Deutschen Physikalischen Gesellschaft*, Münster, Germany, Mar. 1997.

[T-38] M. Mundbrod, K. Thonke, R. Sauer, M. Mayer, A. Pelzmann, M. Kamp, and K.J. Ebeling, "Temperaturabhängige bandkantennahe Photolumineszenz von MBE–GaN–Schichten auf Saphirsubstrat", *Frühjahrstagung der Deutschen Physikalischen Gesellschaft*, Münster, Germany, Mar. 1997.

Publications and Conference Contributions

[P-1] Z. Dai, R. Michalzik, P. Unger, and K.J. Ebeling, "Numerical simulation of broad-area high-power semiconductor laser amplifiers", *IEEE Journal of Quantum Electronics*, vol. 33, pp. 2240–2254, 1997.

[P-2] Z. Dai, P. Unger, and K.J. Ebeling, "Numerical simulation of tapered semiconductor laser amplifiers", in *Proc. Conf. on Lasers and Electro-Optics CLEO '97*, pp. 241–242, Baltimore, Maryland, USA, May 1997.

[P-3] K.J. Ebeling, M. Grabherr, R. Jäger, and R. Michalzik, "Diode cascade quantum well VCSEL", in *Proc. IEEE Summer Topical Meetings 1997, Vertical-Cavity Lasers*, pp. 61–62, Montreal, Quebec, Canada, Aug. 1997.

[P-4] K.J. Ebeling, M. Grabherr, R. Jäger, C. Jung, R. King, R. Michalzik, G. Reiner, P. Schnitzer, B. Weigl, and D. Wiedenmann, "Advanced vertical cavity laser diodes and arrays for high speed optical interconnects", in *Proc. 11th Japanese - German Forum on Information Technology*, Nagano, Japan, Nov. 1997.

[P-5] K.J. Ebeling, R. Michalzik, B. Weigl, G. Reiner, P. Schnitzer, C. Jung, R. Jäger, M. Grabherr, D. Wiedenmann, and W. Schmid, "57 % wallplug efficiency oxide-confined GaAs VCSELs for 1 Gbit/s bias-free data transmission", in *Proc. Phantoms Strategic Domain Meetings, PHASDOM 97, paper D2.10*, Aachen, Germany, Mar. 1997.

[P-6] M. Grabherr, R. Jäger, R. Michalzik, G. Reiner, and K.J. Ebeling, "Efficient single-mode oxide-confined GaAs VCSELs emitting in the 850 nmm wavelength regime", *IEEE Photon. Technol. Lett.*, vol. 9, pp. 1304–1306, 1997.

[P-7] J. Heerlein, M. Grabherr, R. Jäger, and P. Unger, "Improved performance of single-mode lasers by using native-oxide lateral-confinement layers", in *Proc. IEEE Summer Topical Meetings 1997, Advanced Semiconductor Lasers and Applications*, pp. 11–12, Montreal, Quebec, Canada, Aug. 1997.

[P-8] J. Heinrich, M. Rode, K. Pressmar, and E. Zeeb, "Low-cost VCSEL-transceiver module for optical data buses", in *Proc. Conf. on Lasers and Electro-Optics LEOS'97*, pp. 58–59, San Francisco, CA, USA, Nov. 1997.

[P-9] J. Heinrich, E. Zeeb, and K.J. Ebeling, "Butt-coupling efficiency of VCSEL's into multimode fibers", *IEEE Photon. Technol. Lett.*, vol. 9, pp. 1555–1557, 1997.

[P-10] R. Jäger, M. Grabherr, C. Jung, R. Michalzik, B. Weigl, and K.J. Ebeling, "57 % wallplug efficiency oxide-confined 850 nm wavelength GaAs VCSELs", *Electron. Lett.*, vol. 33, pp. 330–331, 1997.

[P-11] R. Jäger, M. Grabherr, C. Jung, P. Schnitzer, and K.J. Ebeling, "Optical data transmission over large temperature range using highly efficient oxide-confined GaAs VCSEL sources", in *Proc. GAAS 97*, pp. 271–274, Bologna, Italy, Sept. 1997.

[P-12] C. Jung, M. Grabherr, R. Jäger, P. Schnitzer, D. Wiedenmann, R. Michalzik, U. Martin, S. Müller, and K.J. Ebeling, "Sub-half-mA single-mode 1-D vertical-cavity laser arrays for 1 Gbit/s data transmission", in *Proc. ECOC 1997*, vol. 1, pp. 111–114, Edinburgh, Scotland, UK, Sept. 1997.

[P-13] C. Jung, R. Jäger, M. Grabherr, P. Schnitzer, R. Michalzik, B. Weigl, S. Müller, and K.J. Ebeling, "4.8 mW single-mode oxide confined top-surface emitting vertical-cavity laser diode", *Electron. Lett.*, vol. 33, pp. 1790–1791, 1997.

[P-14] C. Jung, M. Grabherr, R. Jäger, D. Wiedenmann, R. Michalzik, U. Martin, S. Müller, and K.J. Ebeling, "Sub-half-mA single-mode 1-D vertical-cavity laser arrays for 1 Gbit/s data transmission", *Trends in Optics and Photonics (TOPS), Advances in Vertical Cavity Surface Emitting Lasers*, vol. 15, p. 130, 1997.

[P-15] M. Kamp, M. Mayer, A. Pelzmann, and K.J. Ebeling, "Fundamentals, material properties and device performances in GaN MBE using on-surface cracking of ammonia", *MRS Internet J. Nitride Semicond. Res., article 26*, vol. 2, 1997.

[P-16] M. Kamp, M. Mayer, A. Pelzmann, and K.J. Ebeling, "On surface cracking of ammonia for MBE of GaN (invited)", *Mat. Res. Soc. Symp. Proc., article 161*, vol. 449, 1997.

[P-17] C. Kirchner, A. Pelzmann, M. Schauler, M. Mayer, F. Eberhard, M. Kamp, P. Unger, and K.J. Ebeling, "GaN LEDs grown by MOVPE", in *Proc. EW-MOVPE VII, paper F8*, Berlin, Germany, June 1997.

[P-18] M. Mayer, A. Pelzmann, C. Kirchner, M. Schauler, F. Eberhard, M. Kamp, P. Unger, and K.J. Ebeling, "Device performance of ultra-violet emitting diodes grown by MBE", in *Proc. 2nd International Conference on Nitride Semiconductors (ICNS'97)*, pp. 512–513, Tokushima, Japan, Oct. 1997.

[P-19] M. Mayer, A. Pelzmann, M. Kamp, K.J. Ebeling, H. Teisseyre, G. Nowak, M. Leszczynski, I. Grzegory S. Porowski, and G. Karczewski, "High quality homoepitaxial GaN grown by molecular beam epitaxy with NH_3 on surface cracking", *Jap. J. Appl. Phys., part 2, No. 12b*, vol. 36, pp. 1634–1636, 1997.

[P-20] R. Michalzik, B. Weigl, G. Reiner, M. Grabherr, and K.J. Ebeling, "Realization and modeling of extremely efficient VCSELs", in *Proc. Progress in Electromagn. Res. Symp., PIERS'97*, vol. 2, Hong Kong, Jan. 1997.

[P-21] R. Michalzik, R. Jäger, B. Weigl, M. Grabherr, C. Jung, G. Reiner, and K.J. Ebeling, "High efficiency 850 nm wavelength GaAs VCSELs (invited)", in *Proc. IEEE Summer Topical Meetings 1997, Vertical-Cavity Lasers*, pp. 13–14, Montreal, Quebec, Canada, Aug. 1997.

[P-22] R. Michalzik, K.J. Ebeling, M. Grabherr, D. Wiedenmann, R. Jäger, C. Jung, and B. Weigl, "High power and high efficiency GaAs based VCSELs (invited)", in *Proc. Conf. on Lasers and Electro-Optics LEOS'97*, p. 347, San Francisco, CA, USA, Nov. 1997.

[P-23] R. Michalzik, D. Wiedenmann, B. Weigl, P. Schnitzer, R. King, C. Jung, R. Jäger, M. Grabherr, and K.J. Ebeling, "High efficiency GaAs based VCSELs for optical interconnect applications (invited)", in *Proc. The Rank Prize Funds Symposium on Devices & Systems for Optical Interconnects & Data Links*, Grasmere, UK, Sept. 1997.

[P-24] R. Michalzik, P. Schnitzer, U. Fiedler, D. Wiedenmann, and K.J. Ebeling, "High-bit-rate data transmission with short-wavelength oxidized VCSEL's: Toward bias-free operation", *IEEE J. Select. Topics Quantum Electron.*, vol. 3, pp. 396–404, 1997.

[P-25] A. Pelzmann, S. Strite, A. Dommann, C. Kirchner, M. Kamp, K.J. Ebeling, and A. Nazzal, "Improved optical activation of ion-implanted Zn acceptors in GaN by annealing under N_2 overpressure", *MRS Internet J. Nitride Semicond. Res., article 4*, vol. 2, 1997.

[P-26] A. Pelzmann, C. Kirchner, M. Mayer, M. Schauler, M. Kamp, and K.J. Ebeling, "Blue light-emitting diodes on GaN substrates, growth and characterization", in *Proc. 2nd International Conference on Nitride Semiconductors (ICNS'97)*, pp. 434–435, Tokushima, Japan, Oct. 1997.

[P-27] M. Schauler, C. Kirchner, M. Mayer, A. Pelzmann, F. Eberhard, M. Kamp, P. Unger, and K.J. Ebeling, "GaN based LED's with different recombination zones", *MRS Internet J. Nitride Semicond. Res., article 44*, vol. 2, 1997.

[P-28] W. Schmid, P. Schnitzer, M. Grabherr, R. Jäger, G. Reiner, C. Jung, B. Weigl, and K. J. Ebeling, "High temperature range GaAs VCSELs for 1 Gbit/s data transmission", in *Proc. Semiconductor and Integrated Opto-Electronics SIOE'97*, Cardiff, Wales, UK, Mar. 1997.

[P-29] P. Schnitzer, M. Grabherr, G. Reiner, B. Weigl, W. Zick, and K.J. Ebeling, "High temperature 1 Gbit/s data transmission using $\lambda = 835\,\mathrm{nm}$ GaAs VCSELs", *Electron. Lett.*, vol. 33, pp. 595–597, 1997.

[P-30] P. Schnitzer, D. Wiedenmann, and K.J. Ebeling, "Vertical-cavity surface-emitting lasers of 12 GHz modulation bandwidth for 10 Gbit/s data transmission", in *Proc. MIOP 97*, p. 332, Sindelfingen, Germany, Apr. 1997.

[P-31] P. Schnitzer, M. Grabherr, R. Jäger, C. Jung, R. Michalzik, G. Reiner, W. Schmid, B. Weigl, D. Wiedenmann, and K.J. Ebeling, "Bias-free 1 Gb/s data transmission using high efficiency VCSELs", in *Proc. ECTC 97*, p. 371, San Jose, CA, USA, May 1997.

[P-32] P. Schnitzer, M. Grabherr, R. Jäger, C. Jung, U. Koerbler, and K.J. Ebeling, "Bias-free 2.5 Gbit/s data transmission using GaAs VCSELs at 835 nm emission wavelength", in *Proc. ECOC 1997*, pp. 35–38, Edinburgh, Scotland, UK, Sept. 1997.

[P-33] P. Schnitzer, R. Jäger, C. Jung, S. Müller, and K.J. Ebeling, "Linear 1×8 single-mode GaAs VCSEL arrays for 24 Gb/s data rate transmission", in *Proc. Conf. on Lasers and Electro-Optics LEOS'97*, pp. 53–54, San Francisco, CA, USA, Nov. 1997.

[P-34] P. Schnitzer, U. Fiedler, G. Reiner, B. Weigl, W. Zick, and K.J. Ebeling, "Bias-free 1-Gb/s data transmission using top vertical-cavity surface-emitting laser diodes", *IEEE Photon. Technol. Lett.*, vol. 9, pp. 693–695, 1997.

[P-35] B. Weigl, M. Grabherr, C. Jung, R. Jäger, G. Reiner, R. Michalzik, D. Sowada, and K.J. Ebeling, "High performance oxide confined GaAs VCSELs", *IEEE J. Select. Topics Quantum Electron.*, vol. 3, pp. 409–415, 1997.

[P-36] D. Wiedenmann, C. Jung, M. Grabherr, W. Schmid, G. Reiner, K. Splitthof, R. Michalzik, and K.J. Ebeling, "Measurement of Ultrafast Oscillations in Vertical Cavity Lasers after Pulse Perturbation", in *Proc. Microwave Photonics '97*, pp. 281–284, Duisburg, Germany, Sept. 1997.

[P-37] S. Christiansen, M. Albrecht, W. Dorsch, H. P. Strunk, A. Pelzmann, M. Mayer, M. Kamp, K.J. Ebeling, C. Zanotti-Fregonara, and G. Salviati, "Microstructure and growth morphology as related to electro-optical properties of heteroepitaxial wurtzite GaN on sapphire (0001) substrates", *Mat. Sci. Eng. B43*, pp. 296–302, 1997.

[P-38] O. Galjukov, Y.E. Egorov, Y.N. Makarov, R.A. Talalaev, C. Kirchner, M. Kamp, and K.J. Ebeling, "Modeling of MOVPE of group III-nitrides in horizontal tube reactor (extended abstract)", in *Proc. Conference on Microscopy of Semiconducting Materials*, Oxford, UK, 1997.

[P-39] G. Salviati, C. Zanotti-Fregonara, M. Albrecht, S. Christiansen, H.P. Strunk, M. Mayer, A. Pelzmann, M. Kamp, K.J. Ebeling, M.D. Bremser, R.F. Davis, and Y.G. Shreter, "Crystal defects and optical properties of GaN grown with different techniques: stacking faults related luminesence", in *Proc. Conference on Microscopy of Semiconducting Materials*, Oxford, UK, 1997.

[P-40] S. Strite, A. Pelzmann, T. Suski, M. Leszcynski, J. Jun, A. Rockett, M. Kamp, and K.J. Ebeling, "Efficient optical activation of ion-implanted Zn acceptors in GaN by annealing under 10 kbar N_2 overpressure", *MRS Internet J. Nitride Semicond. Res., article 15*, vol. 2, 1997.

[P-41] H.Y.A. Chung, G. Stareev, J. Joos J. Maehnss, and K.J. Ebeling, "Very low threshold current density 1.3 μm-InAsP/InGaAsP strained quantum well GRIN-SCH laser grown by Gas Source MBE", *to be presented at IPRM '98*, Tsukuba, Japan, May 1998.

[P-42] J. Heerlein, M. Grabherr, R. Jäger, and P. Unger, "Single-mode AlGaAs-GaAs lasers using lateral confinement by native-oxide layers", *IEEE Photonics Technology Lett., in press*, vol. 10, 1998.

[P-43] R. King, R. Michalzik, C. Jung, M. Grabherr, F. Eberhard, R. Jäger, and K.J. Ebeling, "Oxide confined 2D VCSEL arrays for high-density inter/intra- chip interconnects", *Proc. SPIE Photonics West, Optoelectronics'98 - Vertical-Cavity Surface-Emitting Lasers II*, San Jose, CA, USA, Jan. 1998.

[P-44] R. King, R. Michalzik, R. Jäger, F. Eberhard, C. Jung, M. Grabherr, and K.J. Ebeling, "Vertical-cavity surface-emitting laser diode arrays for parallel optical interconnects within multichip modules", *submitted to PIERS 98 - Progress in Electromagnetics Research Symposium*, Nantes, France, July 1998.

[P-45] M. Mayer, A. Pelzmann M. Kamp, M. Albrecht, S. Christiansen, H.P. Strunk, G. Salviati, C. Zanotti-Fregonara, and K.J. Ebeling, "Luminescence related to stacking faults in GaN/sapphire (0001)", *submitted to Appl. Phys. Lett.*, 1997.

[P-46] R. Michalzik, M. Grabherr, and K.J. Ebeling, "High-power VCSELs: Modeling and experimental charaterization (invited)", *Proc. SPIE Photonics West, Optoelectronics'98 - Vertical-Cavity Surface-Emitting Lasers II*, San Jose, CA, USA, Jan. 1998.

[P-47] W. Schmid, D. Wiedenmann, M. Grabherr, R. Jäger, R. Michalzik, and K.J. Ebeling, "CW-operation of a diode cascade InGaAs quantum well VCSEL", *Electron. Lett.*, vol. 34, pp. 553–555, 1998.

[P-48] P. Schnitzer, M. Grabherr, R. Jäger, C. Jung, and K.J. Ebeling, "Linear 1×8 GaAs VCSEL arrays for 24 Gbit/s data rate transmission", *Electron. Lett.*, vol. 34, pp. 187–189, 1998.

[P-49] P. Schnitzer, M. Grabherr, R. Jäger, C. Jung, R. King, R. Michalzik, D. Wiedenmann, and K.J. Ebeling, "Short distance polymer optical fiber data transmission at 2.5 Gb/s using GaAs vertical cavity surface emitting lasers at λ = 780 nm", *Proc. OFC'98*, San Jose, CA, USA, Febr. 1998.

[P-50] P. Schnitzer, M. Grabherr, R. Michalzik, R. Jäger, J. Joos, C. Jung, R. King, , W. Schmid, D. Wiedenmann, and K.J. Ebeling, "High performance VCSEL arrays for optical interconnection", *to be presented at ECTC'98*, Seattle, Washington, USA, May 1998.

[P-51] P. Schnitzer, M. Grabherr, R. Michalzik, R. Jäger, J. Joos, C. Jung, R. King, , W. Schmid, D. Wiedenmann, and K.J. Ebeling, "Hochbitratige Datenübertragung mit Vertikallasermatrizen", *Proc. MMONT'98*, p. 12, Günzburg, Germany, Mar. 1998.

[P-52] P. Schnitzer, M. Grabherr, R. Jäger, J. Jung, and K.J. Ebeling, "Bias-Free 2.5 Gbit/s Data Transmission Using Polymide Passivated GaAs VCSELs", *Electron. Lett., in press*, vol. 34, 1998.

[P-53] D. Wiedenmann, C. Jung, M. Grabherr, R. Jäger, W. Schmid, U. Martin, R. Michalzik, and K.J. Ebeling, "Oxide Confined Vertical-Cavity Semiconductor Optical Amplifier for 980 nm Wavelength", *Proc. OFC'98*, San Francisco, CA, USA, May 1998.

[P-54] M. Albrecht, S. Christiansen, G. Salviati, C. Zanotti-Fregonara, Y. T. Rebane, Y. G. Shreter, M. Mayer, A. Pelzmann, M. Kamp, K.J. Ebeling, M. D. Bremser, R. F. Davis, and H. P. Strunk, "Luminescence related to stacking faults in heteroepitaxially grown wurtzite gan", *to be published in Mat. Res. Soc. Symp.*, vol. 468, 1998.

[P-55] S. Christiansen, M. Albrecht, H.P. Strunk, M. Mayer, A. Pelzmann, M. Kamp, K.J. Ebeling, C. Zanotti-Fregonara, and G. Salviati, "Nitridation affecting the epitaxial orientation relationships, the defect population and the related luminescence properties", *submitted to MRS Internet J. Nitride Semicond. Res.*, 1997.

[P-56] S. Christiansen, M. Albrecht, H.P. Strunk, C. Zanotti-Fregonara, G. Salviati, M. Mayer, A. Pelzmann, and M. Kamp, "Structural and luminesence properties of homoepitaxial gan layers", *submitted to MRS Internet J. Nitride Semicond. Res.*, 1998.

[P-57] B. Holländer, S. Mantl A. Pelzmann, C. Kirchner, M. Mayer, M. Kamp, K.J. Ebeling, S. Christiansen, and H. P. Strunk, "Ion scattering studies of defects in GaN thin films on C-orientated sapphire", *submitted to MRS Internet J. Nitride Semicond. Res.*, 1998.

[P-58] B. Holländer, S. Mantl A. Pelzmann, C. Kirchner, M. Mayer, M. Kamp, K.J. Ebeling, S. Christiansen, and H. P. Strunk, "Ion channeling studies of GaN layers on C-oriented sapphire", *accepted for Nucl. Inst. Meth B*, 1997.

[P-59] K. Kornitzer, M. Mayer, M. Mundbrod, K. Thonke, A. Pelzmann, M. Kamp, and R. Sauer, "Donor-acceptor pair transitions in GaN", *to be published in Mat. Sci. Forum, Trans. Tech. Publ.*, Switzerland, 1998.

[P-60] K. Kornitzer, K. Thonke, R. Sauer, M. Mayer, , M. Kamp, and K.J. Ebeling, "Photoluminesence measurements in the near-band-edge region of 6h gan", *submitted to J. Appl. Phys. Lett.*, 1997.

[P-61] T. Suski, J. Jun, M. Leszcynski, H. Teisseyre, S. Strite, A. Rocket, A. Pelzmann, M. Kamp, and K.J. Ebeling, "Optical activation and diffusivity of ion-implanted Zn acceptors in GaN under high pressure, high temperature annealing", *submitted to J. Appl. Phys. Lett.*, 1997.